U. S. DEPARTMENT OF THE INTERIOR • GEOLOGICAL SURVEY
NATIONAL CARTOGRAPHIC INFORMATION CENTER

Utah

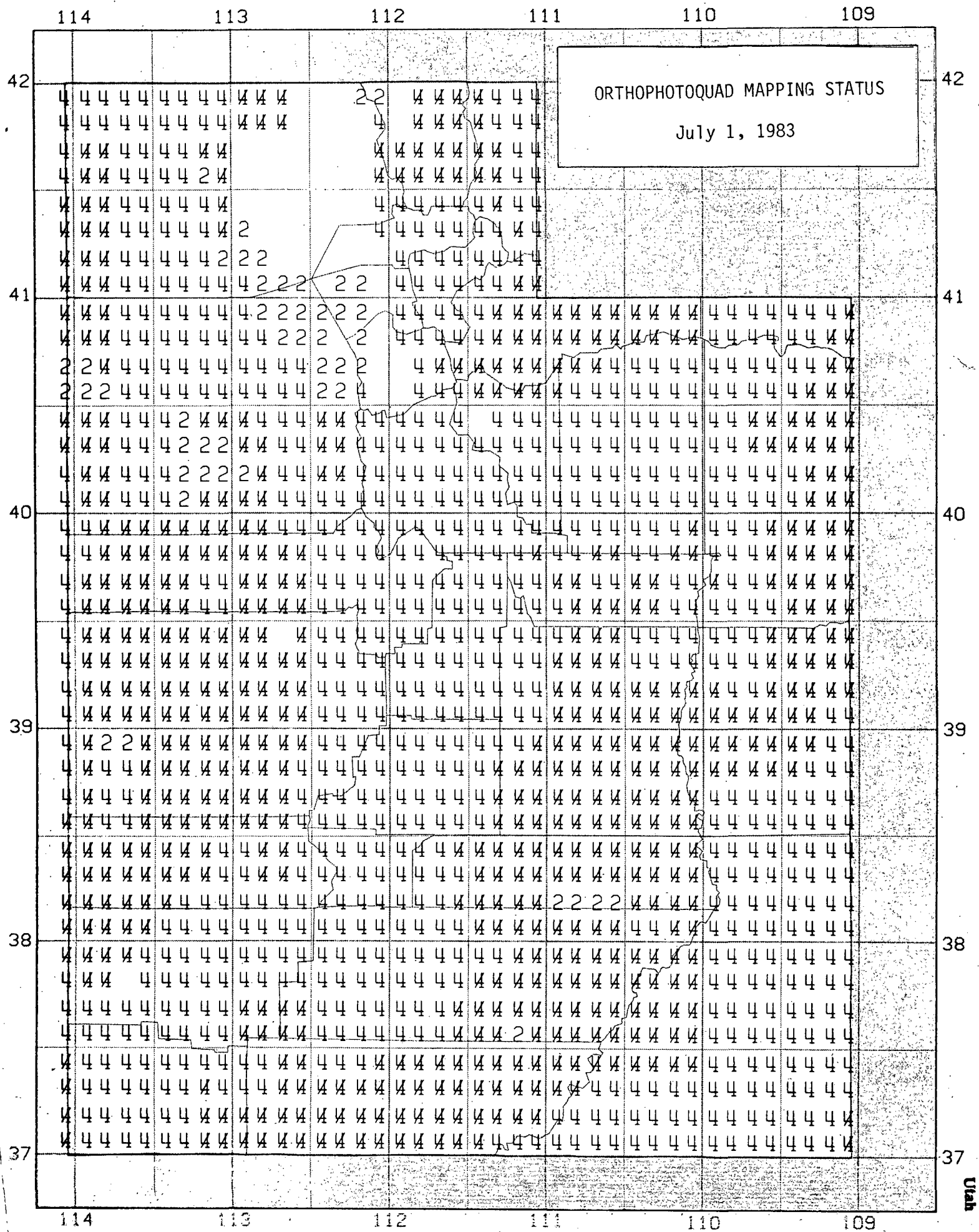

U. S. DEPARTMENT OF THE INTERIOR • GEOLOGICAL SURVEY
NATIONAL CARTOGRAPHIC INFORMATION CENTER

Utah

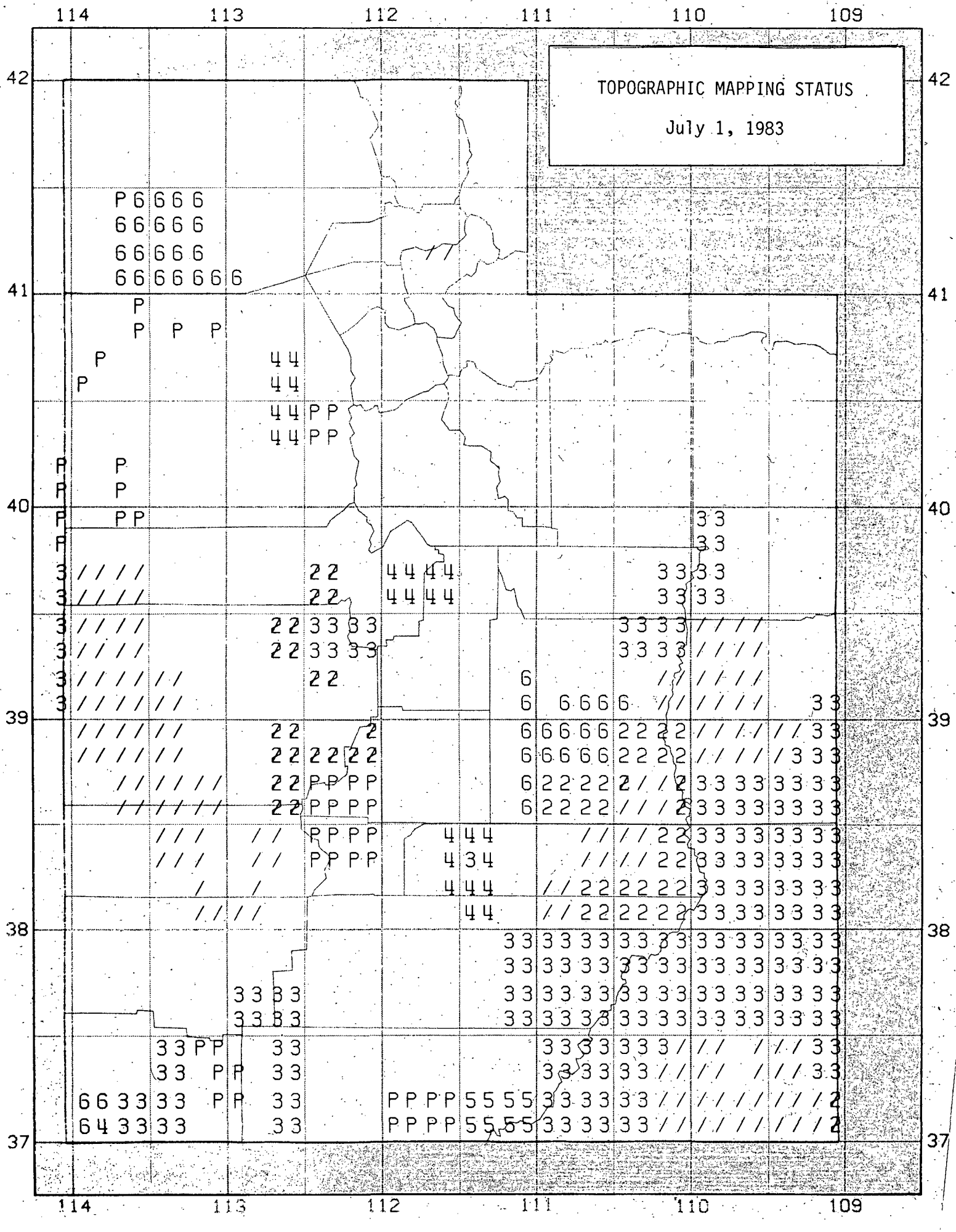

U. S. DEPARTMENT OF THE INTERIOR • GEOLOGICAL SURVEY
NATIONAL CARTOGRAPHIC INFORMATION CENTER

Utah

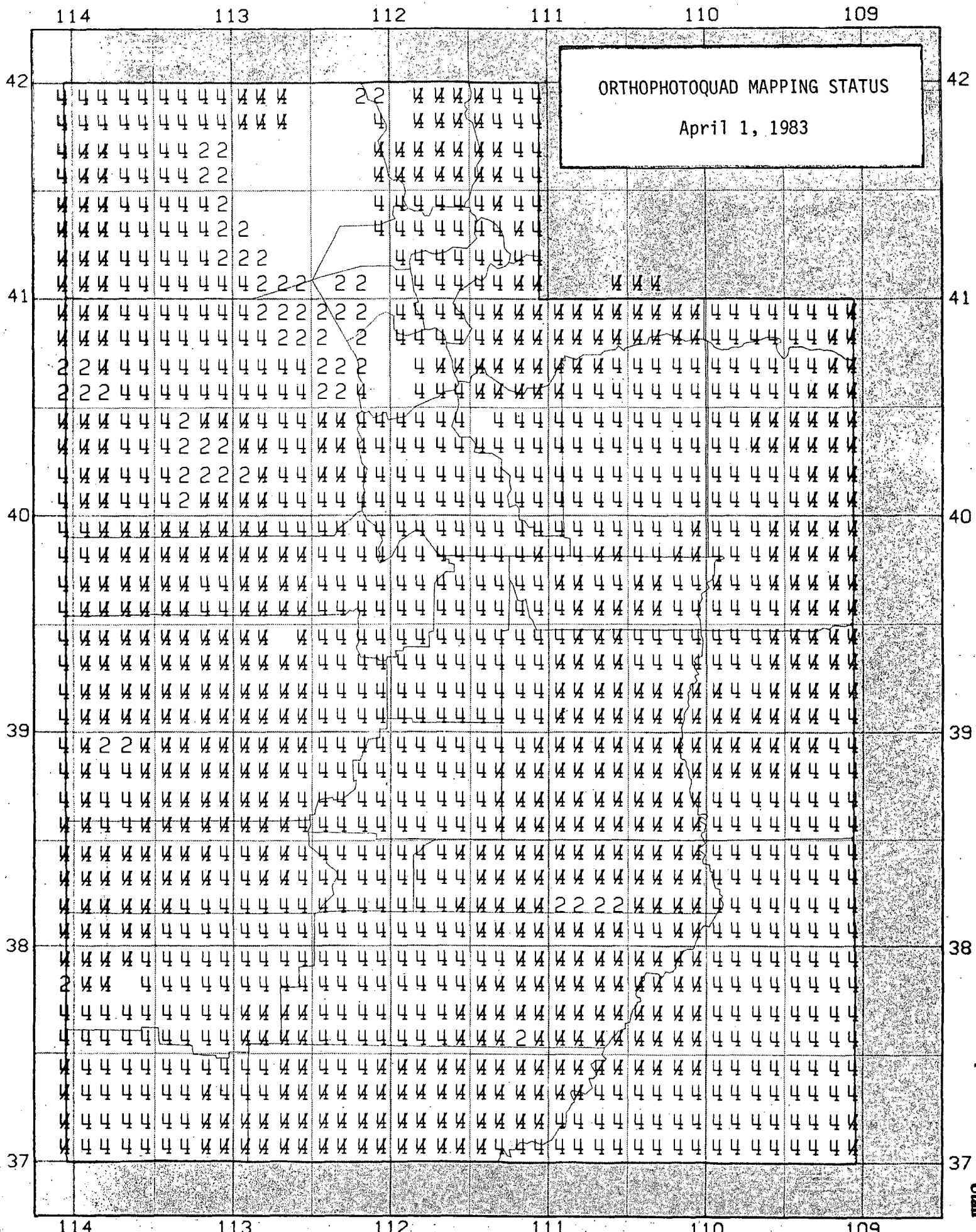

Utah

U. S. DEPARTMENT OF THE INTERIOR • GEOLOGICAL SURVEY
NATIONAL CARTOGRAPHIC INFORMATION CENTER

Utah

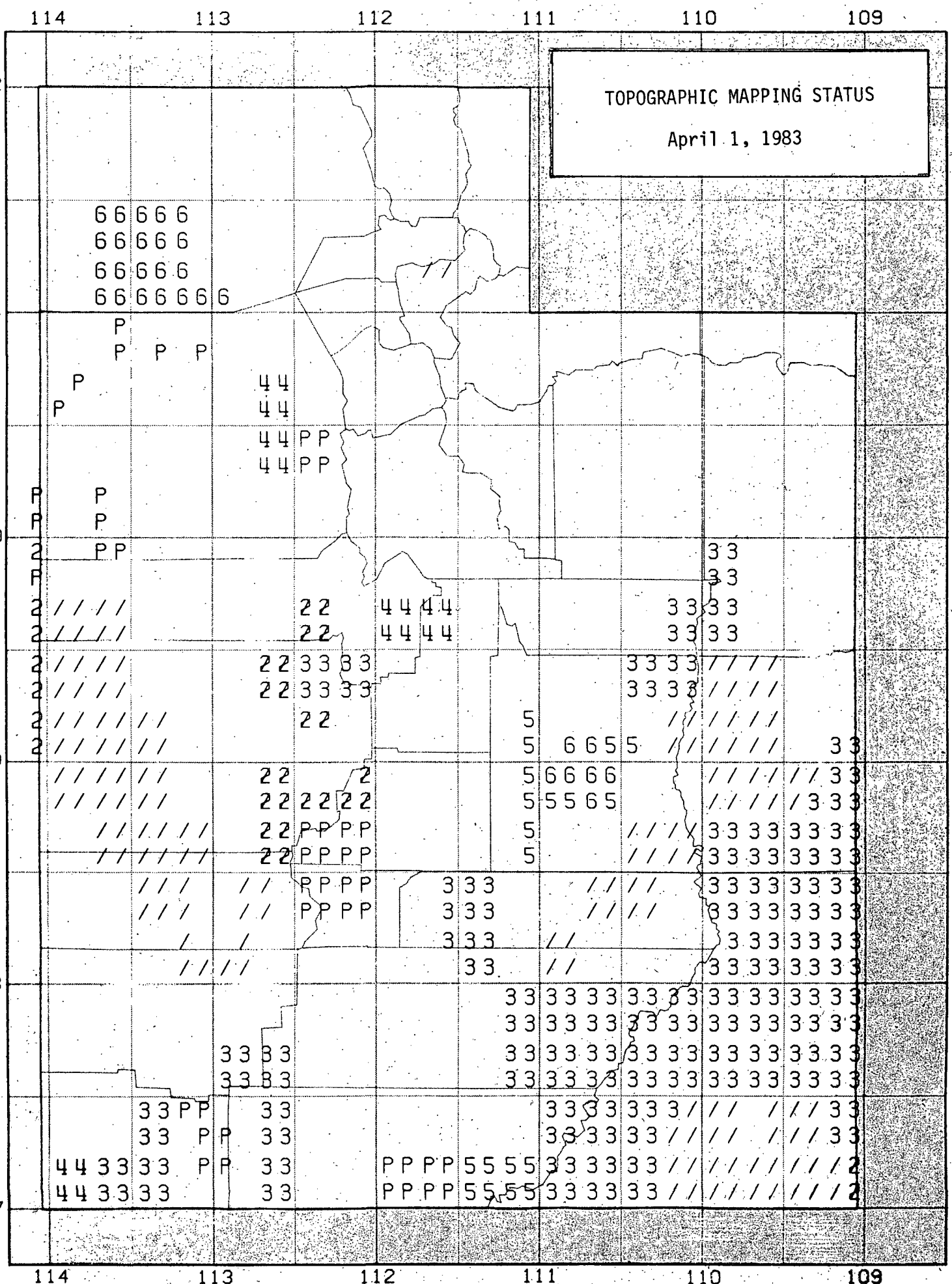

STATUS of LINE MAPPING in UTAH

Rocky Mountain Mapping Center

April 1, 1991

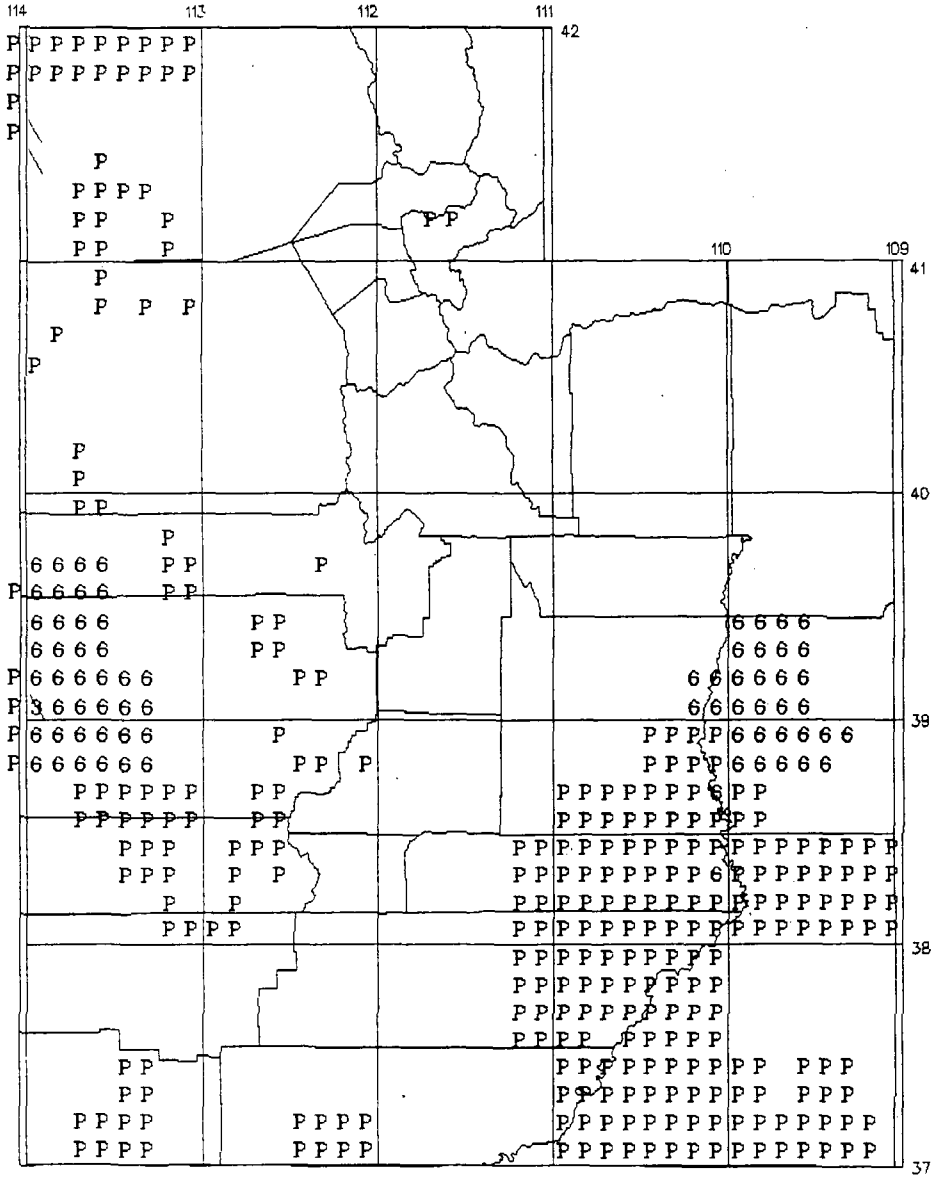

Prepared in Branch of Program Management - RMMC

Utah

STATUS of ORTHO MAPPING in UTAH

Rocky Mountain Mapping Center

April 1, 1991

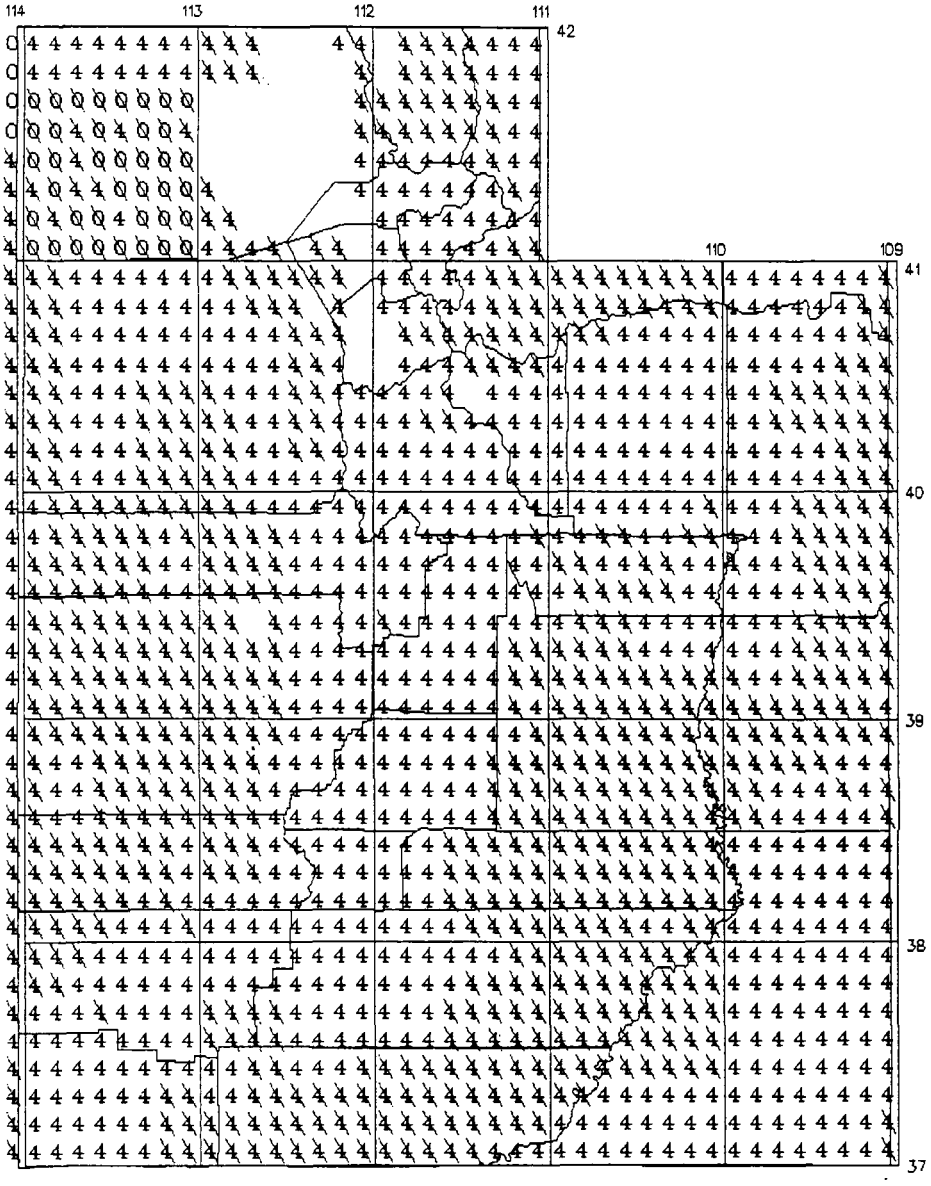

Prepared in Branch of Program Management - RMMC

Utah

U.S. GEOLOGICAL SURVEY
NATIONAL MAPPING DIVISION
EARTH SCIENCE INFORMATION CENTER - LAKEWOOD
ROCKY MOUNTAIN MAPPING CENTER
DENVER, COLORADO
(303) 236-5829
FTS 776-5829

ADVANCE MATERIAL INDEX

The accompanying pages show the status of Topographic Mapping and Orthophotoquad Mapping, and the availability of advance materials. These indexes are produced on a quarterly basis and are furnished to requestors free of charge. Following is an explanation of symbolization and ordering information.

TOPOGRAPHIC MAPPING

2 Aerial photography completed. For ordering address, see note (a).

3 Basic horizontal and vertical control surveys completed. Monumented control may or may not have been established in this quadrangle. Descriptions and unadjusted coordinates and/or elevations are published in 15-minute quadrangle lists. Advance maps are not available at this stage. Price is $1.25 per list (horizontal or vertical). For ordering address, see note (a).

4 Prints of manuscripts (without feature classification, names, boundaries or land net) compiled from aerial photographs are available for $2.50 each. See note (a) and (b).

5 Field mapping and checking completed. One-color unedited advance prints (without names) are available for $2.50 each. See notes (a) and (b).

6 Final drafting completed. Partially-edited one-color advance prints (with names) are available for $2.50 each. See notes (a) and (b).

P Maps published since the latest edition of the State Sales index to published maps. See note (c).

\ Maps published at 1:62,500-scale in 15-minute quadrangles. However, 1:24,000-scale one-color prints in 7 1/2-minute format, with appropriate accuracy and contour intervals are available at $2.50 each. See notes (a) and (b).

Screened areas represent projects in progress at Mid-Continent Mapping Center. Indicated advance materials are available through ESIC-M, USGS Building, 1400 Independence Road, Rolla, Missouri 65401. (314) 341-0851 or FTS 277-0851.

Screened areas represent projects in progress at Western Mapping Center. Indicated advance materials are available through ESIC-W, 345 Middlefield Road, Mail Stop 532, Menlo Park, California 94025. (415) 329-4309 or FTS 459-4309.

ORTHOPHOTOQUAD MAPPING

2 Aerial photography completed, generally quad-centered at 1:80,000-scale. See notes (a) and (b).

4 Advance copy available. See notes (a) and (b). Price per copy for screened image on diazo paper is $3.00; for halftone print on waterproof diazo or single weight positive paper is $15.00; for continuous tone image on photographic paper is $20.00; for screened image on mylar or continuous tone image on opaque scale stable film is $36.00.

4 Same materials available as 4, however, land net (General Land Office) is shown.

0 Second generation advance copy available. Refer to 4, above, for ordering information and prices.

0 Same materials available as 0, however, land net (General Land Office) is shown.

D Third generation advance copy available. Refer to 4, above, for ordering information and prices.

D Same materials available as D, however, land net (General Land Office) is shown.

NOTES

(a) Requests for aerial photography, control lists or advance prints should be sent to the U.S. Geological Survey, Earth Science Information Center-Lakewood, Federal Center, Box 25046, Stop 504, Denver, Colorado 80225. Payment in the exact amount must accompany order. Check or money order should be made payable to the Department of the Interior, USGS. Please do not send stamps or two party checks. Purchase orders from commercial sources must include Federal tax identification. Discount agreements are not honored. Postage and handling charges are $1.00 on all map orders of less than $10.00.

(b) In ordering material or requesting information, mark your area of interest on the accompanying index and forward it with your order. A new copy of the index will be returned to you for future use.

(c) Requests for State sales indexes (free of charge) and for published maps and charts should be sent to the Branch of Distribution, Central Region, U.S. Geological Survey, Federal Center, Box 25286, Denver, Colorado 80225. (303) 236-7477. Remittance must be made payable to Department of Interior, USGS.

(d) This explanation sheet refers to the Advance Materials Indexes for the states of Alaska, Arizona, California, Colorado, Hawaii, Idaho, Montana, Nevada, New Mexico, Oregon, Texas, Utah, Washington and Wyoming. Questions about the mapping program for the remainder of the United States should be directed to ESIC-M, USGS Building, 1400 Independence Road, Rolla, Missouri 65401. (314) 341-0851, FTS 277-0851.

Earth Science Information Center office hours are from 8 a.m. to 4 p.m. Monday through Friday.

AREA
UT
USGS

UTAH

Map ref.

Aeromagnetic map of Hayden Peak and vicinity, Uinta Mtns., Utah, by J. L. Meuschke and J. R. Kirby, scale 1:125,000, (OF 1966) ..... A
Copies on file at 1, 2, 3, 4, 5, 6.
Reproductions may be ordered from 6.

A gravity and aeromagnetic survey of Heber and Rhodes Valleys, Wasatch County, Utah, by D. L. Peterson, 1970, in Water resources of the Heber-Kamas-Park City area, north-central Utah, State of Utah, Dept. Nat. Resources Tech. Pub. No. 27, p. 54-59 (fig. 23, p. 59 is an aeromagnetic map, scale 1:250,000) ..... B

*Professional Paper 316-A Regional geophysical investigations of the Uravan area, Colorado, by P. E. Byerly and H. R. Joesting, 1958, (magnetic coverage shown on pl. 2, scale 1:125,000, extends into Utah)..... C

A comprehensive system of automatic computation in magnetic and gravity interpretation, by R. G. Henderson, 1960, Geophysics, v. 25, no. 3, p. 569-585, (fig. 5 on p. 581 is an aeromagnetic map of the Mexican Hat area, scale 1:250,000)..... D

*Professional Paper 316-C Regional geophysical investigations of the Lisbon Valley area, Utah and Colorado, by P. E. Byerly and H. R. Joesting, 1959, (pl. 8 is an aeromagnetic map, scale 1:125,000)..... E

Geophysical studies of the Upheaval Dome area, San Juan County, Utah, by H. R. Joesting and Donald Plouff, 1958, Intermountain Association of Petroleum Geologists, 9th annual field conference guidebook of the Paradox basin, p. 86-92..... F

*Salt anticlines and deep-seated structures in the Paradox basin, Colorado and Utah, by H. R. Joesting and J. E. Case, 1960, in Professional Paper 400-B, p. 252-256..... G

*Precambrian structures in the Blanding basin and Monument Upwarp, southwest Utah, by J. E. Case and H. R. Joesting, 1961, in Professional Paper 424-D, p. 287-291 ..... H

*Professional Paper 316-F Regional geophysical investigations in the La Sal Mountains area, Utah and Colorado, by J. E. Case, H. R. Joesting, P. Edward Byerly, 1963, (aeromagnetic map shown on pl. 15, scale 1:125,000) I

Regional geophysical studies in Salt Valley - Cisco area, Utah and Colorado, by H. R. Joesting and J. E. Case, 1962, Bulletin of the American Association of Petroleum Geologists, v. 46, no. 10, p. 1879-1889, (fig. 3, p. 1884 is an aeromagnetic map of the Salt Valley - Cisco area)..... J

*Out-of-print

rev. 2-1-79

Map ref.

*Professional Paper 516-B Geologic interpretation of an aeromagnetic survey of the Iron Springs District, Utah, by H. R. Blank, Jr. and J. H. Mackin, 1967 ..... K

*Professional Paper 516-C Regional geophysical investigations of the Moab-Needles area, Utah, by H. R. Joesting, J. E. Case, and Donald Plouff, 1966, (pls. 2 & 3 are aeromagnetic maps at scale 1:125,000) ..... KK

*Professional Paper 516-D Geologic interpretation of aeromagnetic and gravity maps of Tintic Valley and adjacent areas, Tooele and Juab Counties, Utah, by D. R. Mabey and H. T. Morris, 1967 L

Geophysical anomalies over Precambrian rocks, northwestern Uncompahgre Plateau, Utah and Colorado, by J. E. Case, 1966, Bulletin of the American Association of Petroleum Geologists, v. 50, no. 7, p. 1423-1443, (fig. 7, p. 1435 is an aeromagnetic map of area shown on attached index map) ..... M

*Bull. 1230-I Mineral resources of the High Uintas Primitive Area, Utah, by M. D. Crittenden, C. A. Wallace, and M. J. Sheridan, 1967 (interpretation of aeromagnetic survey on p. 20-22, fig. 7 is a small size aeromagnetic contour map) ..... N

Misc. Geol. Invest. Map I-532-A Magnetic map from 112° W longitude to the coast of California, by Isidore Zietz and J. R. Kirby, 1968, scale 1:1,000,000 (coverage in Utah is a combination of data from U. S. Naval Oceanographic Office and U.S. Geol. Survey), 50 cents ..... O

Misc. Geol. Invest. Map I-533-A Magnetic map from 100° to 112° W longitude, by Isidore Zietz and J. R. Kirby, 1968, scale 1:1,000,000 (coverage in Utah is a combination of data from U. S. Naval Oceanographic Office and U.S. Geol. Survey), 50 cents ..... P

Aeromagnetic investigation of crustal structure for a strip across the western United States, by Isidore Zietz and others, 1969, Geol. Soc. America Bull., v. 80, no. 9, p. 1703-1714, (pl. 1 shows tectonic features, aeromagnetic map with contour intervals of 20 and 100 gammas, and location of major magnetic trends and patterns) ..... Q

Thickness of unconsolidated to semiconsolidated sediments in Jordan Valley, Utah, by R. E. Mattick, 1970, in Professional Paper 700-C, p. 119-124 (fig. 3, p. 121 is an aeromagnetic map of southern Jordan Valley), $3.25 ..... R

Morphological study of geophysical maps by viewing in three dimensions, by S. Parker Gay, Jr., 1971, Geophysics, v. 36, no. 2 (this paper is not by a U.S.G.S. author but the southern 3/4 of GP-598 is used as an example) ..... S

*Out-of-print

rev. 2-1-79

Map ref.

Reconnaissance geology and mineral potential of Thomas, Keg, and Desert calderas, central Juab County, Utah, by D. R. Shawe, 1972, in Professional Paper 800-B, p. 67-77 (fig. 2 contains 100 gamma aeromagnetic contours), $2.25 ..... T

Professional Paper 736 Regional geophysical investigations in the central Colorado Plateau, by J. E. Case and H. R. Joesting, 1972 (1973), (pl. 2 is an aeromagnetic map, scale 1:125,000), $6.85 ..... U

Aeromagnetic map of part of west-central Utah, by U.S. Geol. Survey, scale 1:250,000 (OF 1971) V
Copies on file at 1, 2, 3, 4, 5, 6, 10, 11.
Reproductions may be ordered from 6.

Aeromagnetic map of parts of the Richfield and Cedar City 1° by 2° quadrangles, Utah, by U.S. Geol. Survey, scale 1:250,000, OF (1972) ..... W
Copies on file at 1, 2, 3, 4, 5, 6.
Reproductions may be ordered from 6.

Aeromagnetic map of parts of the Delta and Richfield 1° by 2° quadrangles, Utah, by U.S. Geol. Survey, scale 1:250,000 (OF 1972) X
Copies on file at 1, 2, 3, 4, 5, 6.
Reproductions may be ordered from 6.

Seismic reflection and aeromagnetic surveys of the Great Salt Lake, Utah, by M. J. Mikulich and R. B. Smith, 1974, Geol. Soc. America Bull., v. 85, no. 6, p. 991, (fig. 3 is an aeromagnetic map) ..... Y

Mineral resources of the Lone Peak Wilderness Study Area, Utah and Salt Lake Counties, Utah, by C. S. Bromfield and L. L. Patten, with a section on Interpretation of aeromagnetic data by D. R. Mabey (report contains an aeromagnetic map at scale 1:48,000), (OF Rept. 75-382, 1975) ..... Z
Copies on file at 1, 2, 3, 4, 5.

GP-127 Airborne radioactivity survey of the Myton area, Duchesne and Uintah Counties, Utah, by R. W. Johnson, 1955, scale 1:31,680, 50 cents 127

GP-422 Aeromagnetic and generalized geologic map of part of north-central Utah, by D. R. Mabey, M. D. Crittenden, Jr., H. T. Morris, R. J. Roberts, and E. W. Tooker, 1964, scale 1:250,000, 50 cents ... 422

GP-597 Aeromagnetic and gravity profiles of the United States along the 37th parallel, by Isidore Zietz and J. R. Kirby, 1967, scale 1:2,500,000, 50 cents 597

GP-598 Aeromagnetic map of the San Francisco Mountains and vicinity, southwestern Utah, 1966, scale 1:62,500, 50 cents 598

Map ref.

GP-907 Aeromagnetic map of Utah, by Isidore Zietz, Ralph Shuey and John R. Kirby, Jr., scale 1:1,000,000, 1976 907

1. U.S.G.S. Library, Rm. 4-A-100, 12201 Sunrise Valley Dr., Reston, Va.
2. Rm. 8105 Federal Bldg., 125 South State St., Salt Lake City, Utah
3. Rm. 1012 Federal Bldg., 1961 South St., Denver, Colorado
4. U.S.G.S. Library, Stevinson Bldg. #3, Denver West Office Park, 1526 Cole Blvd., Golden, Colo.
5. U.S.G.S. Library, 345 Middlefield Rd., Menlo Park, Calif.
6. Utah Geol. and Mineral Survey, 606 Black Hawk Way, Salt Lake City, Utah
7. Rm. 504 Custom House, 555 Battery St., San Francisco, Calif.
8. Rm. 7638 Federal Bldg., 300 N. Los Angeles St., Los Angeles, Calif.
9. Colorado Geological Survey, 254 Columbine Bldg., 1845 Sherman St., Denver, Colo.
10. Idaho Bureau of Mines and Geology, Montana College of Mineral Science and Technology, Butte, Mont.

UNITED STATES
DEPARTMENT OF THE INTERIOR
GEOLOGICAL SURVEY

UTAH

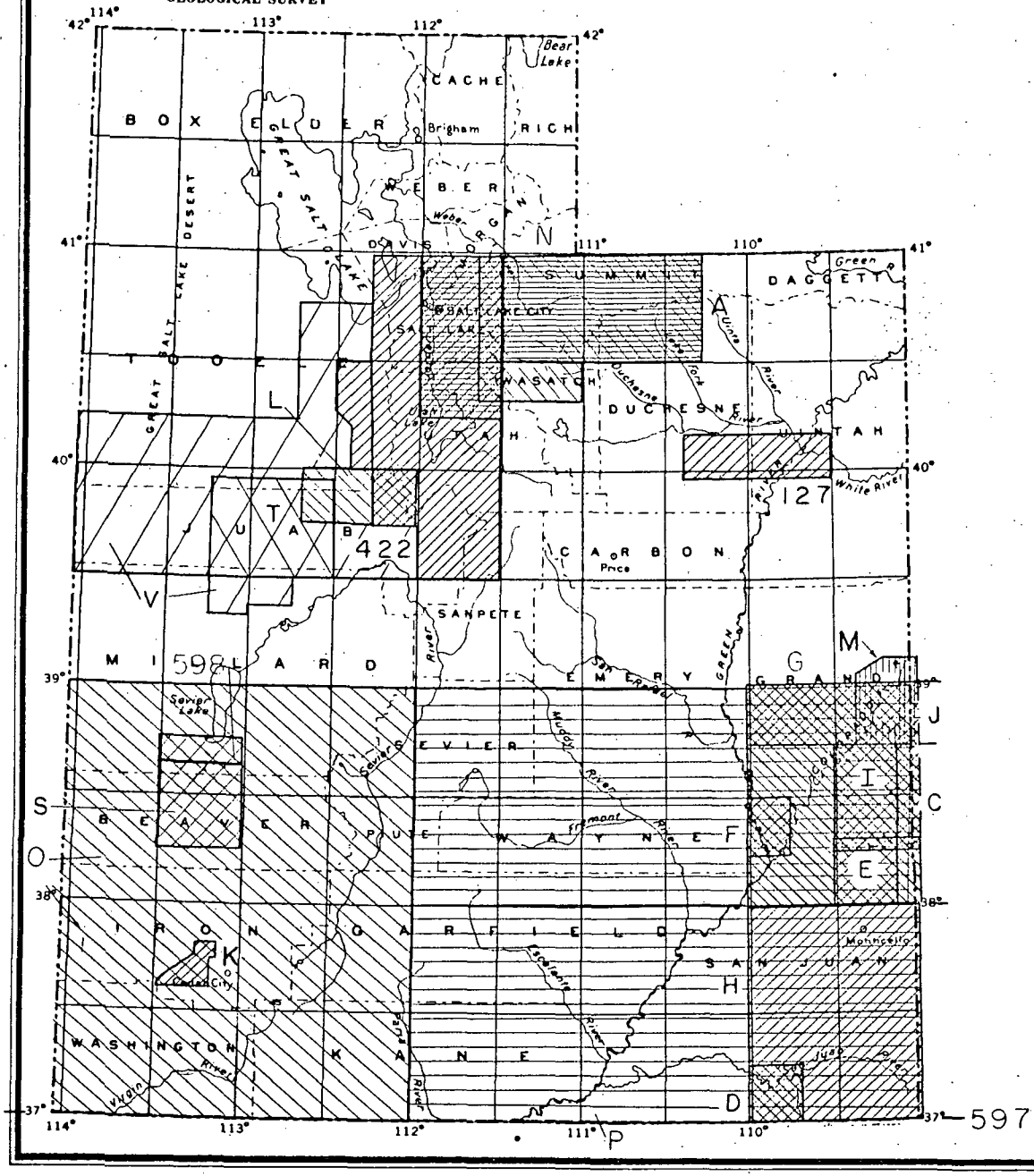

907 COVERS THE
WHOLE STATE

MAP NO. 1

UTAH

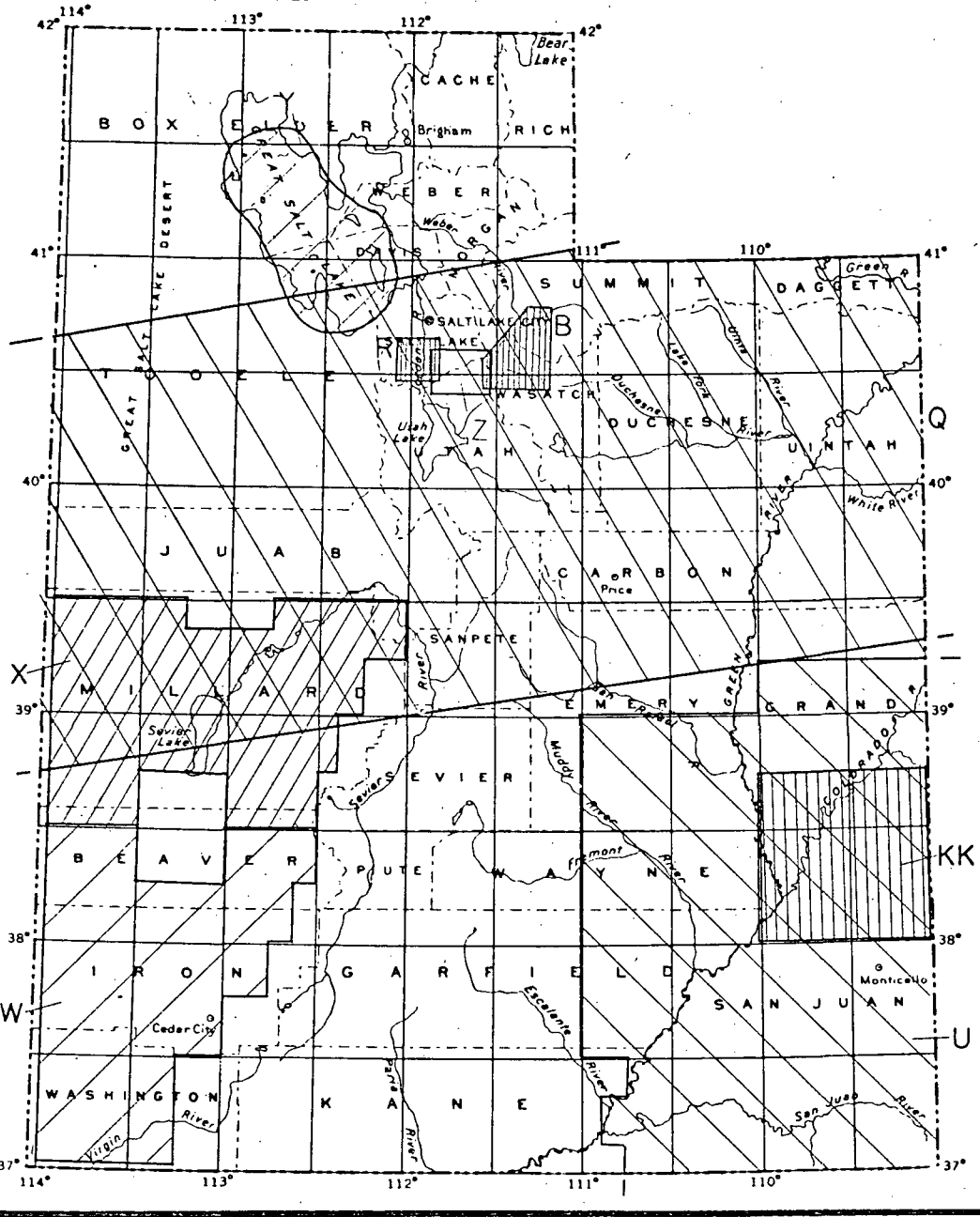
UNITED STATES
DEPARTMENT OF THE INTERIOR
GEOLOGICAL SURVEY
BOX ELDER
CACHE
RICH
Bear Lake
Brigham
WEBER
DAVIS
SALT LAKE
SALT LAKE CITY
TOOELE
GREAT SALT LAKE DESERT
Great Salt Lake
Utah Lake
Jordan River
Weber River
Provo River
Duchesne River
Lake Fork
Green R.
SUMMIT
DAGGETT
WASATCH
DUCHESNE
UINTAH
White River
JUAB
CARBON
Price
SANPETE
MILLARD
EMERY
GRAND
San Rafael River
Sevier River
Sevier Lake
Muddy River
Fremont River
Dirty Devil River
Colorado River
BEAVER
PIUTE
WAYNE
IRON
GARFIELD
SAN JUAN
Monticello
Cedar City
Escalante River
WASHINGTON
KANE
Virgin River
Paria River
San Juan River
B
Q
U
W
X
Z
KK
114°
113°
112°
111°
110°
42°
41°
40°
39°
38°
37°

MAP NO. 2

With Compliments of
Ken Cook

REPRINT

Botton Gravity Meter Regional Survey of the Great Salt Lake, Utah

by

Kenneth L. Cook, Edward F. Gray, Robert M. Iverson, and Martin T. Strohmeier

Reprint from

Great Salt Lake -- a Scientific, Historical and Economic Overview
Edited by J. Wallace Gwynn
Utah Geological and Mineral Survey Bulletin 116, p. 125-143
June 1980

BOTTOM GRAVITY METER REGIONAL SURVEY OF THE GREAT SALT LAKE, UTAH

by Kenneth L. Cook[1], Edward F. Gray[2], Robert M. Iverson[3], and Martin T. Strohmeier[4]

[1] Department of Geology and Geophysics, University of Utah, Salt Lake City, Utah, 84112
[2] Formerly Department of Geology and Geophysics, University of Utah, Salt Lake City, Utah, 84112
[3] Formerly Defense Mapping Agency, Topographic Center, 6500 Brookes Lane, Washington, D. C., 20315
[4] Defense Mapping Agency, Hydrographic/Topographic Center, Geodetic Survey Squadron, F. E. Warren Air Force Base, Wyoming 82001

ABSTRACT

A bottom gravity meter regional survey of the Great Salt Lake (64 stations during 1968) resulted in the compilation of a simple Bouguer gravity anomaly map (with 5-mgal contour interval) and interpretive geologic cross sections along four east-west gravity profiles across the lake that provided information concerning the geologic structures beneath the lake. The large gravity low, that extends for a distance of about 70 miles, essentially the entire length of the lake, indicates a large north-northwestward trending graben beneath the lake, herein designated the Great Salt Lake graben. The closely spaced gravity contours, with steep gravity gradients, indicate that the graben is bounded on each side by large Basin and Range fault zones. On the northwestern side is the East Lakeside Mountains fault zone; on the southwestern side is the East Carrington-Stansbury Islands fault zone; and on the east side is the East Great Salt Lake fault zone. All fault names are newly designated. The large gravity low centers that lie north and south of the gravity saddle that extends between Bird (Hat) Island and the Promontory Point-Fremont Island area, indicate that at least two Cenozoic structural basins of deposition probably formed within the great graben between the Dolphin Island-Rozel Hills area and the Tooele Valley graben. The two basins are designated the "northern Cenozoic basin" and "southern Cenozoic basin" to the north and south, respectively, of the gravity saddle.

The geologic cross sections along the gravity profiles, based on a density contrast of 0.5 gm/cc between the bedrock and valley fill, indicate that the maximum thickness of the Cenozoic structural basins (valley fill) is more than 7,100 feet and 9,700 feet in the northern and southern Cenozoic basins, respectively. An assumed larger or smaller density contrast would result in correspondingly smaller or larger thicknesses, respectively.

The new gravity data over the Great Salt Lake, used in conjunction with the previous gravity data over the adjoining mainland (Cook and others, 1966), afforded an interpretation of the continuity and interrelationships of the geologic structures. For example, the Great Salt Lake graben is continuous with the Tooele Valley graben. Also, an arm of the northern Cenozoic basin within the Great Salt Lake graben probably extends southward, with some constriction, between the Lakeside Mountains and Carrington Island, to connect with the Cenozoic structural basin within the Lakeside-Stansbury graben.

INTRODUCTION

During July and August 1968 a regional gravity survey of the entire Great Salt Lake, Utah was made by the U. S. Defense Mapping Agency, Topographic Center (formerly designated U. S. Army Map Service) in cooperation with the Utah Geological and Mineral Survey (formerly designated Utah Geological and Mineralogical Survey). Figure 1 shows an index map of the survey area.

Sixty-four new gravity stations were taken at the bottom of the Great Salt Lake, (plate 2, in pocket) using a bottom gravity meter. The new gravity data were combined with the gravity data on land peripheral to the Great Salt Lake and along the Southern Pacific Railroad causeway across the lake that was previously published by Cook and others (1966).

The combined gravity data were used in compiling 1) a simple Bouguer gravity anomaly map of the Great Salt Lake and vicinity (plate 2) and 2) four interpretive geologic cross sections indicating the general geologic structures under and adjacent to the Great Salt Lake. A knowledge of the geologic structures will be helpful not only in deciphering the tectonic patterns and geologic

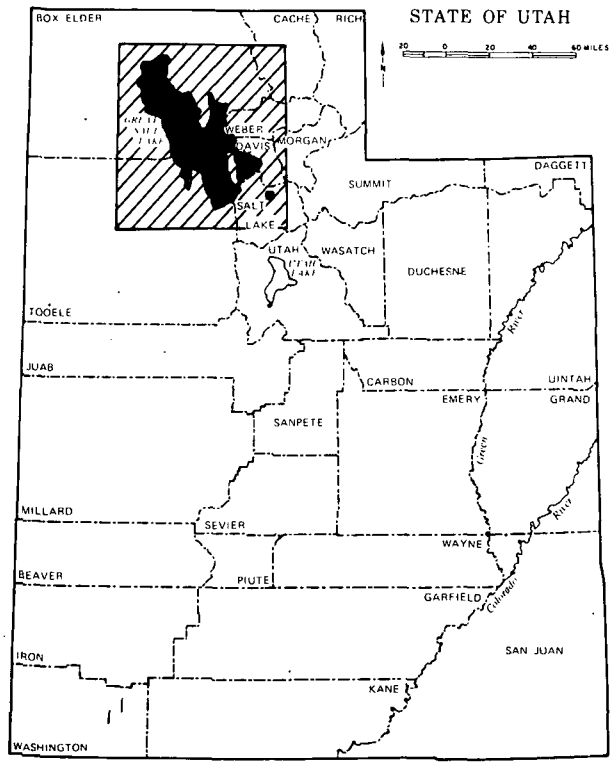

Figure 1. Index map of Utah, showing survey area.

history of the region, but also in the evaluation of the potential for natural resources. For example, the existence of deep Cenozoic (including Quaternary and Tertiary) basins beneath the Great Salt Lake makes the area favorable for the exploration of petroleum and/or natural gas.

TECHNIQUES AND BACKGROUND DATA

Using a LaCoste and Romberg bottom gravity meter, readings at 64 stations were taken along east-west profiles spaced approximately 5 miles apart. The stations were at 2- and 5-mile intervals on alternate traverses. Plate 2 shows the station coverage over the Great Salt Lake and surrounding areas. In the extreme northern part of the lake, the gravity coverage was less detailed than in other parts of the lake because of the difficulty in taking gravity readings in the shallow water. In this area, the wave action on the surface of the lake caused motion of the water at the bottom and hence instability (i.e., accelerations) of the bottom gravity meter that prevented the taking of accurate measurements. To await periods of perfectly calm surface water conditions for satisfactory gravity measurements would have prolonged the survey unduly.

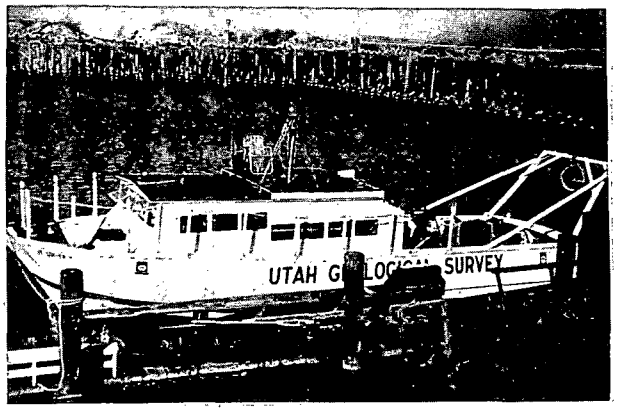

Figure 2. The boat *G. K. Gilbert* at dock in Little Valley Harbor, Great Salt Lake. Tellurometer on tripod on top of cabin. Bottom gravity meter and power winch inside boat at stern. Note cable to pulley on wooden yoke over stern of boat. Photograph taken by K. L. Cook on August 4, 1968.

The *G. K. Gilbert*, a boat owned by the Utah Geological and Mineral Survey, was used for the survey (figure 2). The boat, which was 42 feet long, 13 feet wide and 6 tons in weight, was propelled by two water-jet-type propulsion engines and had a draft of 1½ feet. The gravity meter was lowered over the stern of the boat on a cable that passed through a pulley to a power winch (figure 3).

Horizontal control was obtained to an accuracy of generally a few meters with a Tellurometer (Model MRA3). The master was mounted on top of the cabin of the boat (figure 2) and the two slave stations were either on the mainland or on the islands of the lake. Vertical control was obtained to an accuracy of half a foot with a lead line dropped over the side of the boat.

Two principal base stations on land were used for the survey (plate 2): (1) for the survey of the southern part of the lake, the station was on the breakwater forming the County Boat Harbor at Silver Sands Beach and (2) for the survey of the northern part of the lake, the station was adjacent to the wharf at Little Valley Harbor (northwest of Promontory Point). Using LaCoste and Romberg land gravity meter No. 123, these base stations were tied to the Salt Lake City K base station (at the Salt Lake City airport), which is a United States National Gravity Base Net station (Cook and others, 1971). A description of the location of each of these base stations is given in Appendix I.

Figure 3. LaCoste and Romberg bottom gravity meter being lifted over side of boat before lowering by cable and power winch into Great Salt Lake. Note metal flanges on tripod legs of instrument housing to facilitate stability in muddy bottom of lake. Photograph taken by K. L. Cook on August 4, 1968.

The gravity data were reduced during 1968 by the Gravity Division of the U. S. Army Map Service in Washington, D.C. to give simple Bouguer gravity anomaly values. In making the Bouguer corrections, an average density of 1.22 gm/cc was used for the salt water of the lake, and a density of 2.67 gm/cc was used from the bottom of the lake to mean sea level. Listings of the elevations of the Great Salt Lake during the gravity survey, the density of the salt waters of the Great Salt Lake during the summer of 1968, and the principal facts of the bottom gravity stations are given in Appendices 2, 3, and 4, respectively.

The simple Bouguer gravity anomaly values for the bottom gravity stations were contoured on a map using a 5-milligal (mgal) contour interval. This map was then fitted to the corresponding gravity map values of Cook and others (1966) along the shores of the lake and the causeway across the lake. The resulting simple Bouguer gravity anomaly map, at a 5-mgal contour interval, is shown in plate 2. Four profiles (A-A′ through D-D′, plate 2) were selected for the construction of the interpretive geologic cross sections, which were computed using the two-dimensional modeling technique of Talwani and others (1959).

The resulting interpretive geologic cross sections, in conjunction with the characteristics and patterns on the gravity map and the mapped surface geology, were used to delineate the major geologic structures of the region. The results of the gravity studies were also compared with the results of the available seismic data to provide as reasonable a geologic interpretation as possible.

GEOLOGY

The Great Salt Lake lies along the active rift system in the eastern part of the Basin and Range province (Cook, 1969). The region is characterized by north-south trending mountains and valleys which generally are large horsts and grabens, respectively. The mountain ranges are generally bounded by major Basin and Range fault zones, many of which are seismically active today.

North-south trending mountain ranges surround the Great Salt Lake in most areas. These mountains, which are generally composed of Paleozoic rocks, include the Hogup Mountains, Terrace Mountains, Lakeside Mountains, Promontory Mountains, Oquirrh Mountains, and Stansbury Mountains (plate 2).

Several islands and peninsulas of the Great Salt Lake are composed of Precambrian and/or Paleozoic rocks (plate 2). Antelope Island, Fremont Island, Carrington Island, and Bird (Hat) Island are composed of Precambrian rocks. Stansbury Island and Promontory Point are composed of Precambrian and Paleozoic rocks. South Little Mountain is composed of Precambrian rocks.

Volcanic rocks of Tertiary age are the principal composition of (1) the Rozel Hills, (extending northwest of Rozel Point) which lie along the northeastern margin of Great Salt Lake and (2) the Wildcat Hills and Cedar

Hill, both of which lie near the northern margin of Great Salt Lake and off the map of plate 2.

Most of the surficial valley fill surrounding the Great Salt Lake is Quaternary alluvium. However, several isolated outcrops of Tertiary age (including the Salt Lake group) occur along or near the flanks of the mountain ranges adjacent to the lake.

Within several of the mountain ranges, major north-south trending faults and minor east-west trending faults have been mapped (plate 2). Examples of such faulting are found in the Stansbury Mountains, Lakeside Mountains, Terrace Mountains, and Hogup Mountains.

The Great Salt Lake is approximately 75 miles long and up to 30 miles wide. At the time of the gravity survey (1968), the lake had a maximum depth of 30 feet, and the surface elevations were 4,194 feet and 4,195 feet (i.e., a difference of 1 foot) for the north and south arms, respectively (see Appendix 2). The Great Salt Lake itself is a playa lake, the remanent of the historic Lake Bonneville which covered most of western Utah and parts of Nevada and Idaho during Pleistocene time. In modern times, the lake has receded to its present size and has no outlet.

The Southern Pacific Railroad causeway, completed during 1959 between Lakeside and Promontory Point, isolates the northern portion of the lake from the southern part, except for two small culverts between them. Because all surface water inflow is into the southern part of the lake, the southern part is much less saline than the northern part and at a higher elevation (about 1 foot during 1968). The density of the lake waters during 1968 was 1.21 to 1.23 gm/cc in the north arm and 1.14 gm/cc (shallow water) to 1.21 gm/cc (deep water) in the south arm (See Appendix 3).

INTERPRETATION

Gravity Patterns and Geologic Structures

The simple Bouguer gravity anomaly map (plate 2) of the Great Salt Lake and vicinity contains gravity patterns which correspond to geologic structures. The correspondence of the broader gravity patterns with the broader regional geologic structures of the Great Salt Lake region, especially the land region peripheral to the lake, are given in a previous publication (Cook and others, 1966), and will not be discussed in detail here. In the present paper, emphasis will be given to the correspondence of the gravity patterns and geologic structures in the Great Salt Lake area proper. However, the interrelationships of geologic structures and those of the surrounding mainland areas will be treated briefly to provide an overview.

On the gravity map (plate 2), the large elongate gravity lows indicate grabens. These are generally Cenozoic basins that contain sedimentary and/or volcanic rocks of Quaternary and Tertiary age possibly up to 12,000 feet in thickness (Cook and others, 1966, p. 69). The large elongate gravity highs indicate horsts, which generally form the mountain blocks in the region. The zones of closely spaced ("tight") gravity contours, with steep gravity gradients, generally indicate Basin and Range fault zones. These fault zones generally result in a large density contrast between the rocks in the mountain blocks and the valley fill material within the grabens.

The main trend of the gravity contours is north to north-northwest and parallel to the principal Laramide and older structures, as well as the major Basin and Range faults in the region (Cook and Berg, 1961). However, some locally pronounced trends are northeastern and are probably caused by Basin and Range or perhaps earlier faulting.

Horsts. On the northwestern end of the Great Salt Lake, the Lakeside Mountains horst (newly designated herein) is indicated by an elongate northward-trending gravity high (maximum of about -140 mgal) which is more than 40 miles long. This high overlies the Lakeside Mountains and extends northward over the lake to include Gunnison Island, Cub Island, and the lake area north thereof (plate 2). The horst is interpreted as one large block that includes the Lakeside Mountains, Gunnison Island, and Cub Island as outcrops of the horst.

On the western side of the Great Salt Lake, the Carrington-Stansbury Islands horst (newly designated herein) is indicated by the elongate northward-trending belt of gravity highs which is more than 30 miles long. This belt overlies Stansbury Island (-140 mgal) and extends northward over Carrington Island (maximum of about -130 mgal), Bird (Hat) Island (-133 mgal) and the lake area north thereof. The horst is interpreted as one large block that includes all three islands as outcrops of the horst.

Along the eastern margin of the Great Salt Lake, the continuous belt of gravity highs over the Promontory Range (maximum of about -130 mgal), Fremont

Island (-130 mgal) South Little Mountain (-135 mgal) and Antelope Island (-130 mgal) indicates a large essentially continuous fault block throughout this area. This interpretation was first suggested by Cook and others (1966, p. 60). For convenience of nomenclature, however, the newly designated "Promontory Mountains horst" and "Antelope Island horst" shown on plate 2 are used for the respective portions of the large block covered by these topographic features, and a single name is not given to the fault block as a whole. Moreover, the existence of previously mapped east-west trending faults within this large block indicates that the block is broken in places. Even as recently as Basin and Range faulting, this block has probably had internal faulting, but presumably on a minor scale. The same principle also applies to the Lakeside Mountains horst and the Carrington-Stansbury Islands horst.

Grabens. In a previous publication (Cook and others, 1966), the following grabens and their corresponding gravity features were described; that discussion will not be repeated here, except in so far as it concerns the overall tectonic interrelationships: the Strongknob graben (minimum simple Bouguer gravity anomaly value of about -155 mgal), the Rozel graben (-165 mgal), the Bear River Bay graben (-160 mgal), the Lakeside-Stansbury graben (-165 mgal), the East Antelope Island graben (-160 mgal); the Farmington graben (-195 mgal), and the Tooele Valley graben (-185 mgal) (plate 2).

The Great Salt Lake graben (newly designated, plate 2) is indicated by the large gravity low that extends for about 70 miles from the Dolphin Island-Rozel Hills area on the north to the Tooele Valley graben area on the south (Cook and others, 1969). The graben constitutes a large Cenozoic structural basin filled with thick sequences of sedimentary and/or volcanic rocks.

In the region between Bird (Hat) Island and the Promontory Point-Fremont Island area, the large Cenozoic structural basin may have been separated at times into at least two major Cenozoic structural basins of deposition within the graben during its development. This is evidenced by the gravity saddle and the constriction of the main gravity low associated with the Great Salt Lake graben. The "northern Cenozoic basin" lies north of the gravity saddle and the "southern Cenozoic basin" lies south thereof.

In that part of the northern Cenozoic basin between the Hogup Mountains and Rozel Hills, the gravity data indicate that the thickness of rocks in the basin is relatively small in comparison with the area within the same basin south thereof. The Bouguer gravity values over the lake in this area are about -150 to -153 mgal in comparison with values of about -140 mgal over the Hogup Mountains and Rozel Hills, a difference of only 10 to 13 mgal.

The gravity data indicate that the deepest part of the northern Cenozoic basin, where the rocks are the thickest, is probably in the area of the Southern Pacific Railroad causeway, at a point about midway between Lakeside and Promontory Point (plate 2). Here the Bouguer gravity anomaly values form a minimum of less than -165 mgal, in contrast with values of about -130 mgal over the Paleozoic bedrock in the Lakeside Mountains to the west and the Promontory Mountains to the east, a difference of about 35 mgal.

The gravity data further indicate that the southern Cenozoic basin, within the Great Salt Lake graben, is probably longer and deeper than the northern Cenozoic basin. South of the gravity saddle (about -160 mgal) between Bird (Hat) Island and the Promontory Point-Fremont Island area, the decrease of the Bouguer gravity values along the axis of the gravity low, to reach values of less than -185 mgal within the Tooele Valley graben, indicates southward deepening of the basin. These low values are in contrast with gravity values of about -130 mgal over Carrington Island and Antelope Island, a difference of about 55 mgal. It should be noted that along the axis of the gravity low, the values do not decrease consistently; rather, there are two subsidiary gravity low centers over the lake: 1) one (about -170 mgal) midway between Carrington Island and the northern tip of Antelope Island; and 2) another (about -175 mgal) midway between Stansbury Island and the southern part of Antelope Island. These gravity low centers are provisionally interpreted as being caused by undulations of the bedrock surface and may be related to subsidiary structural basins along the axis of the main southern Cenozoic basin.

The Great Salt Lake graben is continuous with the Tooele Valley graben, their trends departing from each other by about 45°. An interpretive geologic cross section along a gravity profile across the southern part of the Tooele Valley graben by Cook and others (1966) indicates the depth to bedrock to be 12,000 feet. A density contrast of 0.4 gm/cc between the bedrock and valley fill was assumed. A well (WG1 on plate 2) within the Tooele Valley graben and about 2 miles south of this gravity profile, was drilled to a depth of 7,993 feet without completely penetrating the valley fill of Cenozoic age (Cook and others, 1966, p. 68). The great

thickness of Cenozoic valley fill penetrated in the Tooele Valley graben supports the interpretation that comparable thicknesses should occur beneath the southern Cenozoic basin of the Great Salt Lake graben.

It should be noted that the gravity trough between the Lakeside Mountains and Bird (Hat) Island, that extends southwest of the gravity low center over the northern Cenozoic basin, indicates a southern arm of the northern Cenozoic basin. This gravity trough continues southward, with some constriction between the Lakeside Mountains and Carrington Island, to join the pronounced gravity low center over the Lakeside-Stansbury graben. Such continuation indicates that this arm of the northern Cenozoic basin probably extends southward to connect with the Cenozoic structural basin within the Lakeside-Stansbury graben.

Faults. The gravity data indicate many major Basin and Range fault zones, which are shown on plate 2. The location of each fault, indicated by the gravity data was obtained from either the gravity map (plate 2) or the interpretive geologic cross sections along the four profiles (to be discussed later). Most of the faults shown on plate 2 are newly designated but will be only briefly mentioned.

The Great Salt Lake graben is bounded by the following fault zones: 1) on the northwestern margin, by the East Lakeside Mountains fault zone; 2) on the southwestern margin, by the East Carrington-Stansbury Islands fault zone; and 3) on the eastern margin, by the East Great Salt Lake fault zone, which extends continuously from the Rozel Hills south-southeastward along or near the western margin of the Promontory Range, Fremont Island, South Little Mountain, and Antelope Island.

The Strongknob graben is bounded on the east by the West Lakeside Mountains fault zone. The Bear River Bay graben is bounded on the west by the East Promontory Mountains fault zone. The Lakeside-Stansbury graben is bounded on the west by the East Lakeside Mountains fault zone and on the east by the West Carrington-Stansbury Islands fault zone. The Antelope Island horst is bounded on the east by the East Antelope Island fault zone.

Each of the Basin and Range fault zones are generally comprised of individual step faults that form a sinuous and/or braided pattern on the geologic map (plate 2). The indicated locations and throws of the faults and the configuration of the bedrock are shown in the profiles.

Profiles

Interpretive geologic cross sections were constructed along four east-west profiles (A-A′ through D-D′, figures 4 - 7) across the Great Salt Lake, using the two-dimensional modeling technique of Talwani and others (1959). Simple two-layer models were assumed in each cross section. A density contrast of 0.5 gm/cc was assumed between the bedrock (bottom layer, with rocks of pre-Tertiary age) and the top layer (valley fill, with rocks of Quaternary and/or Tertiary age); vertical or steeply dipping faults were assumed in all models. It should be noted that all interpretive geologic cross sections have a vertical exaggeration so that apparent dips are greatly exaggerated. The water in the Great Salt Lake is too shallow (less than 30 feet during 1968) to be included in the cross sections.

The figure for each profile is divided into three parts: (1) part "a", which shows the "observed" simple Bouguer gravity anomaly values, in milligals, with the assumed regional gravity trend; (2) part "b" which shows the residual gravity values, in milligals, after the assumed regional gravity trend has been removed from the observed gravity values; and (3) part "c" which shows the interpretive geologic cross section with the gravity station locations marked on the profile. In part "c" of three profiles, "contour stations" are indicated at locations along those portions of each profile for which the gravity control was based on contoured values only. These values were taken from the gravity map (plate 2).

Because of the inherent ambiguity of gravity data, the models should not be considered unique; however, based on all available information, they are believed to represent a reasonable interpretation of the structural configuration of the contact between the valley fill and the bedrock. For those faults already mapped at the surface (Stokes, 1963), the locations of the faults shown on the profiles agree with those of the mapped faults. For those faults interpreted from the shallow reflection seismic survey over the lake during 1969, reported by Mikulich (1971) and Mikulich and Smith (1974), the location of the faults shown on the profiles generally agree well with those interpreted from the seismic survey, with a few notable exceptions that will be discussed later. This seismic survey had a maximum depth of penetration of only 4,000 feet below the surface of the lake. It should be noted that the actual number of faults along each profile, especially those at great depth, may be more or less than those shown in the profile. However, for the density contrast assumed for each profile and the total thickness of the valley fill,

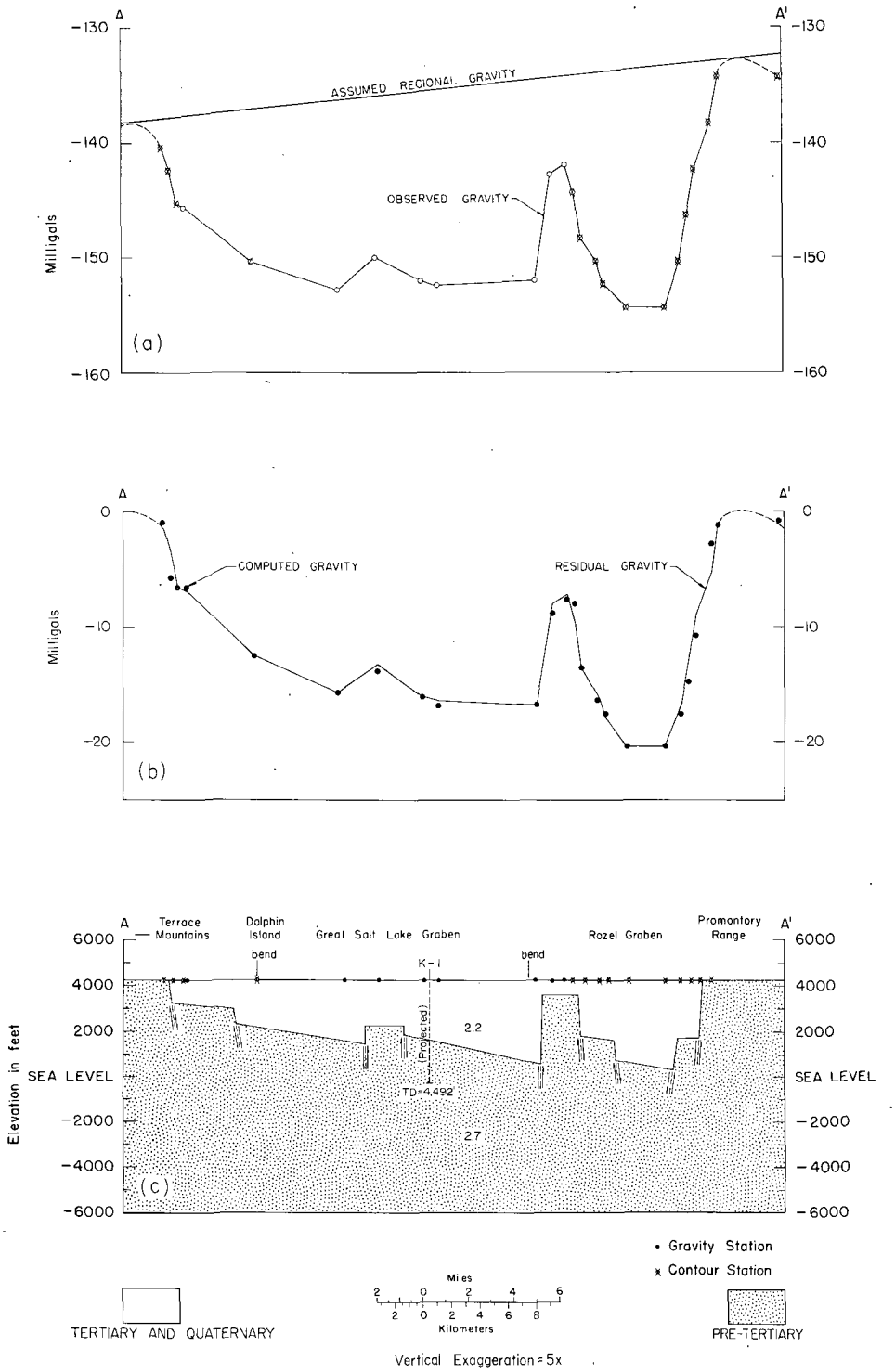

Figure 4. Gravity and interpretive geologic cross section along profile A-A′ across Great Salt Lake and Rozel grabens. Assumed density contrast is 0.5 gm/cc.

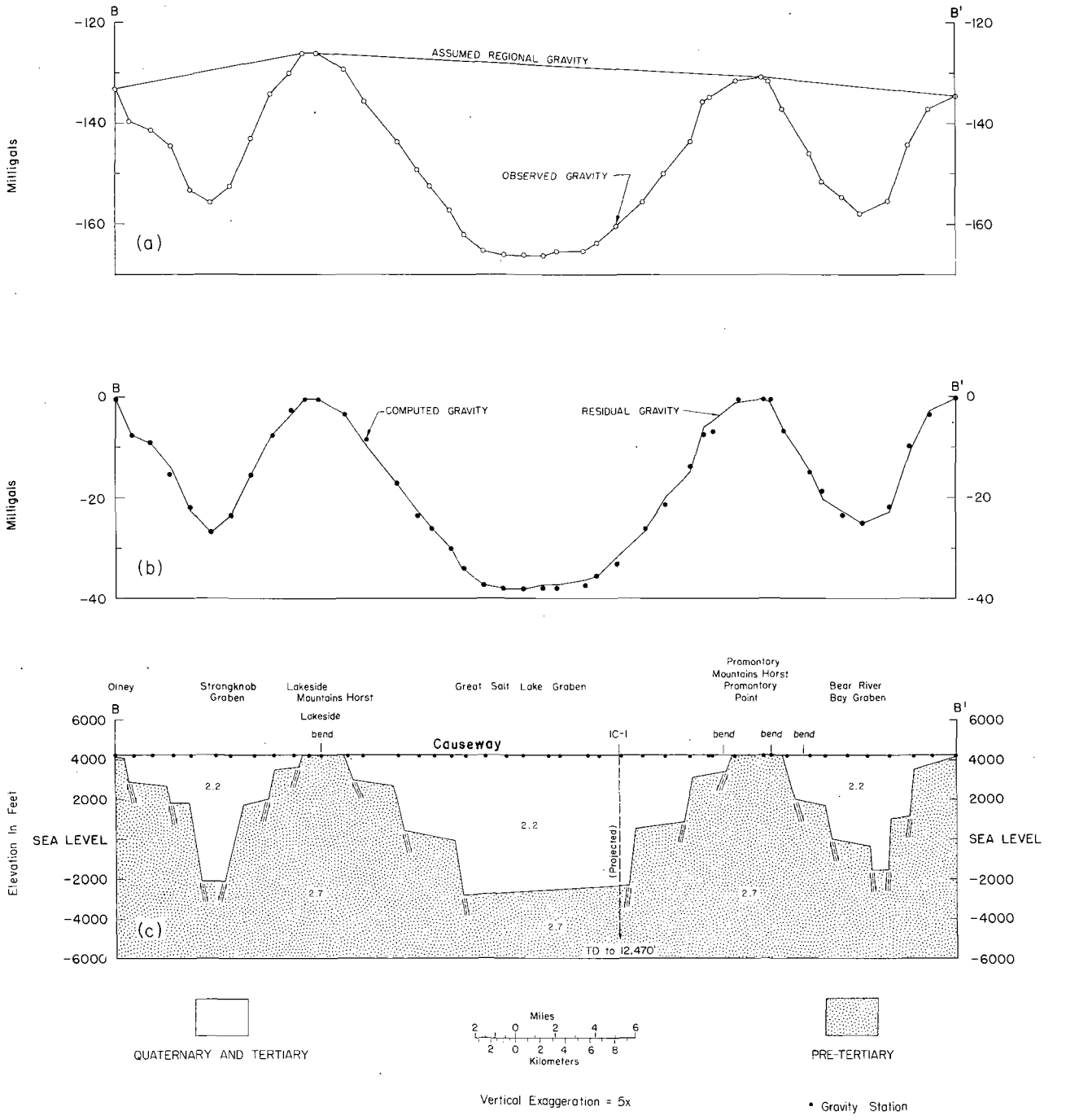

Figure 5. Gravity and interpretive geologic cross section along profile B-B′ across Strongknob, Great Salt Lake, and Bear River Bay grabens and across Lakeside Mountains and Promontory Mountains horsts. Assumed density contrast is 0.5 gm/cc.

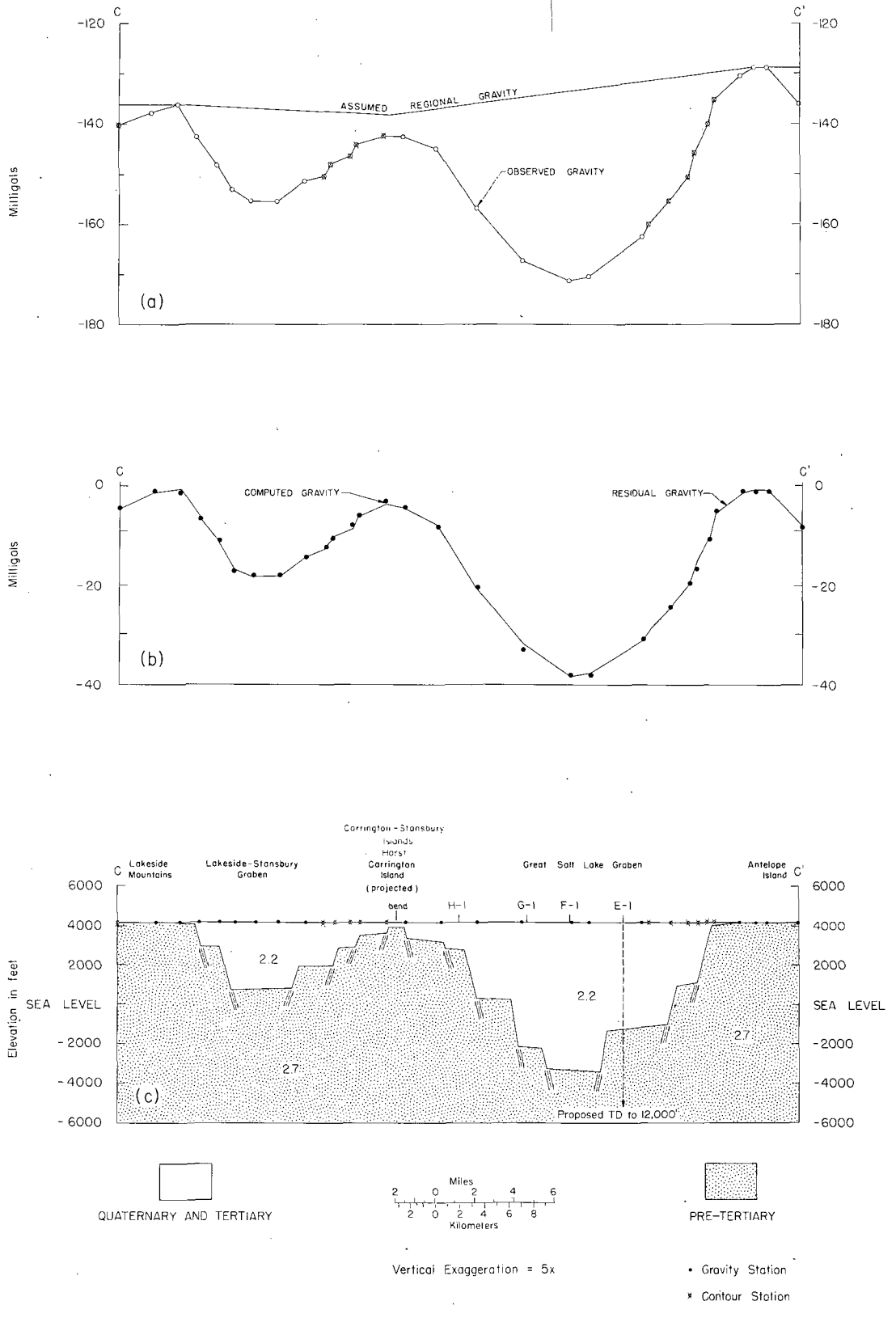

Figure 6. Gravity and interpretive geologic cross section along profile C-C′ across Lakeside-Stansbury and Great Salt Lake grabens and Carrington-Stansbury Islands horst. Assumed density contrast is 0.5 gm/cc.

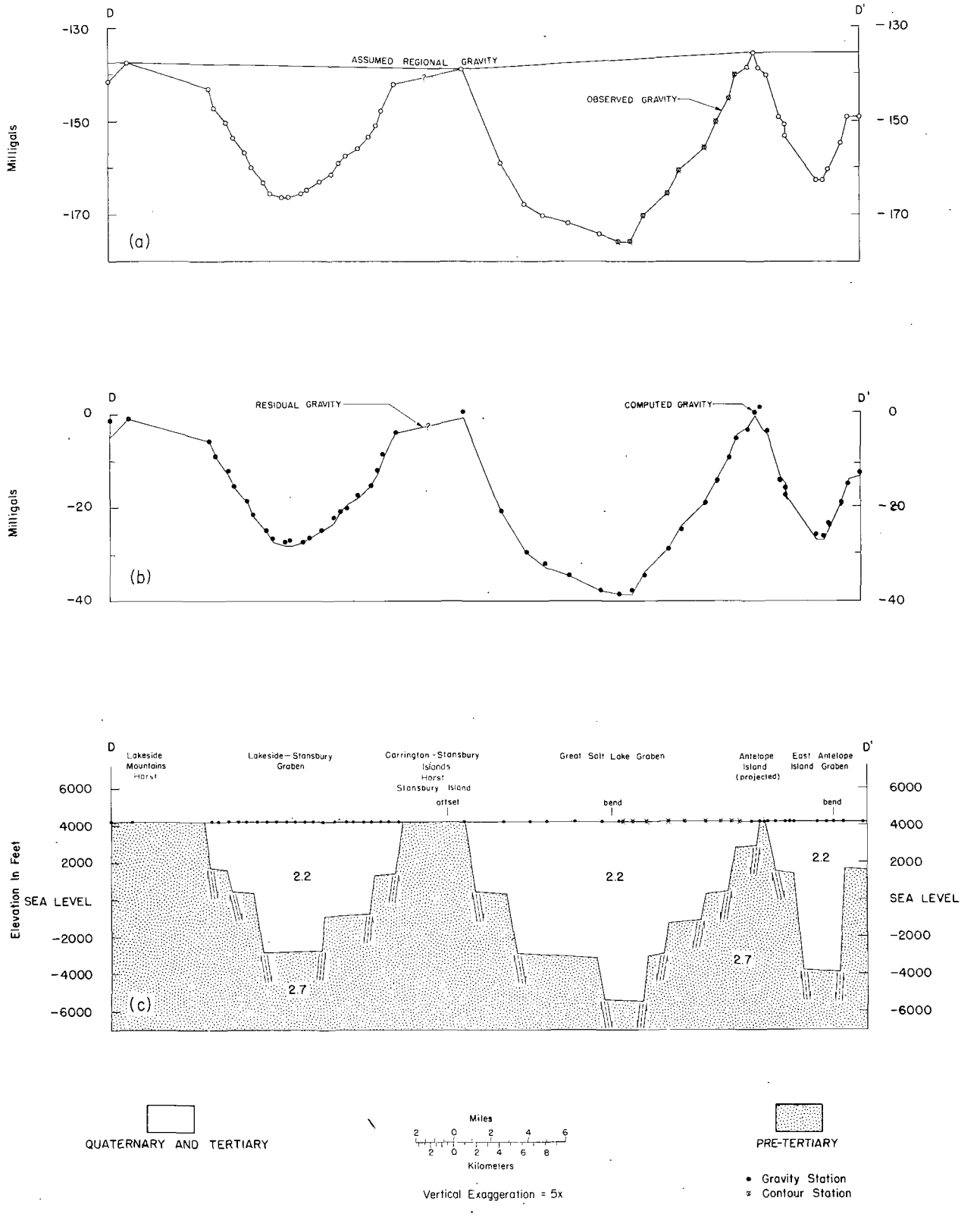

Figure 7. Gravity and interpretive geologic cross section along profile D-D′ across Lakeside-Stansbury, Great Salt Lake, and East Antelope Island grabens and across Lakeside Mountains, Carrington-Stansbury Islands, and Antelope Island horsts. Assumed density contrast is 0.5 gm/cc.

the overall configuration of the bedrock surface is considered reasonable. It should be emphasized that if the true density contrast between the top (valley fill) and bottom (bedrock) layers of rocks is less or greater than the assumed value of 0.5 gm/cc, the thickness of the top layer (valley fill) will be correspondingly greater or less, respectively, than that shown in the models.

Profile A-A'. Profile A-A' (figure 4) extends for about 29 miles along lat 41°28' N approximately across the northern Cenozoic basin between the Terrace Mountains and the western flank of the Promontory Mountains (see plate 2). The model shows the Great Salt Lake graben with a small, buried horst in the bedrock approximately midway between the Terrace Mountains and the Rozel Hills. This small, narrow horst is apparently the northern continuation of the Lakeside Mountains horst, a large block which forms the Lakeside Mountains, and Gunnison and Cub islands, as discussed earlier. The maximum depth to bedrock in the Great Salt Lake graben along profile A-A' is positioned just west of the Rozel Hills, and is indicated as being about 3,600 feet.

Just east of the Great Salt Lake graben is a small horst which comes to within about 600 feet of the surface. This horst separates the Great Salt Lake graben from the Rozel graben, which lies under the Rozel Hills. The Rozel graben has been described elsewhere in detail by Cook and others (1966).

Profile B-B'. Profile B-B' (figure 5) extends for about 38 miles at lat 41°15' N approximately along the Southern Pacific Railroad between the Olney siding, west of Strongknob Mountain, and South Little Mountain, east of Promontory Point (plate 2). The profile passes through Lakeside and Promontory Point. Approximately 19 miles of the profile lie along the causeway which crosses the lake.

On the west, the model shows the Strongknob graben, which has been described elsewhere in detail by Cook and others (1966). To the east of the Strongknob graben are successively, the Lakeside Mountains horst, the Great Salt Lake graben, the Promontory Mountains horst, and the Bear River Bay graben. Along profile B-B', the maximum depth to bedrock is apparently along the deep western margin of the Great Salt Lake graben, which corresponds with the deep eastern base of the Lakeside Mountains horst. Moreover, the northern Cenozoic basin is apparently deepest here; and the maximum basin fill is indicated as about 7,100 feet. The Bear River Bay graben has been described elsewhere in detail by Cook and others (1966).

Profile C-C'. Profile C-C' (figure 6) extends for about 34 miles along lat 40°47' N approximately between the Lakeside Mountains and Antelope Island (plate 2). The profile crosses over a narrow peninsula of Quaternary rocks extending south of Carrington Island and continues eastward for about 20 miles over the lake itself. Beneath the western part of the profile is the Lakeside-Stansbury graben, which has been described elsewhere in detail by Cook and others (1966). Beneath the central part of the profile is the Carrington-Stansbury Islands horst, the top of which is buried beneath a thin cover of Quaternary rocks. The Great Salt Lake graben lies between Stansbury Island and Antelope Island. The maximum depth to bedrock along the profile is approximately midway between the two islands and is indicated as 7,600 feet. It should be noted that this part of the Great Salt Lake graben is in the southern Cenozoic basin.

Profile D-D'. Profile D-D' (figure 7) extends for about 41 miles along lat 40°50' N approximately from the Lakeside Mountains eastward across Stansbury Island (with a slight offset in the profile), the southern part of the Great Salt Lake (with a slight bend in the profile in the central part of the lake), the southern tip of Antelope Island, and along the road causeway between Antelope Island and the mainland (plate 2). The profile crosses the following structures, successively from west to east: Lakeside Mountains horst, Lakeside-Stansbury graben, Carrington-Stansbury Islands horst, Great Salt Lake graben, Antelope Island horst, East Antelope Island graben, and Farmington Bay horst. The East Antelope Island graben and Farmington Bay horst have been described elsewhere in detail by Cook and others (1966).

Along profile D-D', the basement configuration is strikingly asymmetrical. In particular, the Great Salt Lake graben is deepest toward Antelope Island where the maximum depth to bedrock is indicated as about 9,700 feet. It should be noted that although the maximum depth to bedrock within the Great Salt Lake graben is greater along profile D-D' than profile C-C', the deepest part of the southern Cenozoic basin lies south of profile D-D', where the Great Salt Lake graben joins the Tooele Valley graben (plate 2). Consequently the maximum thickness of the valley fill in the southern Cenozoic basin probably exceeds 9,700 feet.

Summary of profiles

The maximum depths to bedrock indicated within the various grabens along the four profiles A-A' through

D-D′ are summarized in table 1. Also in the table, a comparison between the maximum depth to bedrock indicated in this paper with depth estimates given by Cook and others (1966) shows good agreement. The discrepancy in the estimated depths to bedrock for the East Antelope Island graben can be explained partly because an assumed regional gravity trend is removed in this paper, whereas none was removed by Cook and others (1966).

Although the structures shown in the interpretive geologic cross sections are considered a reasonable interpretation, based on the available gravity and geologic control, they should not be considered a unique interpretation. An equally good fit of the computed and residual gravity could be obtained by assuming a larger number of step faults than those actually shown. Also, the angle of dip shown on the faults is subject to much uncertainty, but the values assigned are considered reasonable. For an assumed density contrast greater or less than the value of 0.5 gm/cc used, the interpreted locations of the inferred faults would not have changed appreciably. However, the total throw of the postulated faults would be correspondingly less or greater, respectively, and the maximum thickness of the Cenozoic valley fill in the central part of the grabens would be correspondingly less or greater, respectively, than that shown in the profiles.

A significant result of the interpretive geologic cross sections is that within the Great Salt Lake graben, the maximum thickness of the Cenozoic valley fill in the southern Cenozoic basin (indicated as about 9,700 feet on profile D-D′) is much greater than that in the northern Cenozoic basin (indicated as about 7,100 feet on profile B-B′).

COMPARISON OF RESULTS OF SEISMIC AND GRAVITY SURVEYS

During 1969, an extensive seismic reflection survey was made over the Great Salt Lake (Mikulich, 1971; Mikulich and Smith, 1974). The maximum depth of penetration of the Bolt air gun used for this survey was only 4,000 feet.

A comparison of the results of the seismic and gravity surveys shows that most of the faults that were indicated by the seismic data (not shown on plate 2) correspond well with the faults interpreted from the gravity data (shown on plate 2). In particular, the best correspondence is noted for the larger, elongate, north-south trending Basin and Range faults that delineate the east and west margins of the complexly faulted Great Salt Lake graben. Some of the individual step faults along fault zones marginal to the graben probably have vertical throws of 1,000 feet or more, and are indicated

Table 1. Summary of indicated maximum depths to bedrock along profiles.

Name of graben	Profile	Maximum depth to bedrock -- this paper (feet) [1]	Estimated depth to bedrock (Cook and others, 1966) (feet)[2]
Great Salt Lake (Northern basin)	A-A′	3,600	– –
Rozel	A-A′	3,900	>2,350
Strongknob	B-B′	6,400	>1,500
Great Salt Lake (Northern basin)	B-B′	7,100	– –
Bear River Bay	B-B′	5,800	>1,500
Lakeside-Stansbury	C-C′	3,500	>1,500
Great Salt Lake (Southern basin)	C-C′	7,600	– –
Lakeside-Stansbury	D-D′	7,000	>2,500
Great Salt Lake (Southern basin)	D-D′	9,700	– –
East Antelope Island	D-D′	8,100	6,100[3]
Tooele Valley	[4]	– –	12,000[4]

[1] Based on an assumed density contrast of 0.5 gm/cc between the bedrock and valley fill.

[2] Estimated from the Bouguer approximation and an assumed density contrast of 0.4 gm/cc or 0.5 gm/cc between the bedrock and valley fill – – unless otherwise noted.

[3] Value along profile B-B′, figure 4, Cook and others, 1966, p. 70. Based on an assumed density contrast of 0.5 gm/cc. Also depths to bedrock of 4,600 feet and 7,900 feet are indicated for assumed density contrasts of 0.6 gm/cc and 0.4 gm/cc, respectively.

[4] Value along profile A-A′, figure 3, Cook and others, 1966, p. 66. Based on an assumed density contrast of 0.4 gm/cc between the bedrock and valley fill.

by both gravity and seismic data at approximately the same locations. The faults that show good correspondence are in the following areas: 1) along the East Great Salt Lake fault zone west of Antelope Island (along profile D-D') and west of Promontory Point (along profile B-B') and 2) along the East Lakeside Mountains fault zone east of Lakeside (along profile B-B').

As expected, several faults interpreted from the seismic data were not indicated by the gravity data because the faults were in either Quaternary or Tertiary sediments with insufficient density contrast on either side of the fault. Also some faults interpreted from the seismic data were of insufficient vertical throw to be resolved in a regional-type bottom gravity survey.

SUMMARY AND CONCLUSIONS

The bottom gravity meter survey of the Great Salt Lake made possible the compilation of a simple Bouguer gravity anomaly map and interpretive geologic cross sections along four east-west gravity profiles across the lake that provided helpful information concerning the geologic structures beneath the lake. The large gravity low, that extends for a distance of about 70 miles, essentially the entire length of the lake, indicates a large north-northwestward trending graben beneath the lake. The closely spaced gravity contours, with steep gravity gradients, indicate that the graben is bounded on each side by large Basin and Range fault zones. On the northwestern side is the East Lakeside Mountains fault zone; on the southwestern side is the East Carrington-Stansbury Islands fault zone; and on the east side is the East Great Salt Lake fault zone. All fault names are newly designated. The large gravity low centers that lie north and south of the gravity saddle that extends between Bird (Hat) Island and the Promontory Point-Fremont Island area, indicate that at least two Cenozoic structural basins of deposition probably formed within the large graben between the Dolphin Island-Rozel Hills area and the Tooele Valley graben. The two basins are designated the "northern Cenozoic basin" and "southern Cenozoic basin" to the north and south, respectively, of the gravity saddle.

The geologic cross sections along the gravity profiles, based on a density contrast of 0.5 gm/cc between the bedrock and valley fill, indicate that the maximum thickness of the Cenozoic structural basins (valley fill) are 1) about 7,100 feet in the northern Cenozoic basin, along profile B-B' and 2) about 9,700 feet in the southern Cenozoic basin, along profile D-D'. An assumed larger or smaller density contrast would result in correspondingly smaller or larger thicknesses, respectively.

The new gravity data over the Great Salt Lake, used in conjunction with the previous gravity data over the adjoining mainland (Cook and others, 1966), afforded an interpretation of the continuity and interrelationships of the geologic structures. For example, the Great Salt Lake graben is continuous with the Tooele Valley graben. Also, an arm of the northern Cenozoic basin within the Great Salt Lake graben probably extends southward, with some constriction, between the Lakeside Mountains and Carrington Island to connect with the Cenozoic structural basin within the Lakeside-Stansbury graben.

ADDENDUM

Since the final draft of the simple Bouguer gravity anomaly map (Plate 2) and interpretive geologic cross sections along the four gravity profiles across the Great Salt Lake were completed (during April 1975), in preparation for oral presentation at scientific meetings during 1975 (Cook and others, 1975; Cook and others, 1976), the Amoco Production Company initiated a test drilling program of the Great Salt Lake during May, 1978. Nine drill holes were planned, five in the north arm of the lake and four in the south arm. The locations of the test holes were apparently based on the results of a deep reflection seismic survey started on July 25, 1973, by the Amoco Production Company.[1] This survey used a specially constructed barge 60 feet long, with a total of 14 air guns (7 air guns mounted on each side of the barge). The depth of penetration was at least 12,000 feet.

The locations of all 9 Amoco test holes, presently drilled or proposed, in the Great Salt Lake are shown on plate 2. Some of the test holes are projected into the appropriate nearest interpretive geologic cross sections along the gravity profiles. At the time of submittal of

[1] The information herein concerning the deep reflection seismic survey by the Amoco Production Company is based on notes taken by K. L. Cook during a joint lecture by Craig Hansen and Charles (Bud) Ervin, geophysicists of the Amoco Production Company, Denver, Colorado. The lecture was presented on December 3, 1974, as part of a Great Salt Lake Seminar conducted at the University of Utah, under the supervision of Professor James A. Whelan, Department of Geology and Geophysics.

Table 2. Amoco Production Company, State of Utah drilled or proposed well locations in Great Salt Lake (Source - Utah Geological and Mineral Survey, August 1979 and Survey Notes, August 1979).

Well Designation	Section, Township, Range	Latitude N[8] deg	min	Longitude W[8] deg	min	Total Depth (TD) (feet) and Status[1]	Lithology at TD
NORTH BASIN							
J-1 (South Rozel)	C-NE-SW Sec. 21-8N-7W	41°	24.36′	112°	39.24′	6,802 (D)	Paleozoic carbonates[4]
K-1 (North Gunnison)	C-NE-SE Sec. 11-8N-9W	41°	26.04′	112°	49.21′	4,492 (D)	Paleozoic carbonates
D-1 (West Rozel)	C-NW-SW Sec. 23-8N-8W	41°	24.36′	112°	44.04′	8,503 (T)	[2]
Indian Cove No. 1 (IC-1 on plate 2)	C-SW-SE Sec. 23-7N-7W	41°	19.06′	112°	36.59′	12,470 (D)	Precambrian schist[5]
West Rozel No. 2 (WR-2 on plate 2)	S-NW-SW Sec. 15- 8N-8W	41°	25.25′	112°	45.18′	2,700 (approx.) (T)	Rozel Point basalt[3]
SOUTH BASIN[6] E-1	C-NW-SW Sec. 19-3N-4W	40°	58.56′	112°	21.09′	Proposed to 12,000[7]	– –
F-1	C-NW-SW Sec. 15-3N-5W	40°	59.42′	112°	24.59′	Proposed	– –
G-1	C-SE-NW Sec. 29-3N-5W	40°	57.97′	112°	26.66′	Proposed	– –
H-1	C-NW-SW Sec. 11-3N-6W	41°	00.28′	112°	30.36′	Proposed	– –

[1] (T) = Temporarily abandoned.
(D) = Dry and abandoned.
Source – Survey Notes, August 1979.

[2] Paleozoic carbonates at about 6,325 feet. Tested heavy oil from basalt at 2,300 feet depth. (Survey Notes, August 1979).

[3] Pump tests recovered 8,000 barrels of heavy oil at rates as high as 1,500 barrels per day from 2,300 feet to total depth. (Survey Notes, August 1979).

[4] Paleozoic carbonates at 6,000 feet (Survey Notes, August 1979).

[5] No Paleozoic rocks penetrated. Precambrian at 12,450 feet (Survey Notes, August 1979).

[6] Drilling operations are scheduled to begin in late summer of 1979 (Survey Notes, August 1979).

[7] Survey Notes, August 1979.

[8] Coordinates of latitude and longitude of the wells were determined from a map (on which the well locations had been determined from the citation by section, township, and range) kindly furnished by Howard R. Ritzma, Utah Geological and Mineral Survey.

this paper for publication (August, 1979), the five test holes on the north arm of the lake had been completed, and the first test hole on the south arm of the lake was still in preparation to be drilled. No well logs were available because, under the terms of the state of Utah land leases to the Amoco Production Company, these data are to be considered proprietary until 7 months following the completion of each well.

Table 2 gives 1) the names and locations (both by section, township, and range and also by latitude and longitude) of all 9 Amoco test holes in the Great Salt Lake (both those already drilled and those proposed); 2) the total depth of each test hole drilled to date (August 1979); and 3) miscellaneous lithologic information that has been released by the Amoco Production Company.

It should be emphasized that in projecting the Amoco test holes into the appropriate nearest geologic cross sections along the gravity profiles, the projection was made along the trend of the gravity contours (plate 2), and hence along the indicated trend of the geologic

structure (i.e., Basin and Range fault zones). Because the distances of the projections were necessarily large for the two profiles (A-A′ and B-B′) along which the Amoco test holes have been completed, and especially because the complete well logs are not yet available, any comparison between the available drilling data and the indicated maximum depth to bedrock, as shown on the profiles, is of limited value.

For example, test hole K-1, which is projected onto profile A-A′ (figure 4), actually lies about 3 miles south-southeast of profile A-A′ at a point within the north Cenozoic basin where the lower gravity values indicate a somewhat larger thickness of valley fill than along profile A-A′. Similarly, test hole IC-1, which is projected onto profile B-B′, (figure 5), lies about 7 miles north-northwest of profile B-B′; but here a comparison is more difficult. In particular, it is reported (Survey Notes, August 1979) that in test hole IC-1 (1) no Paleozoic rocks were penetrated and (2) Precambrian rocks were penetrated at a depth of 12,450 feet.

These early drilling results indicate that the maximum depth to bedrock shown along profile B-B′ (figure 5) is probably too small and that therefore the assumed average density contrast of 0.5 gm/cc between the bedrock and valley fill is probably too large for the northern Cenozoic basin. This indication has been corroborated by the measurement of the density of a dense gray siltstone core sample from Amoco test hole IC-1 (the one projected into profile B-B′, figure 5) from a depth of approximately 5,500 feet. The density was 2.54 gm/cc (J. W. Gwynn, Utah Geological and Mineral Survey, August 14, 1979, personal communication).

ACKNOWLEDGMENTS

Appreciation is expressed to Colonel David B. Conard, formerly Commanding Officer, Army Map Service, Corps of Engineers, Department of the Army, Washington, D. C., and William P. Hewitt, former Director, Utah Geological and Mineralogical Survey, Salt Lake City, Utah, for their original authorization of the bottom gravity meter survey. The work was done during 1968 as a cooperative project between the two organizations. Encouragement to publish the results of the survey has been given by Dr. S. H. Ward, Chairman, Department of Geology and Geophysics, University of Utah and Dr. L. H. Lattman, Dean, College of Mines and Mineral Industries, University of Utah.

The U. S. Army Map Service personnel, who performed the bottom gravity meter survey, consisted of: 1) Supervisor - R. M. Iverson; 2) Party Chiefs and bottom gravity meter instrument operators - Lawrence Hunt, during the early part of the survey and M. T. Strohmeier, during the latter part of the survey; 3) Electronic Technician (for repairs and maintenance of gravity meter) - Glen Cobb, 4) Tellurometer operators - Lewis Phillips, in charge, assited by Ronald Creel, James D. Hutchison, Carl Kaywood, and Don Zeal.

The *G. K. Gilbert* was operated for the Utah Geological and Mineralogical Survey by Leonard Hedberg, captain, and Dave Sekino, first mate.

Robert H. Brown, a graduate student in Geophysics at the University of Utah, made the gravity ties between the Salt Lake City airport base station K and the Little Valley and Silver Sands base stations.

The gravity data were reduced under the immediate supervision of Robert Ziegler, Gravity Division, Army Map Service, Corps of Engineers, Department of the Army, Washington, D. C.

Appreciation is expressed to the Gravity Division, Army Map Service, Corps of Engineers, Department of the Army, Washington, D. C., for the loan of LaCoste and Romberg land gravity meter No. 123, which was used to make the ties of the various gravity base stations on land.

Leonard Hedberg and J. A. Whelan provided density values of the waters of the Great Salt Lake given in Appendix 3.

Financial support for the compilation and interpretation of the gravity map and profiles and the preparation of the paper for publication was given by 1) the National Science Foundation under Research Grants GA-30182 and DE71-00422-AO2, 2) the Mineral Leasing Funds, College of Mines and Mineral Industries, University of Utah, and 3) the Utah Geological and Mineral Survey.

REFERENCES

Cook, K. L., 1969, Active rift system in the Basin and Range province: Tectonophysics, v. 8, p. 469-511.

Cook, K. L., and J. W. Berg, Jr., 1961, Regional gravity survey along the central and southern Wasatch front, Utah: U.S. Geological Survey Professional Paper 316-E, p. 75-89.

Cook, K. L., J. W. Berg, Jr., W. W. Johnson, and R. T. Novotny, 1966, Some Cenozoic structural basins in the Great Salt Lake

area, Utah, indicated by regional gravity surveys: *in* The Great Salt Lake, Guidebook to the Geology of Utah, no. 20, W. L. Stokes, Editor, Utah Geological Society, Salt Lake City, Utah, p. 57-75.

Cook, K. L., J. W. Berg, Jr., and Daniel Lum, 1967, Seismic and gravity profile across the northern Wasatch trench: *in* Refraction Seismic Prospecting, edited by A. W. Musgrave, Society of Exploration Geophysicists, Tulsa, Oklahoma, p. 539-549.

Cook, K. L., R. M. Iverson, and M. T. Strohmeier, 1969, Bottom gravity meter survey of the Great Salt Lake, Utah (abstract): EOS, American Geophysical Union Transactions, v. 50, p. 321. Abstract also published in Abstracts with Program, Part 5, Rocky Mountain Section, 22nd Annual Meeting, Geological Society of America, Salt Lake City, Utah, May 7-11, p. 16.

Cook, K. L., R. M. Iverson, M. T. Strohmeier, and E. F. Gray, 1975, Interpretive geologic cross sections along gravity profiles across the Great Salt Lake, Utah (abstract): Abstracts with Programs, v. 7, no. 5, March 1975, 28th Annual Meeting, Rocky Mountain Section, Geological Society of America, Boise, Idaho, May 3-6, 1975, p. 597-598.

Cook, K. L., R. M. Iverson, R. T. Strohmeier, and E. F. Gray, 1976, Interpretive geologic cross sections along gravity profiles across the Great Salt Lake (abstract): Geophysics. v. 41, no. 2, p. 346.

Cook, K. L., T. H. Nilsen, and J. F. Lambert, 1971, Gravity base station network in Utah – 1967: Utah Geological and Mineralogical Survey Bulletin 92, 57 p.

Duerksen, J. A., 1949, Pendulum gravity data in the United States: U. S. Coast and Geodetic Survey Special Publication 244, 218 p.

McDonald, R. E., 1976, Tertiary tectonics and sedimentary rocks along the transition, Basin and Range provinces to Plateau and Thrust Belt province, Utah: *in* Symposium on Geology of the Cordilleran Hingeline, Rocky Mountain Association of Geologists, J. G. Hill, editor, Denver, Colorado, p. 281-317.

Mikulich, M. J., 1971, Seismic reflection and aeromagnetic surveys of the Great Salt Lake, Utah: Ph.D. dissertation, University of Utah, 108 p.

Mikulich, M. J., and R. B. Smith, 1974, Seismic reflection and aeromagnetic surveys of the Great Salt Lake, Utah: Geological Society of America Bulletin, v. 85. p. 991-1002.

Rocky Mountain Region Report, 1979, Southern Rockies, v. 52, no. 126, June 28, 1979. published by Petroleum Information Corporation, Denver, Colorado.

Stokes, W. L., 1963, Geologic map of northwestern Utah: College of Mines and Mineral Industries, University of Utah.

Survey Notes, 1979, Utah Geological and Mineral Survey, August, 1979.

Talwani, Manik, L. J. Worzel, and Mark Landisman, 1959, Rapid gravity computations for two-dimensional bodies with applications to the Mendocino submarine fracture zone: Journal of Geophysical Research, v. 64, p. 49-59.

APPENDIX 1

DESCRIPTION OF GRAVITY BASE STATIONS

1 Little Valley Gravity Base Station

The station is located on U. S. government benchmark "BM 4205" on the land surface at Little Valley

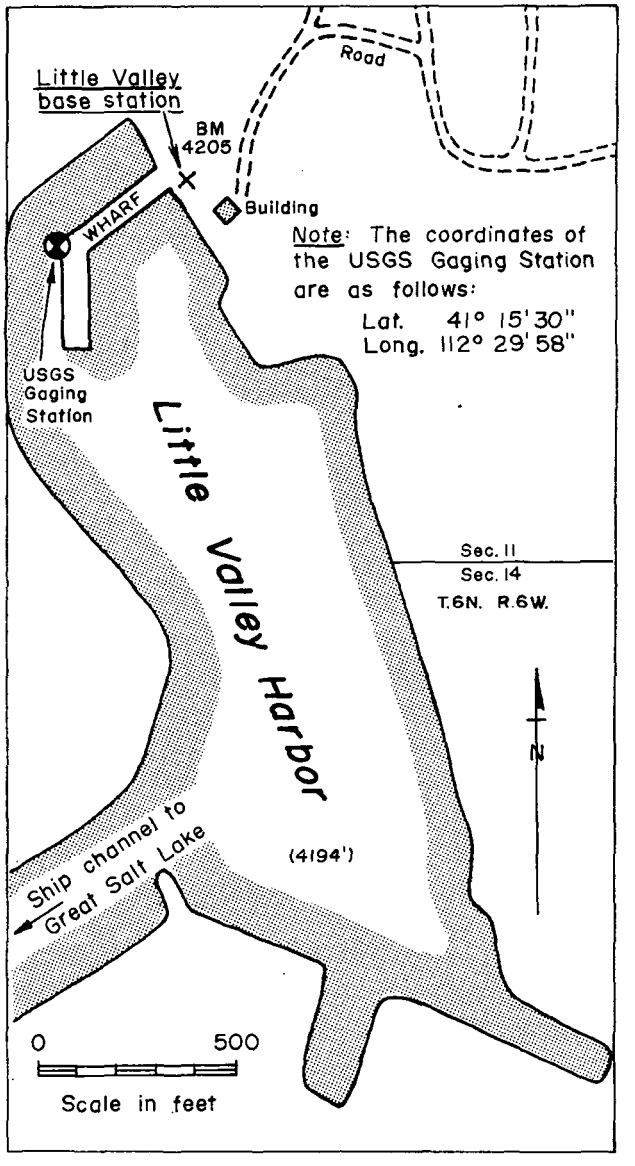

Figure 8. Sketch map showing location of Little Valley gravity base station.

Harbor northwest of Promontory Point (figure 8). The benchmark is shown on 1) the U. S. Geological Survey 7-1/2 minute topographic quadrangle map "Pokes Point, Utah" and 2) the map entitled "Great Salt Lake and Vicinity, Utah" published in 1974 jointly by the U. S. Geological Survey and the Utah Geological and Mineral Survey. The coordinates of the station are: lat 41°15.53′ N and long 112°29.90′ W.

2. Silver Sands Gravity Base Station

The station is located at Silver Sands Beach near the southwest end of the 60-foot-wide breakwater that forms the County Boat Harbor about 0.12 mile (0.2 km) southwest of U. S. government benchmark "BM 4209" that is shown on the 1) Garfield, Utah (1952) 7-1/2 minute topographic quadrangle map of the U. S. Geological Survey and 2) the map entitled "Great Salt Lake and Vicinity, Utah," published in 1974 jointly by the U. S. Geological Survey and the Utah Geological and Mineral Survey. The station is located on top of a sand bar that lies immediately southeast of the breakwater about 120 feet northeast of the southwest end of the breakwater (figure 9). The elevation of the top of the sand bar is about 5 feet below that of the top of the breakwater and was about 2 feet above the level of the south arm of the Great Salt Lake on July 28, 1968 during the time of the gravity survey. The station, which was marked in 1968 by a metal stake driven onto the sand bar, is 15 feet southeast of the bottom of the breakwater and 30 feet northeast of the northeast side of the boathouse which in 1968 contained the water-level marker for the Great Salt Lake in this area. The coordinates of the station are: latitude 40° 44.11′ N and longitude 112° 12.81′ W.

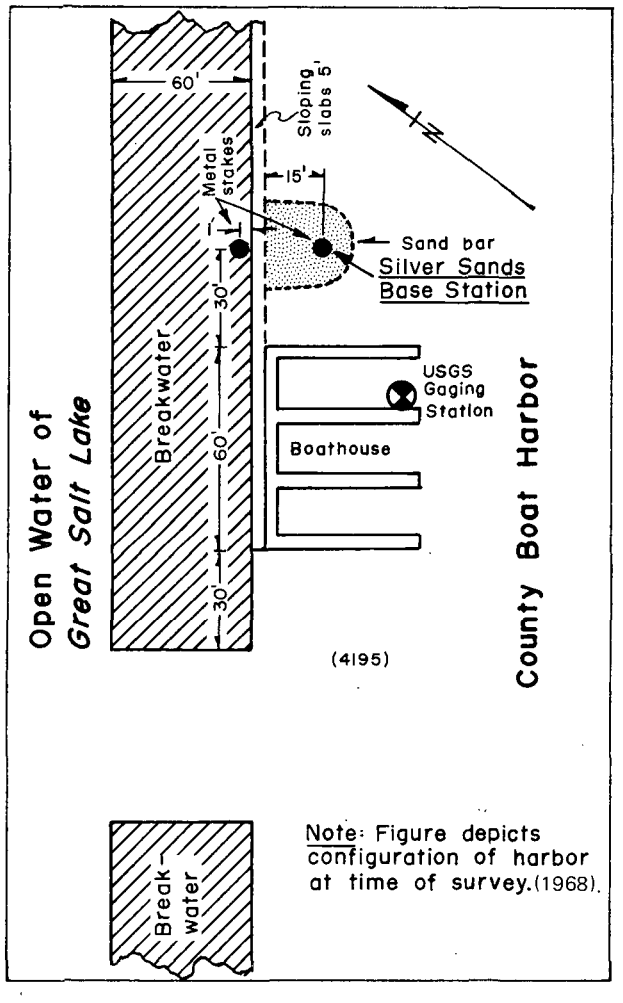

Figure 9. Sketch map showing location of Silver Sands gravity base station.

APPENDIX 2

Elevations of the Great Salt Lake during the gravity survey (data supplied by Leonard Hedberg, Utah Geological and Mineralogical Survey, August 1968).

Elevation of Great Salt Lake –South Arm (Boat Harbor Gage) For Period July 1-27, 1968

Date	Elevation (Ft.) Above MSL
July 1	4,195.48
2	4,195.45
3	4,195.45
4	4,195.40
5	4,195.40
6	4,195.40
7	4,195.38
8	4,195.38
9	4,195.38
10	4,195.35
11	4,195.33
12	4,195.33
13	4,195.33
14	4,195.28
15	4,195.25
16	4,195.25
17	4,195.28
18	4,195.22
19	4,195.18
20	4,195.18
21	4,195.13
22	4,195.05
23	4,195.05

24	4,195.05
25	4,195.05
26	4,195.03
27	4,195.00

Considerable storm activity occurred during July 22-23.

Maximum elevation:	4,195.42
Minimum elevation:	4,194.05

Elevation of Great Salt Lake – – North Arm (Saline Gage) For Period July 28-August 9, 1968

July 28	4,194.30
29	4,194.28
30	4,194.30
31	4,194.30
Aug. 1	4,194.25
2	4,194.23
3	4,194.23
4	4,194.20
5	4,194.20
6	4,194.15
7	4,194.15
8	4,194.15
9	4,194.13

Large storm occurred on August 3, from about 6:00 p.m., until midnight.

Maximum elevation	4,195.25
Minimum elevation:	4,193.32

APPENDIX 3

Data on density of waters of the Great Salt Lake during the summer of 1968 (data supplied by James A. Whelan, Department of Geological and Geophysical Sciences, University of Utah, and Leonard Hedberg, Utah Geological and Mineral Survey, September 1968).

North Arm

Density varies from 1.21 to 1.23 gm/cc.
Average density is 1.22 gm/cc.

South Arm

Density of water from surface of lake to a depth of 20 feet is 1.14 gm/cc.
Density of water layer between this depth (20 feet) and bottom of the lake is 1.21 gm/cc.

APPENDIX 4

Principal facts of gravity stations for the bottom gravity meter survey of the Great Salt Lake (as compiled by the U. S. Army Map Service during December 1968) are shown on table 3.

EXPLANATION

The listing contains consecutively, from left to right:
Station name.
Station number.
Latitude, in degrees and minutes.
Longitude, in degrees and minutes.
Elevation of Great Salt Lake, in meters, when station was taken.
Depth to bottom of lake, in meters, at location of station.
Observed gravity, in milligals.
Free-air gravity anomaly value, in milligals.
Simple Bouguer gravity anomaly value, in milligals (using, for the Bouguer correction, an average density of 1.22 gm/cc for the lake water and 2.67 gm/cc for the material between the lake bottom and mean sea level).
Theoretical gravity at mean sea level, using the International Gravity Formula, in milligals.

Notes: The observed gravity value at Salt Lake City airport base station K was taken as 979,815.444 mgal (Cook and others, 1971). Using this value, the ties to the Little Valley and Silver Sands gravity base stations, which were made with the LaCoste and Romberg land gravity meter No. 123, resulted in observed gravity values of 979,906.540 mgal and 979,825.407 mgal, respectively, for these base stations. It should be noted that the arbitrary (and incorrect) values given in the listing for the latitudes and longitudes of these two base stations only do not affect the accuracy of the values of the observed gravity of these base stations.

The simple Bouguer gravity anomaly values used in contouring the map shown on plate 2 over the Great Salt Lake itself (i.e., for the bottom gravity meter stations only) were obtained by adding algebraically 4.36 mgal to the simple Bouguer gravity anomaly values shown in the listing. This adjustment was made so that the gravity contours over the Great Salt Lake would fit smoothly with the simple Bouguer gravity anomaly contours (obtained from the land gravity meter surveys) over the land adjacent to the lake published by Cook and others (1966). For these land gravity meter surveys (Cook and others, 1966, p. 59), the reference for observed absolute gravity was the U. S. Coast and Geodetic Survey pendulum station No. 49, in the Temple Grounds in Salt Lake City, for which the absolute gravity value was accepted as 979,806 mgal (Duerksen, 1949, p. 8).

PRINCIPAL FACTS AT GRAVITY STATIONS

STA NAME AND NUM	LATITUDE NORTH +	LONGITUDE EAST +	ELEVATION METERS	SUPP ELEV METERS	OBSERVED G MGAL	FREE AIR MGAL	BOUGUER MGAL	THEOR G MGAL
SILVER SANDS 3000	40 60.00	-111 60.00	1278.715	1.524	979826.260	-49.173	-192.156	980269.574
N-1 1	40 44.96	-112 23.38	1278.715	1.067	979826.017	-26.895	-169.910	980247.194
P-1 2	40 42.36	-112 22.07	1278.715	2.134	979803.983	-45.393	-188.335	980243.328
N-2 3	40 45.69	-112 15.10	1278.715	7.010	979815.710	-40.122	-182.727	980248.281
M-1 4	40 49.60	-112 26.00	1278.715	2.591	979840.408	-19.877	-162.786	980254.096
M-2 5	40 49.80	-112 24.40	1278.715	4.724	979832.444	-28.796	-171.559	980254.394
M-3 6	40 49.70	-112 23.30	1278.715	6.096	979830.194	-31.321	-173.989	980254.245
M-4 7	40 49.70	-112 21.60	1278.715	6.248	979828.221	-33.341	-175.998	980254.245
M-5 8	40 49.80	-112 20.00	1278.715	7.010	979826.163	-35.784	-178.389	980254.394
M-6 9	40 49.70	-112 18.80	1278.715	7.772	979824.890	-37.142	-179.695	980254.245
L3 10	40 53.66	-112 18.73	1278.724	7.925	979838.544	-29.425	-171.968	980260.137
L2 11	40 53.72	-112 21.92	1278.724	7.772	979827.201	-40.810	-183.364	980260.226
L1 12	40 54.54	-112 23.31	1278.724	5.639	979841.303	-27.269	-169.970	980261.447
SILVER SAND 4000	40 60.00	-111 60.00	1278.724	3.048	979825.407	-50.493	-193.373	980269.574
SS2 HBR LND 20000	40 60.00	-111 60.00	1278.678	.000	979825.596	-49.379	-192.463	980269.574
K-1 13	40 57.37	-112 31.87	1278.654	1.829	979865.762	-5.668	-148.824	980265.660
K-2 14	40 57.88	-112 27.27	1278.654	6.248	979845.349	-28.405	-171.056	980266.418
K-3 15	40 58.19	-112 23.43	1278.654	8.077	979842.448	-32.331	-174.856	980266.880
J-5 16	41 .86	-112 21.52	1278.654	7.925	979852.737	-25.971	-168.507	980270.855
K-4 17	40 57.63	-112 29.83	1278.654	4.724	979855.371	-17.540	-160.296	980266.047
K-5 18	40 58.24	-112 24.39	1278.654	7.772	979841.432	-33.328	-175.874	980266.955
K-6 19	40 58.66	-112 19.26	1278.654	7.772	979851.332	-24.053	-166.599	980267.579
J-4 20	41 2.02	-112 26.55	1278.654	8.077	979848.140	-32.343	-174.868	980272.582
I-12 21	41 7.80	-112 18.30	1278.654	1.676	979894.963	7.846	-135.120	980281.193
I-11 22	41 7.40	-112 20.70	1278.654	4.724	979886.563	-.899	-143.655	980280.597
I-10 23	41 7.20	-112 22.50	1278.654	6.096	979878.225	-9.362	-152.024	980280.298
I-5 24	41 5.40	-112 35.10	1278.654	2.286	979886.642	2.912	-140.012	980277.617
H-4 25	41 11.60	-112 29.00	1278.648	1.981	979885.738	-7.138	-150.082	980286.856
H-3 26	41 11.40	-112 32.80	1278.648	7.468	979870.846	-23.425	-165.991	980286.557
H-2 27	41 11.60	-112 37.60	1278.648	8.687	979866.515	-28.431	-170.913	980286.856
H-1 28	41 11.60	-112 43.30	1278.639	6.858	979878.335	-16.049	-158.656	980286.856
H-1A 29	41 11.60	-112 47.70	1278.639	1.524	979896.121	3.383	-139.592	980286.856
I-3 30	41 6.10	-112 37.60	1278.639	1.676	979878.929	-5.660	-148.624	980278.660
I-4 31	41 8.10	-112 41.50	1278.639	7.163	979864.605	-24.658	-167.244	980281.640
J-2 32	41 3.90	-112 41.50	1278.639	5.334	979863.455	-18.986	-161.698	980275.383
I-6 33	41 5.90	-112 33.10	1278.639	3.505	979882.202	-2.654	-145.492	980278.362
I-7 34	41 6.00	-112 31.10	1278.639	6.096	979874.893	-10.912	-153.572	980278.511
I-8 35	41 6.00	-112 29.30	1278.639	7.010	979866.236	-19.849	-162.446	980278.511
I-9 36	41 6.10	-112 27.20	1278.639	8.230	979860.136	-26.475	-168.988	980278.660
J-3 37	41 3.50	-112 31.00	1278.639	2.591	979870.939	-10.059	-152.961	980274.788
LITTLE VALLY 50000	40 60.00	-111 60.00	1278.407	.000	979906.540	31.481	-111.573	980269.574
F1 38	41 20.33	-112 50.48	1278.395	1.097	979914.838	9.141	-133.836	980299.871
F2 39	41 19.73	-112 43.72	1278.395	8.534	979887.035	-20.063	-162.528	980298.976
F3 40	41 20.34	-112 39.03	1278.395	7.468	979881.515	-26.163	-168.701	980299.886
F4 41	41 20.09	-112 31.05	1278.395	4.877	979904.792	-1.713	-144.430	980299.513
G-1 42	41 14.11	-112 32.42	1278.395	1.219	979882.121	-14.339	-157.308	980290.597
G-2 43	41 14.93	-112 34.84	1278.395	7.620	979876.434	-23.224	-165.751	980291.819
G-3 44	41 14.97	-112 37.76	1278.395	8.230	979873.605	-26.301	-168.787	980291.679
G-4 45	41 15.14	-112 40.29	1278.395	8.230	979873.207	-26.952	-169.438	980292.132
G-5 46	41 15.40	-112 43.21	1278.395	8.839	979877.052	-23.683	-166.126	980292.520
G-6 47	41 15.54	-112 45.75	1278.395	6.096	979885.210	-14.887	-157.520	980292.729
G-7 48	41 15.63	-112 47.89	1278.395	3.048	979899.812	.523	-142.320	980292.863
E-1 49	41 24.61	-112 39.38	1278.380	3.353	979894.952	-17.831	-160.651	980306.257
E-6 50	41 26.26	-112 48.08	1278.380	4.267	979906.066	-9.461	-152.218	980308.717
E-7 51	41 26.23	-112 49.43	1278.380	3.658	979908.345	-6.948	-149.747	980308.674
E-2 52	41 24.74	-112 41.41	1278.380	5.486	979895.049	-18.586	-161.259	980306.450
E-3 53	41 24.80	-112 43.03	1278.380	6.706	979896.747	-17.353	-159.942	980306.540
E-4 54	41 25.01	-112 44.94	1278.380	5.639	979900.797	-13.287	-155.950	980306.853
E-5 55	41 25.29	-112 47.41	1278.380	4.724	979902.967	-11.253	-153.979	980307.270
E-8 56	41 25.00	-112 53.12	1278.380	2.286	979914.325	1.289	-141.604	980306.837
D-1 57	41 28.41	-112 45.93	1278.380	5.029	979905.697	-13.273	-155.977	980311.926
D-2 58	41 28.58	-112 51.77	1278.380	4.877	979905.798	-13.378	-156.093	980312.180
D-3 59	41 28.61	-112 55.86	1278.380	1.829	979904.732	-13.549	-156.474	980312.224
C-1 60	41 33.71	-112 52.32	1278.380	2.743	979916.163	-10.013	-152.875	980319.837
C-2 61	41 33.80	-112 50.16	1278.380	2.896	979916.963	-9.394	-152.245	980319.971
B-1 62	41 39.01	-112 48.72	1278.380	.914	979920.761	-12.764	-155.752	980327.751
D-4 63	41 28.41	-112 54.04	1278.374	2.743	979907.162	-11.104	-153.965	980311.926
D-5 64	41 28.62	-112 50.99	1278.374	3.962	979905.441	-13.514	-156.291	980312.239

TECTONICS, VOL. 10, NO. 2, PAGES 345-365, APRIL 1991

CENOZOIC EXTENSION AND EVOLUTION OF THE SEVIER DESERT BASIN, UTAH, FROM SEISMIC REFLECTION, GRAVITY, AND WELL LOG DATA

Sverre Planke[1] and Robert B. Smith

Department of Geology and Geophysics, University of Utah, Salt Lake City

Abstract. Seismic reflection profiles (~550 km), gravity data, and well log information from west central Utah, have been interpreted to reveal an asymmetric west-dipping Cenozoic basin beneath the Sevier Desert. The basin is underlain by a 10°-12° westward dipping, slightly undulatory, detachment surface, the Sevier Desert detachment. Finite difference synthetic seismograms were used to constrain the geometry of the interpreted reflectors in the basin. A two-dimensional, one-layer gravity inversion of three gravity profiles in the basin, using a 0.35 g/cm^3 density contrast, corroborated the structure determined from the seismic interpretations. Physical properties and lithological data from eight wells were interpreted to acquire velocity-depth and density-depth functions and to obtain stratigraphic control. A minimum width of the Sevier Desert detachment of 80 km to 130 km and an area of 5600 km^2 to 9100 km^2 was estimated primarily from the reflection data. On the basis of geological and geometrical information, we estimated a minimum post-middle Pliocene extension of 2.5 km to 3.5 km at a rate of 0.6 mm/yr to 0.8 mm/yr, corresponding to a strain rate of 2.7 10^{-16} s^{-1} to 3.5 10^{-16} s^{-1}. Up to 4.0 ± 0.6 km of predominantly post Eocene lacustrine and fluvial sediments overlie the Sevier Desert detachment including a well-defined reflection that is interpreted as a middle Pliocene 4.2 m.y. basaltic flow that is present throughout the central and western part of the basin. The geometry of the middle Pliocene reflector, a variable ~300 to ~1500 m post-middle Pliocene offset of a ~40° eastward dipping western basin-bounding fault, and up to ~6 km east and west stepping of the generally north-trending western basin-bounding fault, suggests a complex late Tertiary deformational history. The varying deformational pattern may be a response to a changing geometry of the underlying detachment surface.

[1]Now at Institute for Geology, University of Oslo, Norway.

Paper number 90TC01948.
0278-7407/91/90TC-01948$10.00

INTRODUCTION

The Sevier Desert, located in west central Utah, Basin and Range province, is here defined to be the region bounded by the Pavant and Canyon ranges on the east, the Cricket Mountains in the west, the Sheeprock Mountains in the north, and the Twin Peaks in the south (Figure 1). The Sevier Desert region has undergone post-middle Oligocene extension, with the development of an asymmetric, up to 4.0 ± 0.6 km deep, westward deepening basin below the Sevier Desert. A 10°-12° west dipping detachment surface, the Sevier Desert detachment (SDD), extends beneath the basin and separates the Cenozoic basin fill from the Paleozoic and Precambrian sedimentary basement formations. A ~40° eastward dipping fault is truncated at the SDD in the western part of the basin, and it is interpreted to be the boundary between Paleozoic and early Tertiary formations to the west and Oligocene to Quaternary basin fill to the east. This fault is referred to as "the western basin-bounding fault" in this paper. The SDD was initially described by McDonald [1976] on the basis of oil industry seismic reflection profiles. It was later traced 70 km to the west, to about 12-15 km depth, on deep crustal reflection profiles [Allmendinger et al., 1983; Smith and Bruhn, 1984].

The Sevier Desert basin is located just west of the Basin and Range-Colorado Plateau boundary and the crustal structure is representative of this transitional margin. Crustal refraction surveys show that the south central Utah has an anomalous crustal P wave velocity structure, with a low-velocity layer at 8-13 km depth, a ~7.4 km/s refraction velocity at ~20 km depth, and a ~7.9 km/s refraction velocity at ~40 km depth [Pechmann et al., 1985; Smith et al., 1989]. In addition, high regional heat flow, ~90 m W m^{-2}, and subdued topography since the Quaternary, Lake Bonneville are characteristic of the region.

The oldest exposed rocks in the Sevier Desert region are Precambrian metamorphosed clastic sediments that are exposed in the Canyon Range, the Sheeprock Mountains, and the San Francisco Mountains (Figure 1). Paleozoic shallow water clastic and carbonate marine shelf sequences generally overlie a basal, transgressive early Cambrian sandstone unit. This unit is overlain by thick Cambrian to Triassic carbonates interbedded with less shale and sandstone [Hintze, 1988]. Continental Mesozoic strata in the region include

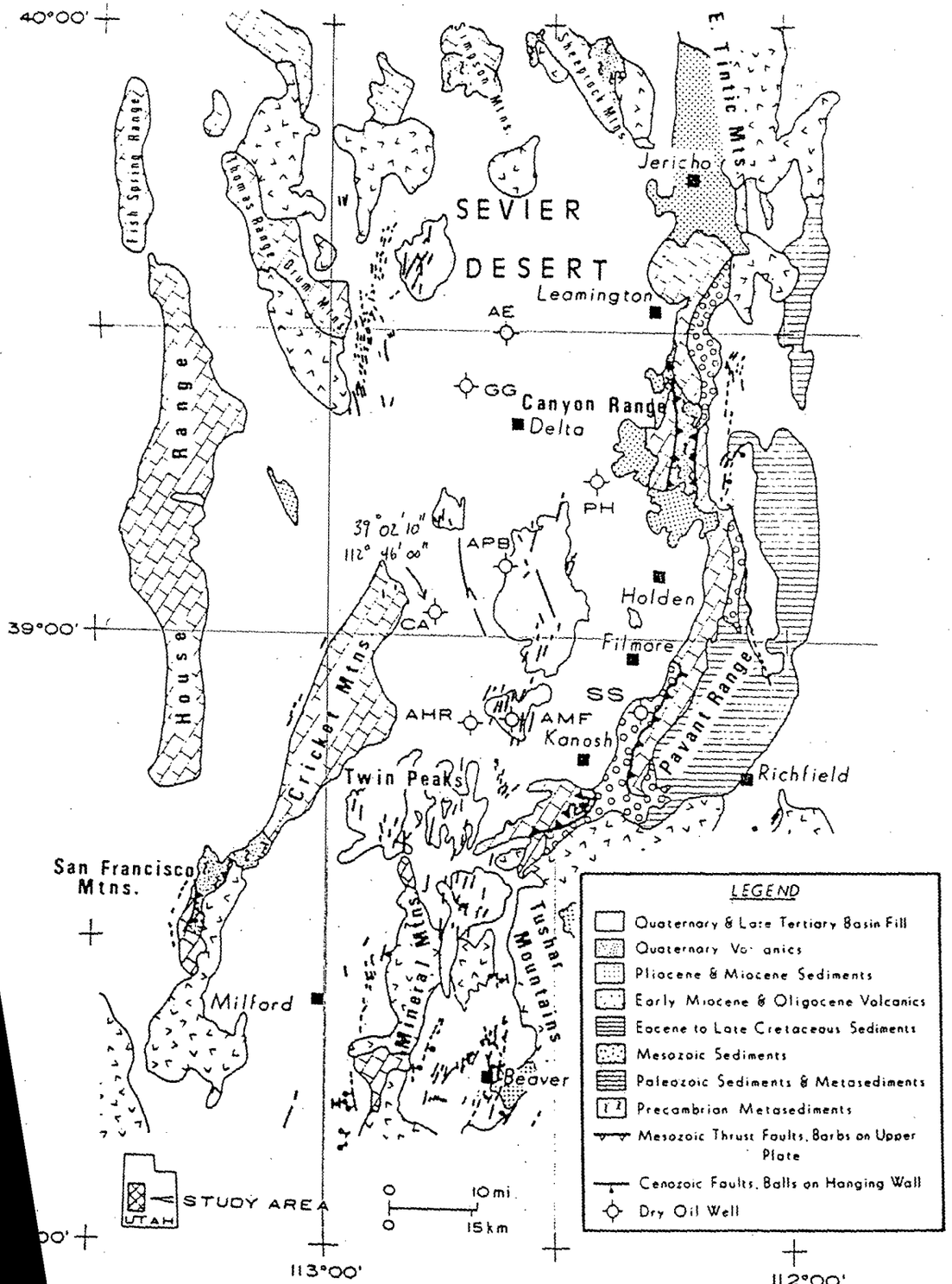

Fig. 1. Geologic base map of the Sevier Desert region, south central Utah. Geology from Hintze (1980). Cenozoic fault scarps from Bucknam and Anderson (1979) and Anderson and Bucknam (1979). Abbreviations are AE, Argonaut Energy 1; AHR, ARCO Hole in the Rock 1; AMF, ARCO Meadow Federal 1; APB, ARCO Pavant Butte 1; CA, Cominco American Inc. 2 Beaver River; GG, Gulf Oil Gronnig 1; PH, Placid Oil Henley 1; SS, and Shell Oil Sunset Canyon 1.

CA well located at 39° 02' 10" N, 112° 46' 00" W } = Utm: 347090.04 E, 4322060.83 N State Plane: 1640192.29 E, 2585253 N

↳ Plots very close to Neels

Near CA well:
• Seis. refl. profile MC3 (W-NE)
5 (W-E)
B (W-E)

Moenkopi and Chinle formations, the Triassic-Jurassic Navajo sandstone, Jurassic evaporites in the Arapien shale, and Cretaceous and early Tertiary lacustrine, fluvial, and alluvial formations. The eastward extension of these Mesozoic formations below the Sevier Desert has not been determined due to erosion associated with late Mesozoic uplift, Mesozoic overthrusting, and Cenozoic extension [Hintze, 1973].

The tectonic history of the Sevier Desert area has been influenced by the tectonic events associated with the Phanerozoic western margin of the North American plate. The main tectonic phases were (1) late Precambrian rifting with the development of a passive continental margin until the end of Devonian [Hintze, 1973; Picha and Gibson, 1983; Allmendinger et al., 1986]; (2) development of a late Jurassic to Eocene "Andean type" convergent margin, associated with the Laramide-Sevier foreland fold and thrust belt developed in central Utah [Hintze, 1973; Hamilton, 1978; Coney et al., 1980]; and (3) post-middle Tertiary change to Basin-Range extension [Hamilton, 1978; Coney et al., 1980; Eaton, 1982]. The spatial correlation of the eastern termination of the lower Paleozoic formations, the eastern termination of the Sevier orogenic foreland fold and thrust belt, and the Basin and Range to Colorado Plateau transition is noteworthy and, likely not coincidental [Hintze, 1973; Smith and Sbar, 1974]. It may have been related to a zone of crustal weakness due to thermal weakening and sedimentary loading at the western edge of the North American craton.

The main extensional phase of the Great Basin was initiated in Oligocene and lower Miocene, but extensional events earlier in the Tertiary have also been noted [Davis, 1979; Zoback et al., 1981, p. 198; Von Tish et al., 1985]. One style of deformation, dominated by low-angle faults and average deformation rates of 0.43 to 1.9 mm/yr, has been interpreted from deep seismic reflection data in the Sevier Desert region [Von Tish et al., 1985], while Zoback et al. [1981] suggested two modes of extension in the Basin and Range province, where the change in deformational mode correlates with a ~45° clockwise rotation of the Basin and Range stress field about 10 m.y. ago.

Three major Cretaceous thrust systems have been mapped in the Sevier Desert region (Figure 1): the Canyon Range thrust (structurally highest), the Pavant Range thrust, and the "sub-Pavant Range" thrust (structurally lowest). These thrusts are generally controlled by the local stratigraphy. Eocambrian, Cambrian, Mississippian, and middle Jurassic shales are considered as possible glide planes in western Utah [Armstrong, 1968]. The SDD was initially interpreted as a reactivated thrust [McDonald, 1976; Mitchell and McDonald, 1986], but Wernicke [1981] and Wernicke et al. [1985] interpreted the fault as a crustal penetrating, primarily normal fault, analogous to the early stages of development of detachment faults in the Cordilleran metamorphic core complexes. Based on hanging wall truncations and palinspastically restored cross sections, Sharp [1984] also interpreted the SDD as a mostly or entirely new Cenozoic low-angle normal fault.

Seismic reflection data and well log data show up to 4.0 ± 0.6 km of post Eocene continental strata in the Sevier Desert basin. Stratigraphic names are normally not assigned to these sequences due to the limited surface exposures and large lateral variations in the basin. These sedimentary sequences are mainly alluvial, fluvial, and lacustrine clastic and sedimentary formations, with less limestone and salt [Mitchell, 1979]. Oligocene ash flow tuffs and welded tuffs are exposed in most of the mountain ranges surrounding the Sevier Desert basin (Figure 1), whereas 6.9 m.y. to 11,000 year old tholeiitic high alumina basalt flows and rhyolite cinder cones occur in the central part of the basin [Condie and Barsky, 1972; Lindsey et al., 1981; Carrier and Chapman, 1981].

Geothermal and oil exploration in the late 1970s and early 1980s in the Sevier Desert region provided modern geological and geophysical data available for this study. This paper focu[illegible]roseis seismic refle[illegible]wave equation synt[illegible]interpretation. Wel[illegible]reflection data wer[illegible]structure, and grav[illegible]nensional, one-layer approach to corroborate the seismic interpretation. The main objectives of this investigation were (1) to analyze seismic reflection data and to interpret structures in the Sevier Desert basin of west central Utah; (2) to estimate the regional extent and the total extension of the Sevier Desert detachment; and (3) to interpret the late Cenozoic geologic history of the Sevier Desert basin and the surrounding region based on these data.

SEISMIC REFLECTION DATA

Data Acquisition and Processing

About 550 km of seismic reflection profiles were interpreted in this study (Figure 2). Seismic profiles 1 to 10 (Figure 2) were recorded in 1980 by the Arco Oil and Gas Company using 4 to 5 in-line Vibroseis sources. The main field parameters include end-on and split-spread layouts with far offsets from 2.5 to 3.5 km, a 14 to 56 Hz vibrator upsweep, a 4 ms sampling rate, and a 20 s recording time. A vibrator interval of 134, 100, or 50 m, with a corresponding group interval of 61, 25, and 50 m, and recording 96 or 48 channels gave 24-fold data with a vertical fold of 10 to 14. A standard processing sequence including 62 Hz anti-aliasing filtering, 60 Hz notch filtering, reduction to a 1433 m datum using a 1.8 km/s datum velocity, spherical divergence gain recovery, time domain minimum phase deconvolution, statics corrections, normal move out correction, zero-phase time domain filtering, mean absolute automatic gain control (AGC) with a 0.5 s window, coherency statics, and trace editing provided the final CDP displays. Time and finite difference migration of lines 1, 2, 3, 5, 7, and 8 was used to enhance the data. Field and processing parameters for ancillary reflection profiles are reported by McDonald [1976], Smith and Bruhn [1984], and Barker [1986].

Figures 3, 4, and 5 show three seismic reflection profiles in the south Sevier Desert used for this investigation. The main reflectors that could be correlated across these profiles are interpreted to be the SDD (D), a middle Pliocene horizon (B), and a lower Paleozoic-Tertiary unconformity (T). Lithologic information of the reflecting horizons and the basin fill comes from eight exploratory oil wells drilled in the Sevier Desert region between 1957 and 1982 (Figures 1 and 6) and from surface geology (Figure 1). Detailed lithologic descriptions and mechanical log parameters of the eight wells are given by Planke [1987] and will not be discussed in detail here.

Seismic Signature of The Sevier Desert Detachment (D)

A strong two-to three-cycle reflector, D (Figures 3, 4, and 5), was penetrated by four wells (Figure 6) and has been identified as the Sevier Desert detachment (SDD). The reflector corresponds to the boundary between Tertiary basin fill and calcareous Paleozoic marine shelf formations and was first interpreted by McDonald [1976] as the SDD. The multi-cycle nature of reflector D may be due to sedimentary layering, hydrothermal alteration, or a brecciated fault zone [Allmendinger et al., 1983]. There is no indication of excess fluid flow from the temperature log, nor is there evidence of hydrothermal alterations or a brecciated zone in the lithological logs. Sedimentary layering in the basin formations in the unit above the SDD was interpreted in the ARCO Hole in the Rock 1, the ARCO Meadow Federal 1, and the ARCO Pavant Butte 1 wells. Impedance layering and noise therefore seems to be the most plausible hypothesis for the multi-cyclic nature of reflector D.

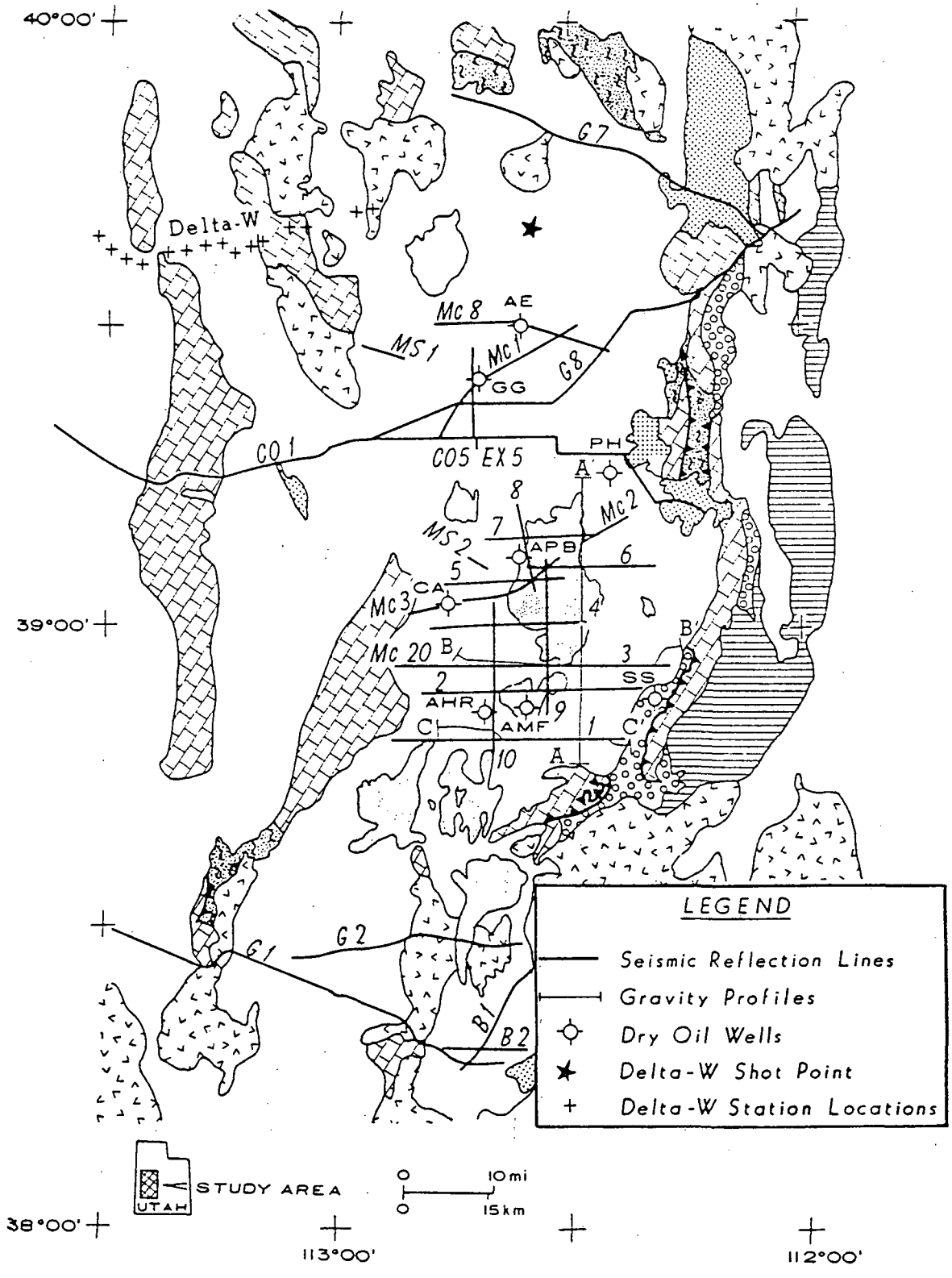

Fig. 2. Map of seismic reflection and refraction lines and gravity profiles of Sevier Desert area. Mc reflection profiles from McDonald [1976], the CO lines from Allmendinger et al. [1983] and Von Tish et al. [1985], the G lines from Barker [1986] and Smith and Bruhn [1984], and the MS lines from Crone and Harding [1984]. Delta-W is a refraction profile shot by U. S. Geological Survey in 1963, while the EX5 is a wide-offset profile shot by Consortium for Continental Reflection Profiling (COCORP). Both profiles are reproduced by Gants [1985]. This study concentrates on reflection lines 1-10.

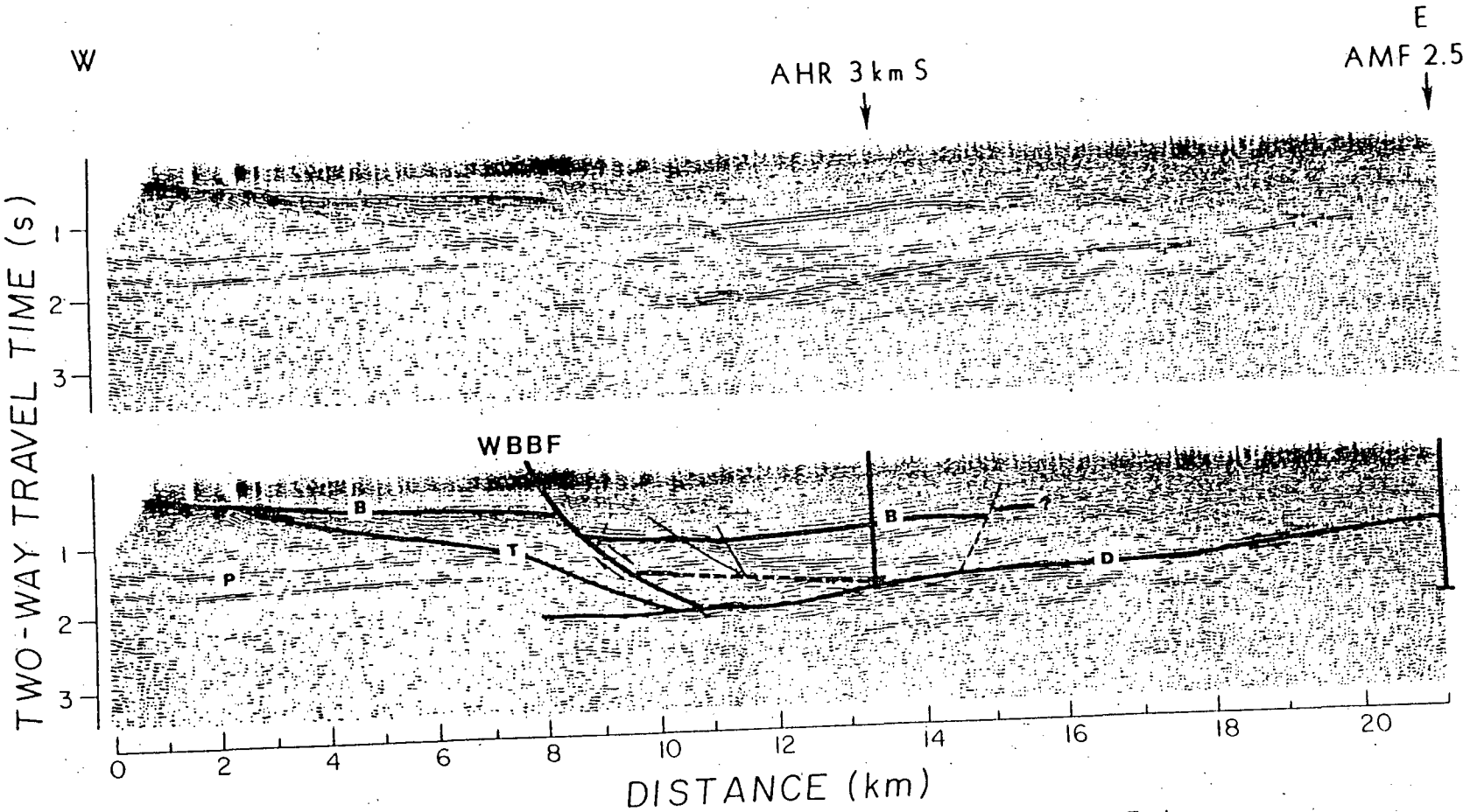

Fig. 3. Western part of seismic reflection line 2. The interpreted reflectors are discussed in the text. Total depths of the ARCO Hole In The Rock 1 (AHR) and the ARCO Meadow Federal 1 (AMF) wells are shown. The reflection data are 24-fold CDP stack, and deconvolved. Finite difference migration was performed from 11.5 to 21 km. WBBF is the western basin-bounding fault. Sevier Desert Detachment = D; Middle Pliocene horizon = B and Paleozoic-Tertiary unconformity = T. Approximate horizontal exaggeration is 1.2 (0-11.5 km) and 1.7 (11.5-21 km).

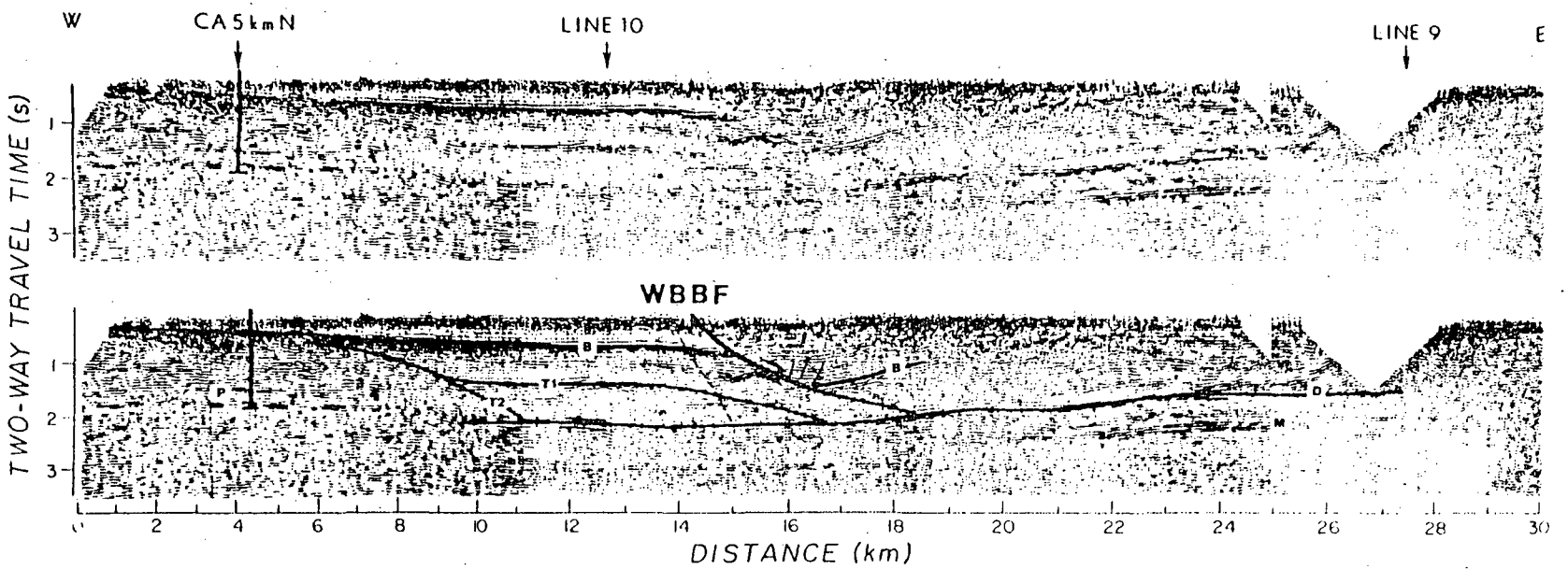

Fig. 4. Western part of seismic reflection line 4. The interpreted reflectors are discussed in the text. Total depth of the Cominco American Inc. 2 Beaver River (CA) well is shown. The reflection data are 24-fold CDP stack, and deconvolved. Migration was performed from 0 to 11 km. Sevier Desert Detachment = D; Middle Pliocene horizon = B and Paleozoic-Tertiary unconformity = T. WBBF is the western basin-bounding fault. Approximate horizontal exaggeration 1.2 (0-11 km) and 1.7 (11-30 km).

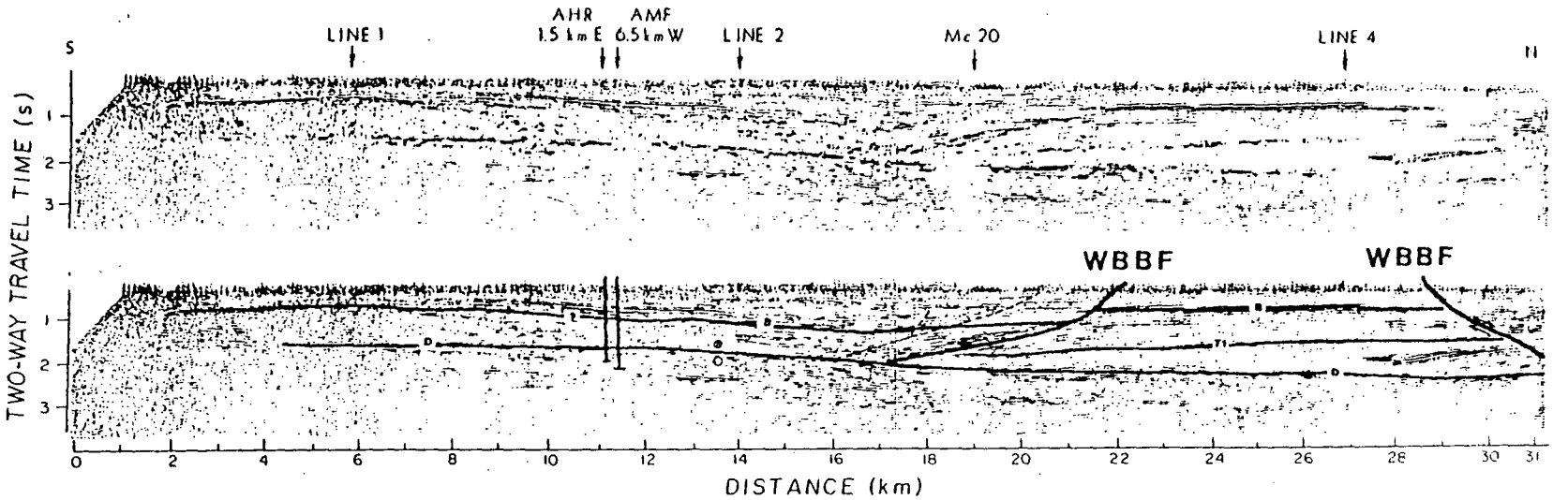

Fig. 5. Seismic reflection line 10. The interpreted reflectors are discussed in the text. Total depths of the ARCO Hole In The Rock 1 (AHR) and the ARCO Meadow Federal 1 (AMF) wells are shown. The reflection data are 24-fold CDP stack, track and cost, and deconvolved. WBBF is the western basin-bounding fault. Approximate horizontal exaggeration is 1.7.

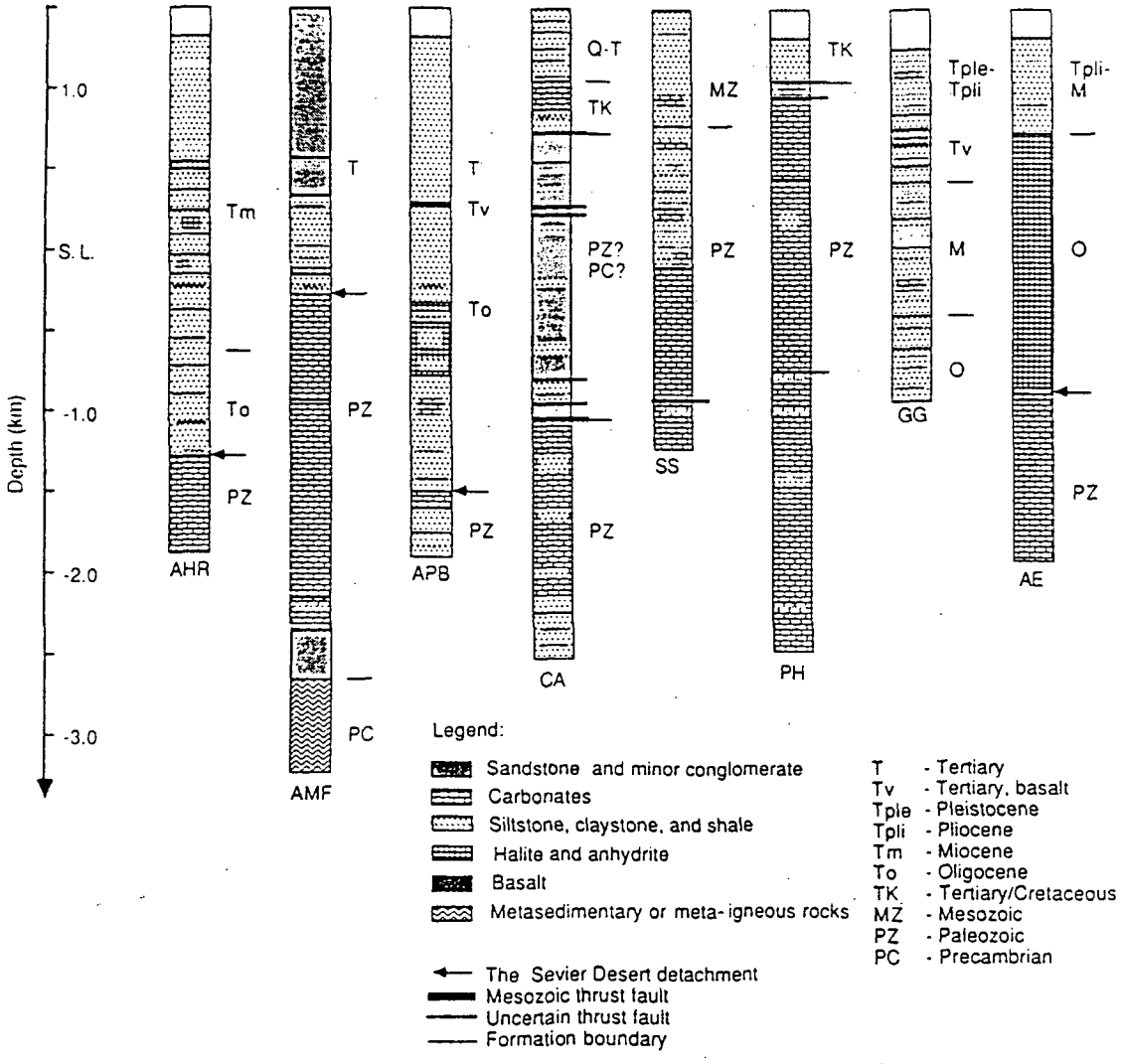

Fig. 6. Simplified lithologic columns of the wells in the Sevier Desert region. The lithologies are from Planke [1987, Appendix B]. See Figure 1 for well name abbreviations. Arrows indicate the Sevier Desert detachment identified in the well logs.

The apparent truncation of faults at the D reflector (e.g., the western basin-bounding fault on Figures 3 and 4) suggests that it is a fault, and not just the Tertiary-Paleozoic basin boundary. Furthermore, there are no significant offsets seen on the D reflector, and lack of lateral continuity is mainly attributed to high noise levels and strong scattering. Hanging wall truncation of the interpreted Pavant Range thrust on line CO-1 [Allmendinger et al., 1983] also supports the detachment fault interpretation. Finally, it is possible to trace a weak and discontinuous D reflector up to 8 km west of the western basin-bounding fault (Figures 3, 4, and 5) on the industry vibroseis data, and a stronger and more continuous D reflector up to 70 km to the west on deep seismic reflection lines [Allmendinger et al., 1983; Smith and Bruhn, 1984]. The westward decrease of the reflection quality is due to both a lower impedance contrast and a lower transmission coefficient of an overlying thick basalt sequence (reflector B) west of the western basin- bounding fault.

A depth contour map of reflector D was made from the seismic reflection data in Figure 2 (Figure 7). The travel times to the D reflector were depth converted using a mean velocity-depth function estimated from the acoustic well logs in the Tertiary basin fill (Figure 8a) and a mean velocity-depth function determined from modeling and inversion of seismic refraction data in the pre- Tertiary sedimentary formations. Due to large lateral velocity variations (Figure 8) and poor lateral control, only one mean velocity-depth function was used to depth convert the Cenozoic basin fill. Upper and lower bounds for the velocity-depth profile in Figure 8a are estimated as v_u = 4.4-0.3 z and v_l = 3.0-1.0 z, where z is depth in kilometers using sea level as the reference depth. These bounds give an error of about ± 0.4 km at 0.5 km below mean sea level and ± 0.6 km at 1.0 km below mean sea level, while a picking error of ± 0.05 s gives an estimated error of ± 0.1 km at 1.0 km below mean sea level. To check the accuracy of the average basin velocity-depth function, the depth to the

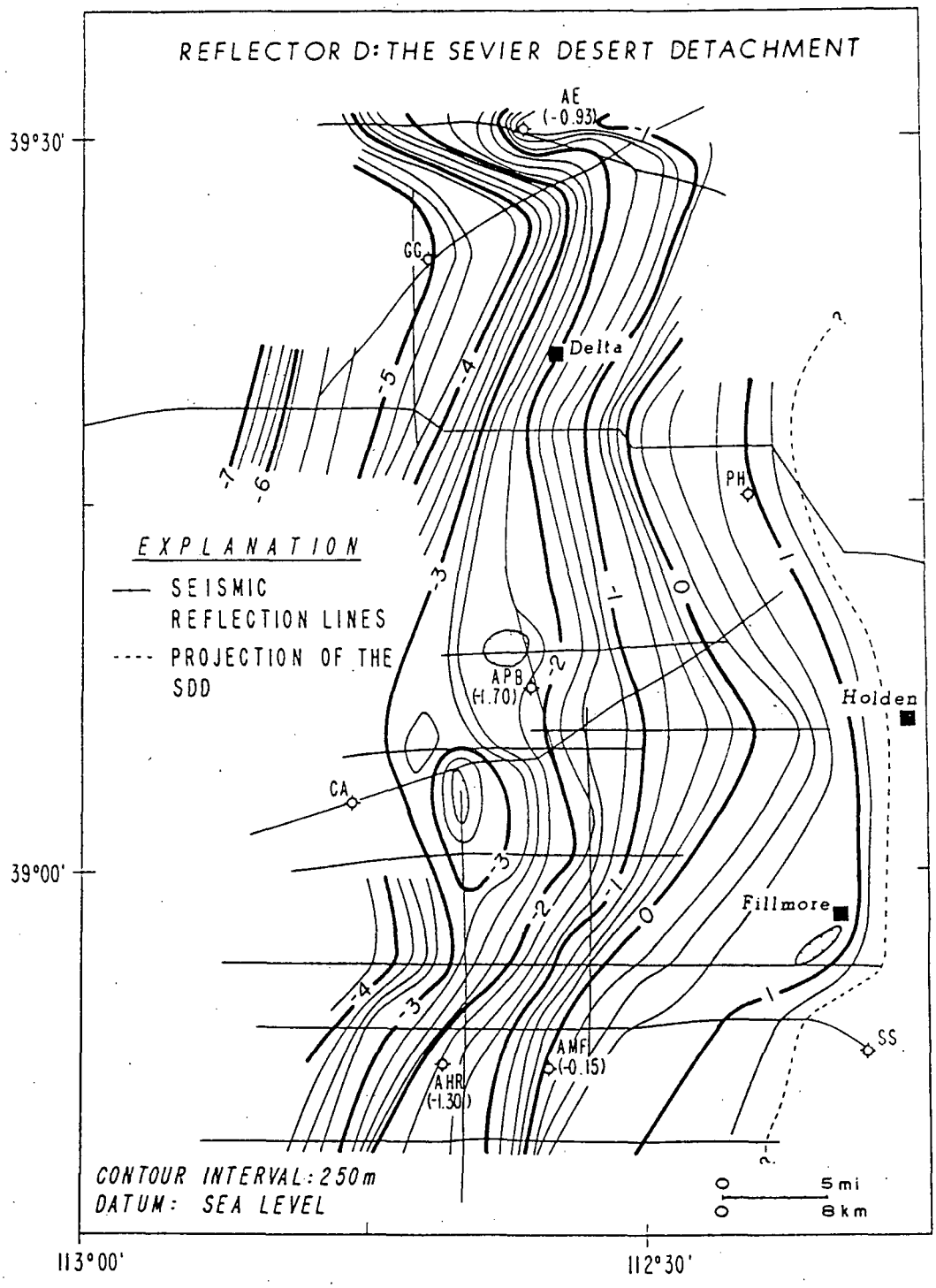

Fig. 7. Depth contour map of the Sevier Desert detachment (SDD). Depths are in kilometers; positive values are above sea level. Measured depths (in kilometers) to the SDD are annotated below the well names. Well name abbreviations are as in Figure 1.

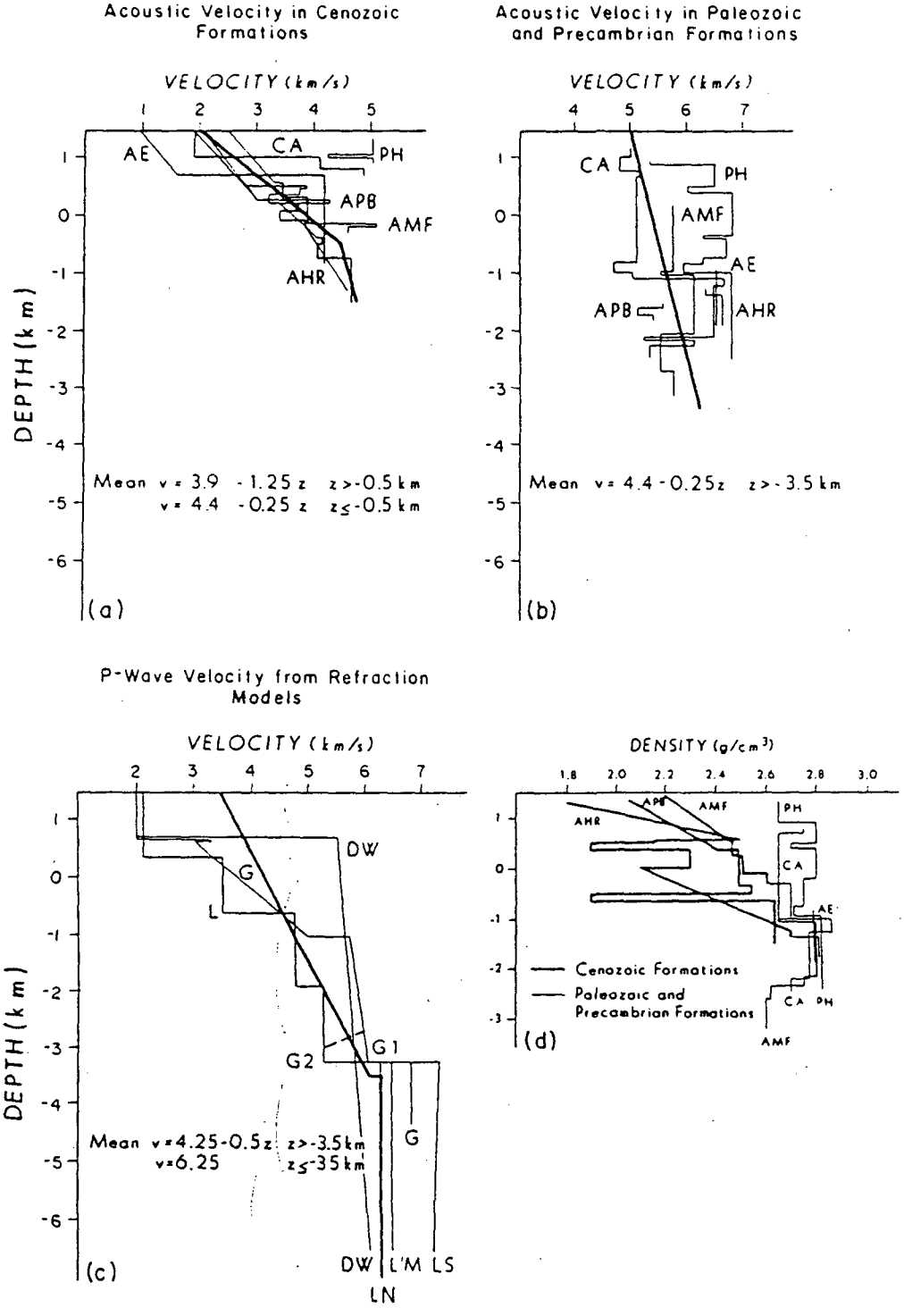

Fig. 8. Velocity-depth functions derived from (a) BHCS well logs, (b) BHCS well logs, (c) modeling of seismic refraction data, and (d) density-depth functions derived from the CNFD well logs. Well name abbreviations are as in Figure 1. DW is Delta-W modeled by Gants [1985].
G is EX5 modeled by Gants [1985]; G1 is without a low-velocity layer, while G2 is with a low-velocity layer. L is EX5 finite-element modeling of EX5 by Liu et al. [1986]; LS is representative of the southern part of the line, LM is representative of the middle part of the line, while LN is representative for the northern part of the line.

basement in the well logs was time converted using the respective acoustic logs, and then depth converted using the average basin velocity-depth profile. All the depths were within ± 0.5 km of the true depth.

To obtain additional information on the geometry of the Sevier Desert basin, three Bouguer-corrected gravity profiles were inverted (Figures 2 and 9). A two-dimensional, one-layer forward model [Pedersen, 1977] was linearized, and the gravity data were iteratively inverted using a singular value decomposition algorithm [Lawson and Hanson, 1974]. Density constraints were provided by density logs from the Sevier Desert basin (Figure 8d), giving an average density of pre-Tertiary formations of ~2.75 g/cm^3 and an average density of Tertiary basin fill of ~2.40 g/cm^3. The good fit between the depth estimates obtained from the gravity data, the depth-converted seismic data, and the well data (Figure 9) strengthens the seismic interpretation and shows that a relatively simple gravity inversion gives a good estimate of the basin geometry.

The main features of the depth-converted contour map of the SDD (Figure 7) are (1) a smooth, ~10° west dipping detachment surface beneath the entire eastern part of the basin, which changes from a north-northeast trend to a north-northwest trend at ~39°5'N, and then back to a north-northeast trend at ~39°20'N; (2) a laterally variable geometry of basin layers below the west central part of the Sevier Desert, characterized by depressions and domes with amplitudes up to

↑ ~2.67

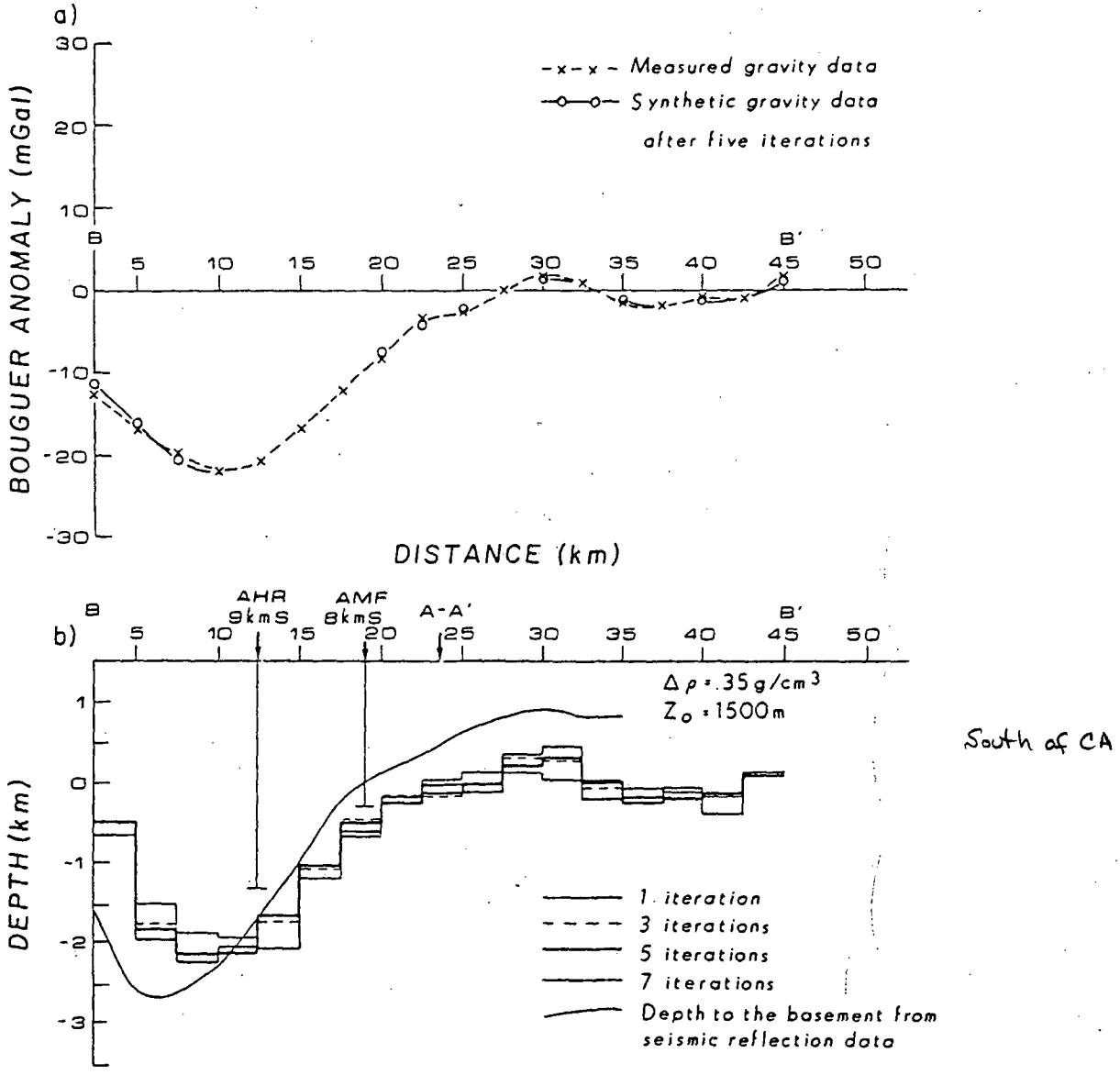

South of CA

Fig. 9. Gravity profile B-B'. (a) Bouguer gravity anomaly from Serpa [1980] normalized to -172 mGal level, and the theoretical gravity response after the 5. iteration. (b) Solution of the depth inversion of the gravity anomaly after the 1, 3, 5, and 7 iteration. Z_0 is the reference depth, and $\Delta\rho$ is the density contrast. AHR and AMF show the depth to the basement in the ARCO Hole In The Rock 1 and the ARCO Meadow Federal 1 wells.

0.5 km associated with a flattening of the detachment; and (3) a 1.5 km structural high beneath a thick salt unit penetrated by the Argonaut Energy 1 well. Some of these interpreted structures may be artifacts due to uncorrected lateral velocity variations, but they are most likely real structures that have formed in response to deformation or result from lateral variations in the local stratigraphy.

Regional Extent of the Sevier Desert Detachment

The seismic reflection and refraction profiles, shown on Figure 2, were interpreted to estimate the regional extent of the Sevier Desert detachment. The projection of the detachment surface is shown on Figure 7 in the eastern part of the Sevier Desert. The surface projection of the SDD intersects the surface east of the towns of Filmore and west of Holden, at the west side of the Pavant Range. However, no Cenozoic fault scarps that would be expected at the surface projection of the SDD are readily apparent from mapping in this region (Figure 1). The location of the SDD surface projection suggests that it is structurally lower than the Canyon Range thrust and that it can possibly be correlated with the Pavant Range thrust (Figure 1). This correlation requires an anticlinal structure of the detachment/thrust surface between the SDD surface projection and the Pavant Range thrust [Villien and Kligfield, 1986]. Balanced cross sections along the deep reflection line CO- 1 [Sharp, 1984] suggest that correlation between the SDD and the Pavant Range thrust was only possible in the Sevier Desert region, and not at deeper levels east of the Cricket Mountains.

The SDD is interpreted to extend at least 70 km to the west, to about 12-15 km depth on line CO-1, but the depth resolution of the industry data makes it difficult to map the detachment west of western basin-bounding fault (Figures 3 and 4). Northward, the SDD is interpreted on line G8 [Gants, 1985], while on line G7 a weak, discontinuous, westward dipping reflector, whose projection intersects the surface just west of Jericho, may be interpreted as the SDD. A different basin geometry and reflection pattern for the potential SDD reflector on line G7 compared with lines G8 and CO-1 make this correlation unlikely. Furthermore, Gants [1985] suggested on the basis of reflection data in the northern Sevier Desert basin that the northward extension of the SDD may correlate with the Leamington shear zone, located north of the Canyon Range (Figure 1). There were no reflectors that could be correlated with the SDD on a regional east-west line 40 km north of G7, north of the map in Figure 1.

Southward, the SDD is observed on line 1 north of Kanosh (Figure 7). In the Beaver Valley, 40 km south, a 2.5 km (1.6 s) deep sedimentary basin can be interpreted on lines B1 and B2 (Figure 2), but it is not possible to correlate any of the reflectors on those lines with the SDD. A discontinuous reflector at ~7 km (2.7 s) depth is apparent below the northern part of the Milford Valley on a north-south reflection line east of the Cricket Mountains (Figure 1, not shown because it is proprietary), but it could not be correlated with the SDD with any confidence. On lines G1 and G2, across the Milford Valley (Figure 2), a 1.5-2.1 km (1.1-1.4 s) deep eastward dipping, asymmetric basin, with a westward dipping bounding fault has been interpreted [Barker, 1986], but again, no reflectors can be correlated with the SDD. The basin geometry interpreted on lines G1 and G2 is similar to the basin geometry in the central part of the Basin and Range province [e.g., Anderson et al., 1983], suggesting different origins for the extensional properties of the Milford Valley basin and the Sevier Desert basin. Neither the seismic data nor a regional geological map [Hintze, 1980] show a southward surface projection; therefore the SDD is interpreted to splay out into a terminating zone or penetrate to a deeper level that has not been imaged.

On the basis of these data the best estimate of the regional extent of the SDD is (Figure 1) (1) eastward to the west side of the Pavant Range and the Canyon Range; (2) northward, definitely to Leamington and possibly north to Jericho; (3) southward to Kanosh with a possible extent to the northern Mineral Mountains; and (4) westward at least 70 km to a depth of ~12-15 km depth. This gives a 80 km to 130 km north-south extent and an area of 5600 km^2 to 9100 km^2.

Mid Pliocene Reflector (B)

A strong multi-cyclic reflector, B (Figures 3, 4, and 5), can be mapped west of the western basin-bounding fault throughout the Sevier Desert. This reflector can be correlated with five, 6 m to 30 m thick, basalt flows penetrated by the Gulf Oil Gronnig 1 well at depths between 768 and 1010 m. The basalt flow at 812 m has been dated using the whole rock K-Ar method at 4.2 ± 0.3 m.y. [Lindsey et al., 1981]. One 30 m thick basalt flow is penetrated by ARCO Pavant Butte 1 at 1190 m (Figure 6). Synthetic seismograms modeling suggests that this flow would give a strong two-cycle reflection at ~1.0 s [Planke, 1987], that can be correlated with a strong reflector at 1.05 s on line 8, 1.0 km east of the well. A similar seismic signature of reflector B east and west of the western basin-bounding fault and the correlation of basalt flows in the ARCO Pavant Butte 1 and the Gulf Oil Gronnig 1 wells and the B reflector on nearby seismic lines are the justifications for correlating reflection B across the western basin-bounding fault.

This correlation implies that basaltic volcanic flows covered much of the Sevier Desert basin during late Pliocene. Still, of the seven wells in the basin, only the Gulf Oil Gronnig 1 and the ARCO Pavant Butte 1 wells penetrated basalt flows. The Cominco American Inc. 2 Beaver River well (Figure 1) is located west of the basalt reflector on line Mc3, while the basalt reflector is truncated at the salt dome penetrated by the Argonaut Energy 1 well. The Placid Oil Henley 1 and the ARCO Meadow Federal 1 wells are located east of the interpreted basalt reflector. Finally, the ARCO Hole In The Rock 1 well is located in the southern part of the Sevier Desert basin, where the B reflector is weak (Figure 5). The lack of basalt in the ARCO Hole in the Rock 1 may reflect a higher relative elevation or a diminished volcanic activity in the south Sevier Desert in middle Pliocene time.

The quality of the B reflector is, however, variable across the Sevier Desert. Normal incidence synthetic seismograms show that multi-cycle reflectors may be due to a single > 30 m thick flow or two or more thin flows [Planke, 1987]. Lateral discontinuities of the reflector may correspond to faulting or pinch-outs of individual flows. The reflector is generally strongest in the deepest part of the basin, which is expected, since the flows generally follow structural lows.

A few slightly east dipping reflectors terminate below reflector B, west of the western basin-bounding fault on line 2 (Figure 4). A similar relationship on line CO-1 was interpreted as a Pliocene angular unconformity by Von Tish et al. [1985]. Mitchell and McDonald [1986], however, question the existence of this unconformity and interpret the angular relationships of reflectors seen on line CO-5 as noise. The variable reflection character of reflector B obscures reflectors just below it, but it is not possible to interpret any dipping reflectors that terminate at reflector B except possibly on line 2 and line CO-1. It is therefore not possible to interpret a regional middle Pliocene angular unconformity in the Sevier Desert basin from the available seismic data.

A reflector at ~0.6 s depth in the southern part of line 10 (Figure 5) is correlated with reflector B on Figure 10. If this interpretation is correct, then the apparent doming is a post-Pliocene effect and could either be a response to hanging wall movement of the detachment fault or later volcanic intrusions (line 1 crosses a Quaternary rhyolite dome above this part of reflector B). Another interpretation that is problematic is the reflection at ~1.2 s depth between 15 and 16 km on line 2 (Figure 4). The strong multi-cycle character suggests that it may correlated with reflector B, and two major basin-bounding

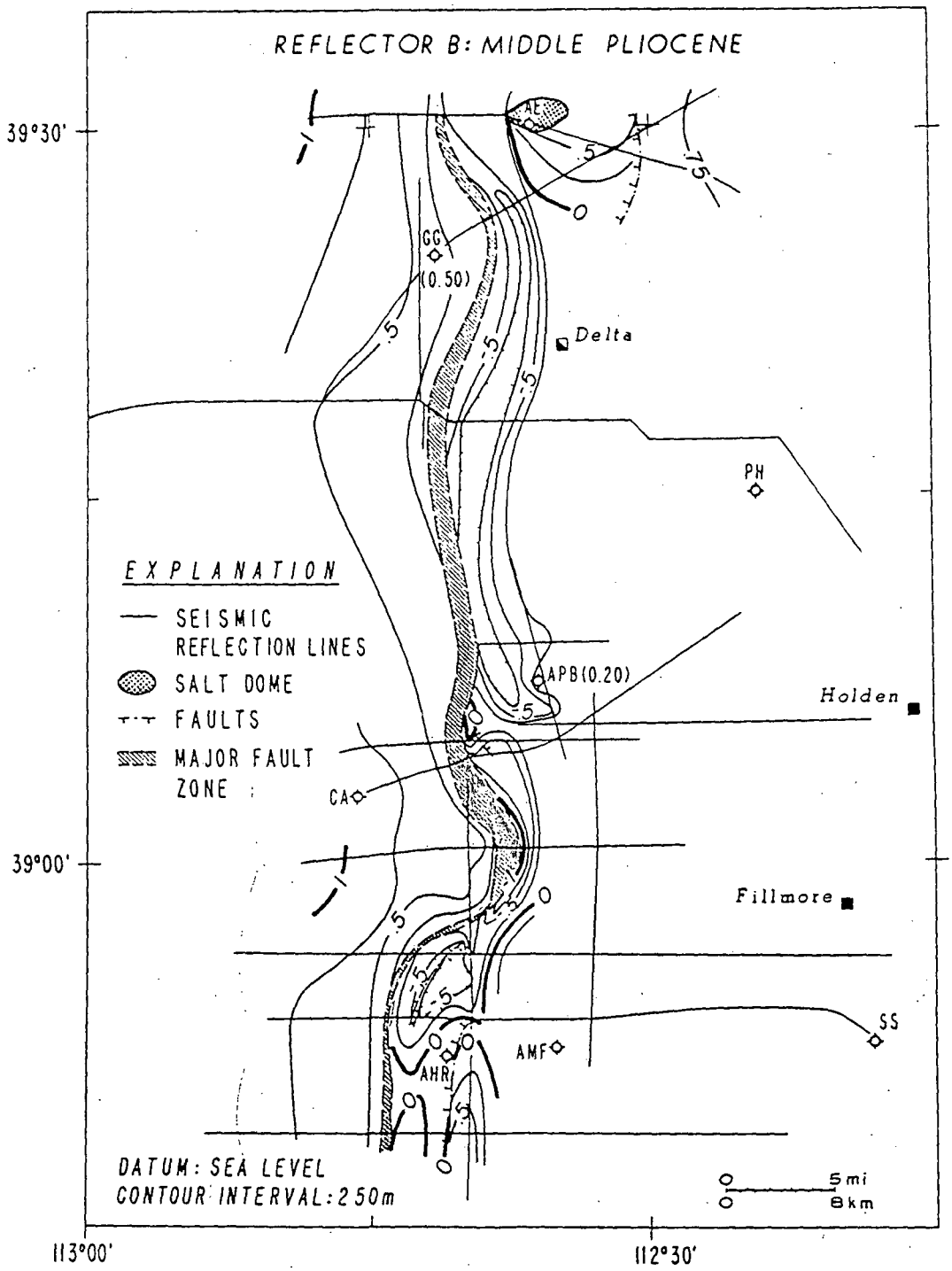

Fig. 10. Depth contour map of the middle Pliocene B reflector. Depths in kilometers. Positive values are above sea level. Measured depths to the reflector are annotated below or beside the well names. Well name abbreviations are described in Figure 1 caption.

faults may then be interpreted. Weak fault reflectors and comparison with nearby seismic reflection lines suggest the interpretation of one major, listric fault. The strong amplitude of this reflector can then be explained either as a volcanic sill intrusion, noise, or diffractions and automatic gain control window (AGCW) effects.

In summary, the major features of the depth contoured map of the mid-Pliocene reflector B (Figure 10) are (1) a gently, 3°-6°, eastward dipping reflector west of the western basin-bounding fault; (2) a simple normal drag on reflector (B) east of the western basin-bounding fault at ~39°N, and a normal and reverse drag (B) reflector north of 39°5'N and south of 38°55'N; (3) a pinchout of the basalt reflector beneath the salt dome penetrated by the Argonaut Energy 1 well, and lack of the B reflector in the eastern part of the basin; (4) a sharp 6 km right-lateral offset of the western basin-bounding fault at ~38°55'N, and a smooth 3 km left-lateral offset of the western basin-bounding fault at ~39°5'N; and (5) a 250 m to 1450 m vertical offset of the western basin-bounding fault, with the largest offset on line 4 (Table 1).

Other Reflectors

A ~30° east dipping, discontinuous and weak reflector, T, is apparent in the hanging wall of the SDD and is interpreted as an angular unconformity between lower Paleozoic and Tertiary formations (Figures 3, 4, and 5). The evidence for this interpretation comes from angular relationships seen on the reflection profiles and from the lithologic well logs. The Gulf Oil Gronnig 1 well reaches a total depth of 2485 m in Tertiary formation above the unconformity (Figure 6) and bottoms in a 1000 m thick sequence of claystone, shale, and tuffaceous sandstone with minor limestone, anhydrite, and gypsum that was assigned an Eocene age by McDonald [1976]. Pollen dating of two cores at 1980 m (6500 feet) and 2110 m (2929 feet) gave an upper Oligocene/early Miocene age, in agreement with fission-track dating of zircon and apatite from the lower core (25.9 ± 1.2 m.y. and 27.8 ± 6.8 m.y., respectively [Lindsey et al., 1981]). To the southwest, the 4021 m deep Cominco American Inc. 2 Beaver River well penetrates a boundary between the Tertiary-Cretaceous North Horn formation and Cambrian or Precambrian sandstone and siltstone at 785 m depth. Deeper formations penetrated by the well are mainly thrust-faulted lower Paleozoic carbonates and clastics. The well data therefore show a Tertiary age for the rocks above the unconformity and a lower Paleozoic and Precambrian age for the rocks below the unconformity. An unconformity of similar age is also found in surface exposures on the east side of the House Range and to the north of the Little Drum Mountains [Von Tish et al., 1985].

C'A-2

TABLE 1. Post-middle-Pliocene Offsets of the Western Basin-Bounding Fault, F

Seismic Reflection Profile	Offset, m
1	500 ± 150
2	750 ± 150
Mc20	650 ± 150
4	1450 ± 250
Mc3	1350 ± 250
5	900 ± 200
CO-1	350 ± 100
Mc1	700 ± 150
Mc8	300 ± 100

See Figure 1 for profile locations.

A rather variable reflection pattern is seen in the wedge bounded by the T, D, and B reflectors and the western basin-bounding fault (Figures 3 and 4). Lines Mc1 and Mc8 show noisy, scattered reflections. Lines Mc3, Mc20, 1, 2, and 5 show an inconsistent, eastward dipping reflection pattern, while line 4 has a few strong, almost horizontal, reflectors. Two interpretations of reflector T, T1 and T2, are possible on line 4 (Figure 4). The increased area of the wedge area compared with the interpreted wedge area on adjacent seismic lines, when T2 is interpreted as the unconformity, suggests that T1 corresponds with the Paleozoic-Tertiary unconformity (Figure 4). Nearby seismic lines, on the other hand, suggest that T2 is the unconformity. T1 may then be a multiple of reflector B, but the southward continuation of the T1 reflector on line 10 (19-22 km, Figure 5) shows that T1 cannot entirely be a multiple. The different reflection patterns in the wedges are probably due to depositional variations and a complex deformational history. Depth contour maps of reflector T are not very accurate due to the poor reflection signature of T, but they show a generally north trending, 30° east dipping, slightly undulatory unconformity [Von Tish et al., 1985; Planke, 1987].

Two strong, gently westward dipping reflectors, P, are interpreted in the lower Paleozoic and Precambrian sequences west of the south Sevier Desert basin (Figures 3 and 4). These reflections probably represent a boundary between low-velocity metamorphic clastic sequences and higher-velocity carbonate formations found in the Cominco American Inc. 2 Beaver River well (Figure 6). Alternatively, they may correspond to Mesozoic thrust faults where allochthonous Paleozoic and Precambrian high-velocity formations overlay autochthonous Mesozoic lower-velocity formations. This hypothesis is not supported by the well data in the Cominco American Inc. 2 Beaver River well or balanced cross-section construction [Sharp, 1984].

One to two deeper reflectors, M, are present beneath the SDD in the eastern part of the basin (Figure 4). The shallow reflectors may be within the lower Mesozoic to upper Paleozoic clastic and carbonate sequences that were penetrated by the Shell Oil Sunset Canyon 1 well, whereas the deeper reflectors are probably within the lower Paleozoic to Precambrian formations penetrated by the ARCO Meadow Federal 1 well. Another possibility is that the reflectors correspond to Sevier aged thrusts (e.g., the lower Pavant thrust), placing allochthonous Paleozoic rocks over autochthonous Mesozoic and Paleozoic rocks [Sharp, 1984; Villien and Kligfield, 1986]. A complex thrust geometry of the Mesozoic-Paleozoic column is proposed just west of the Pavant Mountains and the Canyon Range from the construction of regional cross sections [Sharp, 1984; Villien and Kligfield, 1986]. These complex structures may be the reason for the lack of coherent reflectors in this area.

Abundant subsurface salt has been identified in the Sevier Desert basin. A 1571 m thick crystalline halite formation was penetrated by the Argonaut Energy 1 well and can be correlated with a salt dome interpreted on line Mc8. Mitchell [1979] proposed a Tertiary redeposition of the Jurassic Arapien salt as the origin of this salt dome. The ARCO Pavant Butte 1 well also penetrated halite; one 60 m thick unit at 1825 m and one 300 m thick unit at 1969 m (Figure 6) were found. Pollen of Oligocene age is reported in both units in the lithologic well logs. Possible salt structures are present on lines Mc1, Mc8, CO-1, and 5, but none were identified south of line 5. In the south Sevier Desert basin the reflector at ~0.75 s between 10 and 14 km on line 10 can be correlated with a 36 m thick anhydrite unit penetrated by the ARCO Hole in the Rock 1 well at 924 m (~0.8 s).

Discontinuous, scattered reflections are apparent east of the termination of the B reflector in the Sevier Desert basin (Figures 3 and 4). The good quality of the underlying detachment reflector, D, shows that the lack of reflections is due to a lack of continuous impedance boundaries. Coarse tuffaceous sandstone and poorly sorted conglomerate is reported

in the upper 1123 m of the ARCO Meadow Federal 1 well, whereas the deeper 500 m are mainly tuffaceous siltstone, sandstone, and shale with minor limestone. The well data do not suggest large velocity contrasts in this part of the basin and the lack of reflections may therefore be due to a relatively homogeneous basin fill. Synthetic seismogram modeling shows that abundant small-scale faulting of a constant impedance contrast will lead to scattered reflections. The lack of reflections in the eastern part of the basin is probably due to both homogeneous basin fill and faulting.

SYNTHETIC SEISMOGRAM MODELING

From the initial interpretation of the seismic reflection profiles in the south Sevier Desert, several problems were identified. (1) What constraints can the seismic data give on the shape of the western basin-bounding fault? (2) How does the reflection character of the SDD change from the east to the west side of the western basin-bounding fault? (3) Is the lack of consistent reflectors in the eastern part of the basin due to a relatively homogeneous basin fill or to scattering of waves due

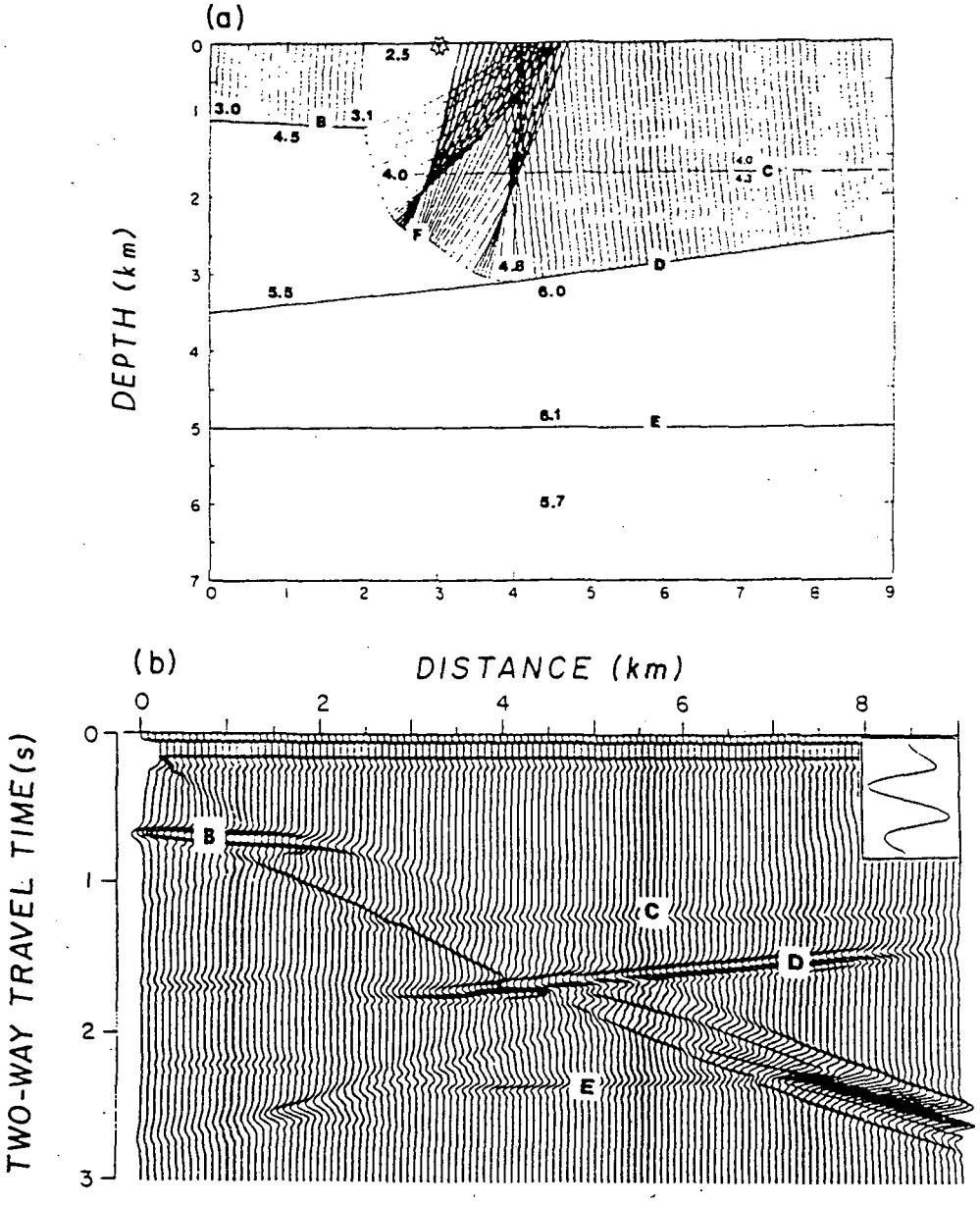

Fig. 11. Synthetic seismograms of an asymmetric basin with a listric basin-bounding fault. (a) Ray traced depth model with acoustic velocities in kilometers per second. Boundary C is included only in Figure 11b. (b) Plane-wave finite difference synthetic seismogram. A grid spacing of 25 m, 361 by 250 grid, and 1150 time steps were used for the finite difference modeling.

to small-scale faulting? To address these questions, synthetic seismogram modeling was undertaken to study the theoretical response of different subsurface velocity models using asymptotic ray theory modeling [Cerveny et al., 1977] as the starting approach and heterogeneous finite difference modeling of the elastodynamic wave equation [Kelly et al., 1976; Clayton and Engquist, 1977] as the final approach. Interval velocities were estimated from the acoustic velocity logs (Figure 8a), modeling of refraction and wide-angle reflection data (Figure 8c) [Ganis, 1985; Liu et al., 1986], and stacking velocities.

A simplified velocity model for the Sevier Desert basin was produced to examine the reflection response across the western basin-bounding fault (Figure 11a). To fulfill the finite difference stability criteria [Kelley et al., 1976], while keeping the size of the model on a manageable size, the dominant frequency of the source wavelet was chosen to be as low as 6.7 Hz. The paraxial wave equation approximation [Clayton and Engquist, 1977] was used as absorbing boundary condition. However, not all side reflections from the model edges were attenuated, for example, the linear event at 8 km and 2.5 s (Figure 11b). The main features of the synthetic plane-wave finite difference seismogram (Figure 11b) are (1) strong reflections from the D reflector east of ~2.5 km and weak reflections west of 2.5 km; (2) a velocity pull-up of 0.2 s and a 1 km reflection gap below and west of the F reflector for reflectors D and E; (3) intersection and complex interference of the F and D reflectors close to their true spatial intersection location; and (4) diffractions from the termination of the B reflector.

Small-Scale Fault Scattering

The seismic reflection data show relatively few continuous reflections above the SDD east of the termination of the B reflector (Figures 3 and 4). The lack of reflections in this area may either be due to low or lack of acoustic impedance boundaries or be due to interference of seismic waves reflected from discontinuous boundaries of small lateral extent. Surface mapping in similar detachment terrains show that small-scale faulting, down to the meter scale, is common in the upper plate (e.g., the Wipple-Buckskin-Rawhide mountains in west Arizona and southeast California [Gross and Hillemeyer, 1982]). To approximate small-scale faulting, a finite difference synthetic seismogram was generated involving a constant impedance boundary with variably spaced, constant offset (Figure 12). The model velocities were derived from the acoustic well logs (Figure 8a). The dominant source frequency was kept proportional to the minimum model velocity and inversely proportional to the grid spacing. The shallow-layer

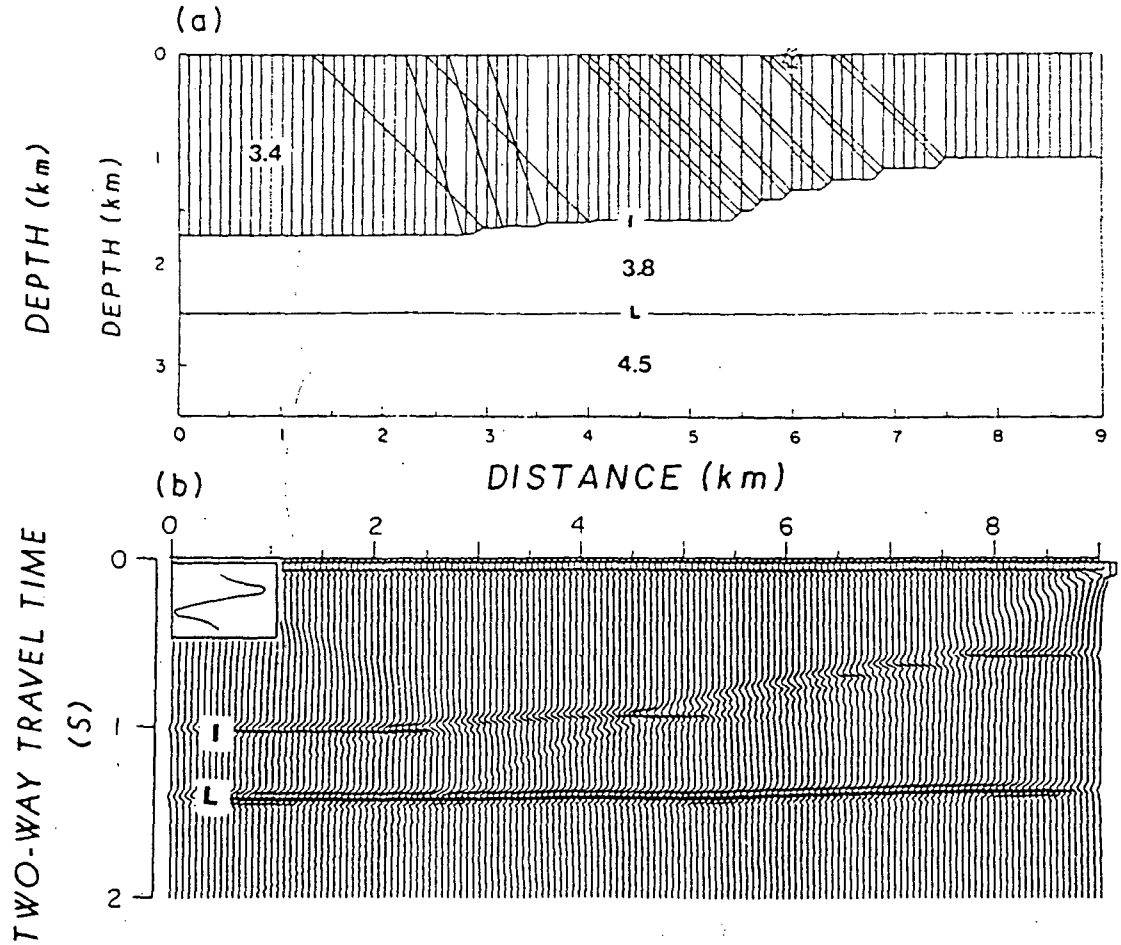

Fig. 12. Synthetic seismograms of constant impedance boundaries with variably spaced offset. (a) Ray-traced depth model with acoustic velocities in kilometers per second. (b) Plane-wave finite difference synthetic seismogram. A grid spacing of 15 m, 601 by 250 grid, and 942 time steps were used for the finite difference modeling.

velocities in the model were purposely set high (3.4 km/s) compared to the velocities derived from the acoustic well logs (Figure 8a), while the dominant frequency was constrained to be low (15 Hz) to maintain a manageable size of the model for computing. Finally, a horizontal, constant impedance boundary was included below the offset interface to examine the influence of the overlying velocity structure on the reflections from the horizontal interface.

The finite difference modeling did not produce reflector segments between the 100 m vertical offset faults with less than ~300-400 m length (Figure 12b). The reflections in this region show a disturbed pattern, with hyperbolic branches and strong variations in amplitude and phase. The 25 m offset faults cannot be resolved, and a weak hyperbolic branch is the only indication that the reflecting model boundary is not smooth in this region. The underlying horizontal reflector is, in neither case, disturbed except for minor velocity pull-up. These results depend of course on the frequency content of the source and the modeling algorithms. The finite difference source had a dominant frequency of 15 Hz, compared to the Sevier Desert vibroseis data that had a dominant frequency of ~20 Hz. Migration may furthermore enhance the reflection image, but the real data will also include artifacts from out-of-profile structures, multiples, processing, and noise that will tend to disturb the seismic reflection image.

Summary of Seismogram Modeling

The magnitude results of the seismic modeling with respect to the Sevier Desert reflection lines are (1) the steeply dipping, high-impedance boundary at the western basin-bounding fault will be poorly imaged by the stacked seismic reflection method employed to acquire the data used in the interpretation; (2) the detachment surface reflector D is poorly imaged beneath the Paleozoic sequence from ~0.5 km west of the western basin-bounding fault and may have a velocity pull-up of up to ~0.2 s; (3) the intersection of the weak reflection from western basin-bounding fault and the reflection from the detachment surface is located within ~0.5 km of the true spatial horizontal intersection position; (4) the disturbed seismic image in the eastern Sevier Desert basin may be due to interference of reflections from inhomogeneities of scale length from ~50 m to ~300 m; and (5) small reflecting interfaces above the SDD will not disturb the D reflector substantially.

ESTIMATE OF CRUSTAL EXTENSION

The magnitude of horizontal extension for a geologic cross section perpendicular to a detachment fault can be estimated from the geometry of the basin fill assuming a balanced area and plane strain [White et al., 1986; Barker, 1986]. In this method the cross-sectional area of the basin is divided by the maximum depth to the detachment surface to estimate the total horizontal displacement. The average extension rate can then be determined by dividing the horizontal displacement by the total time of extension, and the average strain rate can be found by dividing the displacement by the fault length and the total time of extension.

The balanced area method was used to estimate the E-W extension for three east-west seismic reflection profiles in the Sevier Desert (Figure 13; Table 2) using the assumptions that (1) no Tertiary units are pre-extensional; (2) the extension started after middle Oligocene; (3) the thickness of post-middle-Pliocene sediments is constant where no reflectors can be interpreted on the seismic profiles; (4) the maximum depth of the detachment and its length can be extrapolated from lines CO-1 and G8 to be 12-15 km and 70 km; and (5) no significant erosion has occurred since the onset of extension. Pre-extensional Tertiary sequences are penetrated by wells in the Sevier Desert (Figure 6), but they are generally thin, and their aerial extent is poorly defined by the seismic reflection data. A middle Pliocene unconformity has been interpreted on line CO-1 [Von Tish et al., 1985], but the unconformity cannot be interpreted on reflection profiles in the south Sevier Desert. Post-extensional erosion is therefore believed to be of minor importance in the Sevier Desert basin. Note also that no correction for sediment compaction was made. This method has been used to calculate a minimum extension rate for several valleys ~30-50 km to the south of the Sevier Desert, obtaining extension values from 0.05 mm/yr to 0.15 mm/yr (the Wah Wah Valley ~ 0.05 mm/yr, the Milford Valley ~0.09-0.15 mm/yr, the Beaver Valley ~0.08-0.13 mm/yr) [Barker, 1986]. Geological reconstructions, however, suggest 2 to 3 times greater extension rates.

Palinspastically restored cross sections along line CO-1 [Sharp, 1984] suggest 28-38 km of E-W Cenozoic extension along the SDD. The most critical assumptions for this construction were the correlation between the hanging wall and the footwall of the SDD and the interpretation of only one thrust fault intersecting the Cominco American Inc. 2 well where Precambrian clastics overlie Cambrian carbonates. Other interpretations of the well data, however, show no Precambrian formations and up to five thrust faults penetrated by the well [Mitchell and McDonald, 1986; Planke, 1987]. The age of the formations and the number and location of the thrust fault(s) are critically important for the reconstruction of the pre-extensional cross sections. Sharp's [1984] estimate of extension may therefore be an upper bound value. Better dating of the Precambrian and Paleozoic rocks in the wells in the Sevier Desert region is needed to properly determine the stratigraphy interpreted from the well logs and thereby enable the construction of a better palinspastically restored cross-section and extension estimate.

The calculated post-middle Pliocene extension rates determined in this study are 0.6-0.8 mm/yr (Table 2) and are within the error bounds calculated from palinspastically restored cross sections along line CO-1 [Sharp, 1984]. Our middle Oligocene to middle Pliocene extensional rate of ~0.1-0.2 mm/yr is, however, an order of magnitude smaller than the estimate along line CO-1. Possible Pliocene erosion and a shallower detachment depth will both increase the calculated extension rate, but these factors cannot explain the entire difference between the extension rate calculated along line CO-1 and the rate calculated in this study. The calculated regional strain rate of 0.6-3.5 10^{-16} s^{-1} and the total extension rate of ~9% of the Sevier Desert region is of similar magnitude as the results calculated for the Great Basin based on estimates from cumulative seismic moments of historic earthquakes of 1.3-3.2 10^{-16} s^{-1} and 10% extension [Eddington, 1986]. However, the middle Pliocene strain rate and extension rate are also almost an order of magnitude smaller than the palinspastically restored cross section along line CO-1 (Table 2). A minimum post-middle Pliocene horizontal displacement of 2.5 to 3.2 km and a minimum middle Oligocene to middle Pliocene displacement of 3.0 to 4.0 km give a minimum post-middle Oligocene displacement on the SDD of 5.5 to 7.2 km compared with the palinspastically restored cross section that gives a three to eight times larger displacement of 25-38 km.

Extension estimates can also be obtained from summing the horizontal displacement across faults. The horizontal extension of the faults that offset the B reflector gives a 0.8 to 1.5 km post-Pliocene extension (Figures 3 and 4). This is of course a minimum estimate, which is seriously affected by small-scale faulting that cannot be interpreted from the seismic reflection data. Hangingwall-footwall correlation across the SDD gives a different extension estimate, but, as already discussed, the Precambrian and Paleozoic stratigraphy is poorly known in the seismic reflection profiles in the Sevier Desert region.

DISCUSSION

The overall configuration of the Sevier Desert basin is that of an asymmetric north trending Tertiary basin with a maximum depth of 4.0 ± 0.6 km. The Tertiary basin fill is mostly fluvial and lacustrine clastic deposits with minor

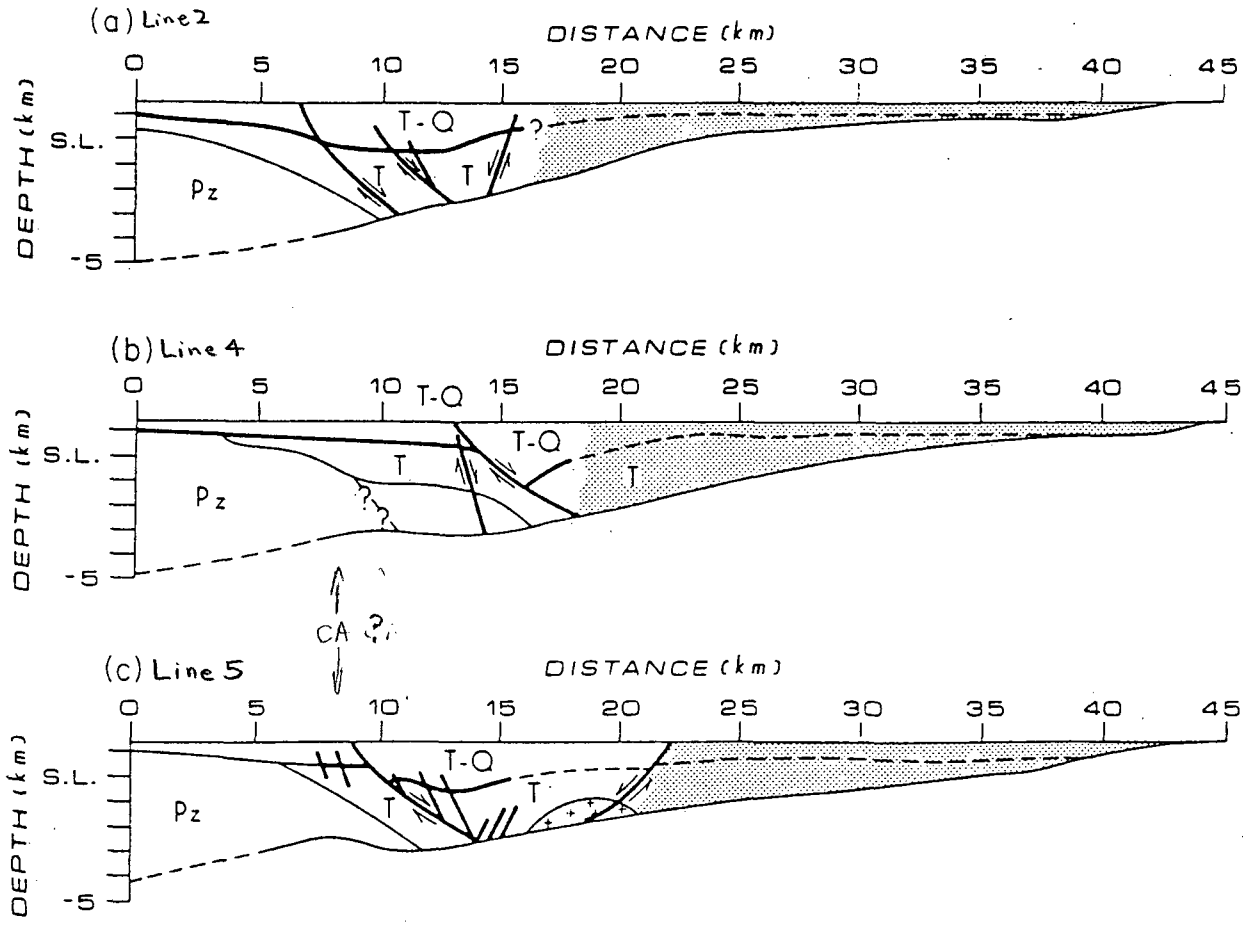

Fig. 13. Geological east-west cross sections of the Sevier Desert basin parallel to (a) line 2, (b) line 4, and (c) line 5 (Figure 2). Only major extensional faults are drawn, while the dotted areas show the location of scattered energy in the seismic sections that is possibly due to small scale faulting. Abbreviations are Pz, Paleozoic and Precambrian basement; T, Oligocene (with minor lower Tertiary) to middle Pliocene formations; and T-Q, middle Pliocene to Recent formations. Pluses indicate a possible salt dome.

carbonates and basaltic flows. Salt is present in the central part of the basin and produces major antiforms. An approximate 10° west dipping, extensional detachment surface, the Sevier Desert detachment, with a width between 80 km and 130 km and an area between 5600 km^2 and 9100 km^2, bounds the eastern part of the basin. The underlying basement rocks are mainly lower Paleozoic and Precambrian clastic and carbonate sediments and metasediments.

Evidence for early Tertiary sediments in the Sevier Desert basin is limited. On the east side of the basin the Placid Oil Henley 1 well penetrates 530 m of dolomitic siltstone and sandstone above the Paleozoic basement, that is possibly the Tertiary-Cretaceous North Horn formation. The Cominco American Inc. 2 Beaver River well penetrates carbonates (the early Tertiary Flagstaff formation?) and carbonates, claystone, and sandstone (the North Horn formation?) from 436 m to 785 m depth in the west side of the basin. Late Cretaceous and early Tertiary formations should be expected to be found in the parts of the Sevier Desert basin that were a part of this early Tertiary basin. Just above the Sevier Desert detachment the ARCO Meadow Federal 1 well penetrates 627 m of Tertiary siltstone and shale with minor very fine grained sandstone and limestone, and the ARCO Hole In The Rock 1 well penetrates 1128 m of Tertiary undivided (upper 634 m Miocene and Oligocene ?) siltstone and very fine grained sandstone (Figure 6). Furthermore, the ARCO Pavant Butte 1 well penetrates 716 m of Tertiary undivided anhydritic shale and limestone, while, finally, the Argonaut Energy 1 well penetrates a 1571 m thick Oligocene (?) rock salt sequence and a 9 m basal red conglomerate. There is therefore no evidence for any pre-Oligocene formations in any of the wells in the central Sevier Desert basin and suggests a post early-Oligocene age of the SDD. This is in agreement with a late Oligocene or early Miocene age of the SDD interpreted from deep seismic reflection data and stratigraphic relationships in the Drum Mountains [Von Tish et al., 1985].

There are no hydrocarbon producing wells in the Sevier Desert basin, and potential traps are limited due to severe Cenozoic deformation, high heat flow, and faulting. The largest reservoir potential is in the least deformed, deeper, central part of the basin. The east part of the basin is shallow, and potential cap rocks are probably more permeable because of Cenozoic faulting. Furthermore, the well data do not suggest the existence of lower Tertiary fluvial, organic rich formations that are source formations in the Uinta basin of eastern Utah (e.g., the Green River Formation), nor any

TABLE 2. Regional Extension Properties of the Sevier Desert Region.

	Line a*	Line b*	Line c*		CO-1†
		Balance Area, km²			
Tertiary‡	89	88	(78)§	84	
Middle Oligocene to middle Pliocene	53	54	(44)§	41	
Post-middle-Pliocene	36	34	—	43	
		Horizontal Displacement, km			
Tertiary‡	6.6	6.5	(5.8)§	6.2	25-38
Middle Oligocene to middle Pliocene	3.9	4.0	(3.3)§	3.0	20-30
Post-middle-Pliocene	2.7	2.5	—	3.2	< 8
		Extension Rate, mm/yr			
Tertiary‡	0.23	0.23	(0.21)§	0.22	
Middle Oligocene to middle Pliocene	0.16	0.17	(0.13)§	0.13	0.9-1.9
Post-middle-Pliocene	0.64	0.59		0.77	0.4-1.9
		Strain Rate, x10^{-16} s^{-1}			
Tertiary‡	1.1	1.1	(0.9)§	1.0	4.0-6.1
Middle Oligocene to middle Pliocene	0.7	0.8	(0.6)§	0.6	3.8-5.7
Post-middle-Pliocene	2.7	2.7	—	3.5	< 8.6
		Total Extension, %			
	0	9	(8)§	9	36-55

The length and the maximum depth of the SDD are 70 km and 12-15 km, respectively, for the balanced area extension calculations. The onset of extension began after middle Oligocene (26-28 m.y.), and the onset of the post-middle-Pliocene extension is correlated with a 4.2 m.y. old basalt flow.

* Refers to Figure 13.

† Extension rates calculated along line CO-1 using palinspastically restored cross sections [Von Tish et al., 1985].

§ Using only wedge area above T1 (see Figure 3).

‡ Average value for the post-middle Oligocene extension.

organic rich middle Tertiary formations. At deeper levels, however, hydrocarbon reservoirs may be found in the Mesozoic and the upper Paleozoic formations below possible overthrusted lower Paleozoic formations, but no wells have demonstrated the existence of any such structures.

West of the western basin-bounding fault in the Sevier Desert basin the middle Pliocene reflector B has a 3° to 6° eastward dip (Figures 3, 4, and 10). The lack of reflectors above B makes it difficult to interpret any sedimentation pattern, but weak reflectors suggest a gradual eastward thickening of the post-middle-Pliocene unit (Figures 3 and 4). Seismic lines G1 and CO-1 (Figure 2) [Smith and Bruhn, 1984; Von Tish et al., 1985] and Quaternary fault scarps and gravity data (Figure 1; Anderson and Bucknam [1979]) show a major westward dipping, normal fault west of the Cricket Mountains and west of the San Francisco Mountains. Wernicke et al. [1985] interpreted this fault to be a normal detachment fault, and using their interpretation of line CO-1, they argued that this detachment fault has not been active the last 4 m.y. The Quaternary fault scarps and the the reprocessed part of the reflection profile CO-1 of Von Tish et al. [1985] clearly suggest that the fault has been recently active.

The fault west of the Cricket Mountains may be interpreted as a normal detachment fault [Allmendinger et al., 1983; Sharp, 1984; Wernicke et al., 1985] or as a normal fault that detached at the SDD at 10-15 km depth east of the House Range. Regional interpretation of line G1 [Smith and Bruhn, 1984] and a speculative correlation of the SDD and the deep detachment mapped below the Milford Valley and the San Francisco Mountains [Baker, 1986, Figure 21] support the latter interpretation. In this case, the backtilt of reflector B may not only be due to rotation of the hanging wall of the SDD but partially also due to uplift of the footwall block of the fault west of the Cricket Mountains. High-quality reflection data south and west of the Cricket Mountains are required to solve this question.

The amount of uplift which may be associated with normal faulting can be inferred from historic earthquakes in the Basin and Range province. Up to 6 m subsidence of the hanging wall and up to 0.5 m of footwall uplift have been mapped after recent large normal fault earthquakes in the Basin and Range province, for example, the Dixie Valley earthquake (1954, M 7.1), the Hebgen Lake earthquake (1959, M 7.5), and the Borah Peak earthquake (1983, M 7.3) [Savage and Hastie, 1966; Smith and Richins, 1984]. The magnitude and the extent of the co-seismic footwall deformation associated with these earthquakes is not conclusive due to measuring errors in a mountainous terrains and the possible compaction of alluvium by the strong ground shake [Savage and Hastie, 1966]. However, using the elastic theory of displacements [Maruyama, 1964], the vertical displacement of the free surface can be calculated for dip-slip motion. This approach was used by Savage and Hastie [1966] and suggests an approximate footwall uplift of 0.5 to 1.0 m for a M 7+ earthquake that would likely nucleate at a 10-20 km depth in the Basin and Range province [Smith and Richins, 1984; Smith et al., 1989].

A 1 to 2 km post-middle-Pliocene vertical displacement of the Cricket Mountains fault can be interpreted from seismic reflection data [Von Tish et al., 1985; Barker, 1986]. Estimating the maximum footwall uplift of a M 7+ earthquake to be 1 m, a total uplift of 100-200 m of the Cricket Mountains is estimated. The distance between the Cricket Mountains fault and the major western Sevier Desert basin-bounding fault is 15-30 km, which gives a dip of 0.2° to 0.8° east for the Cricket Mountains fault block. This is almost an order of magnitude smaller than the observed dip, 3°-6°, of the mid-Pliocene reflector, that would require an 0.8 to 3.2 km uplift of the footwall of the Cricket Mountains fault. The earthquake deformation model can therefore account for only 10% to 25% of the observed dip of the mid-Pliocene reflector.

For a thrust sheet thicker than 5 km it can be shown that a

gravitationally driven wedge moves in the direction of the topographic slope and that the basal shear stress can be described by $\tau = f(\alpha)$, where α is the surface slope [Elliot, 1976; Platt, 1986]. Assuming that the dominant force at shallow levels in an extensional detachment regime is due to the weight of the overburden, this model was applied to the SDD. The Sevier Desert has almost no topography; therefore α may be used as the slope of the detachment surface (Figure 13). From the model equation it can then be seen that the direction of the basal shear stress τ changes direction when the slope of the detachment surface α changes sign. This occurs on profiles b and c in Figure 13 just 2-3 km west of the western basin-bounding fault. On both these profiles a larger post-middle-Pliocene offset is interpreted than on the seismic lines north and south (Table 1). The ~6 km eastward step of the western basin-bounding fault at ~39°55'N (Figure 10) and the variable offset of the western basin-bounding fault is therefore possibly an effect of the direction of the basal shear stress.

A ~6 km eastward step at ~38°55'N and a smoother ~3 km westward step at ~39°5'N is seen on the western basin-bounding fault (Figure 10). Line 4 (Figure 4) was located between these steps of the western basin-bounding fault and is interpreted with one major listric fault with 1.4 ± 0.25 km post-middle-Pliocene offset, minor antithetic faulting, and a normal drag B reflector. A smaller post-middle-Pliocene displacement of the western basin-bounding fault is apparent south of line 4 (~500-800 m), probably because more of the extension is accommodated by smaller east and west dipping listric and planar faults. A more complex fault pattern, local synclines and anticlines, and reversed drag reflections support a more complex deformation (Figures 3 and 10). Similar structures (i.e., smaller offset on the western basin-bounding fault, reverse drag reflectors, local anticlines and synclines, and a complex fault pattern) are also apparent north of ~39°5'N (Figures 10 and 13). Surface fault scarps and Mini-Sosie profiles in this region (Figures 1 and 2) [Crone and Harding, 1984] also support a complex deformational pattern. An even smaller offset of the western basin-bounding fault is mapped on lines CO-1 and Mc8 (~350 m). The extension in the central part of the Sevier Desert basin is therefore accommodated mostly on smaller westward dipping faults. The major strain component is in an east-west direction, while the structures north and south of line 4 suggest a wrench fault component.

Acknowledgments. The seismic reflection data principally used in this study were kindly made available to the University of Utah by ARCO Oil and Gas Company. The American Stratigraphic Company provided the lithological well logs. The seismic modeling programs were kindly supplied by Harley M. Benz and V. Cerveny. The Geophysical Funds program of the Department of Geology and Geophysics, University of Utah, provided support for this project. We would finally like to thank R. W. Allmendinger, J. Thompson, and B. Wernicke for helpful reviews of the paper.

REFERENCES

Allmendinger, R. W., J. W. Sharp, D. Von Tish, L. Serpa, L., Brown, S. Kaufman, J. Oliver, and R. B. Smith, Cenozoic and Mesozoic structure of the eastern Basin and Range province, Utah, from COCORP seismic-reflection data, *Geology, 11*, 532-536, 1983.

Allmendinger, R. W., H. Farmer, E. Hauser, J. Sharp, D.Von Tish, J. Oliver, and S. Kaufman, Phanerozoic tectonics of the Basin and Range-Colorado plateau transition from COCORP data and geological data; a review, in *Reflection Seismology; the Continental Crust*, edited by M. Barazangi et al., Geodyn. Ser., vol. 14, 257-267, AGU, Washington, D.C., 1986.

Anderson, R. E., and R. C. Bucknam, Map of fault scarps in unconsolidated sediments, Richfield 1° by 2° quadrangle, Utah, scale 1:250,000, *U.S. Geol. Surv. Open File Rep. 79-1236*, 1979.

Anderson, R. E., M. L. Zoback, and G. A. Thompson, Implications of selected subsurface data on the structural form and evolution of some basins in the northern Basin and Range province, Nevada and Utah, *Geol. Soc. Am. Bull., 94*, 1055-1072, 1983.

Armstrong, R. L., Sevier Orogenic belt in Nevada and Utah, *Geol. Soc. Am. Bull., 79*, 429-458, 1968.

Barker, C. A., Upper-crustal structure of the Milford Valley and Roosevelt Hot Springs, Utah region, by modeling of seismic refraction and reflection data, M.S. thesis, 101 pp., Univ. of Utah, Salt Lake City, 1986.

Bucknam, R. C., and R. E. Anderson, Map of fault scarps on unconsolidated sediments, Delta 1° by 2° quadrangle, Utah, scale: 1:250,000, *U.S. Geol. Surv. Open File Rep. 79-366*, 1979.

Carrier, D. L., and D. S. Chapman, Gravity and thermal models for the Twin Peaks silicic volcanic center, southwestern Utah, *J. Geophys. Res. 86*, 10287-10302, 1981.

Cerveny, V., I. A. Molotkov, and I. Psencik, *Ray Methods in Seismology*, University of Karlova Press, Prague, Czechoslovakia, 1977.

Clayton, R., and B. Engquist, Absorbing boundary conditions for acoustic and elastic wave equations, *Bull. Seism. Soc. Am., 67*, 1529-1540, 1977.

Condie, K. C., and C. K. Barsky, Origin of Quaternary basalt from the Black Rock Desert region, Utah, *Geol. Soc. Am. Bull., 83*, 333-352, 1972.

Coney, P. J., D. L. Jones, and J. W. H. Monger, Cordilleran suspect terrains, *Nature, 288*, 329- 333, 1980.

Crone, A. J., and S. T. Harding, Relationship of late Quaternary fault scarps to subjacent faults, eastern Great Basin, Utah, *Geology, 12*, 292-295, 1984.

Davis, G. A., Problems of intraplate extensional tectonic, western United States, with special emphasis on the Great Basin, in *1979 Basin and Range Symposium*, edited by G. W. Newman and H. D. Goode, Rocky Mountain Association of Geology and Utah Geological Association, 41-54, 1979.

Eaton, G. P., The Basin and Range province: origin and tectonic significance, *Ann. Rev. Earth Planet. Sci., 10*, 409-440, 1982.

Eddington, P. J., Smith, R. B., and Renggli, Kinematics of Great Basin intraplate extension, eds. Coward, M. P., Dewey, J. F., and Hancock, P. L., in *Continental Extension*, London Geological Soc., Special Publication 28, 371-392, 1987.

Elliot, D., The motion of thrust sheets, *J. Geophys. Res. 81*, 950-963, 1976.

Gants, D. G., Geologic and mechanical properties of the Sevier Desert detachment as inferred by seismic and rheologic modeling, M.S. thesis, 129 pp., Univ. of Utah, Salt Lake City, 1985.

Gross, W. W., and F. L. Hillemeyer, Geometric analysis of upper-plate fault patter in the Whipple Buckskin detachment terrain, in *Mesozoic-Cenozoic Tectonic Evolution of the Colorado River Region, California, Arizona, and Nevada*, edited by E. G. Frost and D. L. Martin, 256-266, Cordilleran Publishers, 1982.

Hamilton, W., Mesozoic tectonics of the Western United States, in *Mesozoic Paleogeography of the Western United States: Pacific Section, Pacific Coast Paleogeography Symposium 2*, edited by D. G. Howell and K. A. McDougall, Society of Economic Paleontologists and Mineralogists, 33-70, Los Angeles, Calif., 1978.

Hintze, L. F., Geologic history of Utah, B. J. Kowallis, ed., *Brigham Young Univ. Geol. Stud*, Special Publication 7, 203 pp., 1988.

Hintze, L. F., *Geologic map of Utah*, scale 1:500,000, Utah Geol. and Miner. Surv., Salt Lake City, 1980.

Kelly, K. R., R. W. Ward, S. Treitel, and R. M. Alford,

Synthetic seismograms: a finite-difference approach, Geophysics, 41, 2-27, 1976.
Lawson, L. L., and R. J. Hanson, *Solving Least Square Problems*, Prentice-Hall, Englewood Cliffs, N.J., 1974.
Lindsey, D. A., R. K. Glanzman, C. W. Naeser, and D. J. Nichols, Upper Oligocene evaporites in basin fill of Sevier Desert region, western Utah, *Am. Assoc. Pet. Geol. Bull.*, *65*, 251-260, 1981.
Liu, C., T. Zhu, H. Farmer, and L. Brown, An expanding spread experiment during COCORP field operation in Utah, in *Reflection Seismology: a Global Perspective*, edited by M. Barazangi, Geodyn. Ser., 13, 327-246, AGU, Washington, D.C. 1986.
Maruyama, T., Statical elastic dislocations in an infinite and semi-infinite medium, *Bull. Earthquake Res. Inst.,Univ. Tokyo*, 42, 289-368, 1964.
McDonald, R. E., Tertiary tectonics and sedimentary rocks along the transition: Basin and Range province to plateau and thrust belt province, Utah, in *Rocky Mountain Association of Geology Symposium*, edited by J. G. Hill, Rocky Mountain Association of Geology, Denver, Colorado, pp. 281-317, 1976.
Mitchell, G. C., and R. E. McDonald, History of Cenozoic extension in central Sevier Desert, west-central Utah, from COCORP seismic reflection data: Discussion, *Am. Assoc. Petrol. Geol. Bull.*, 70, 1015-1021, 1986.
Mitchell, G. C., Stratigraphy and regional implications of the Argonaut Energy no. 1 Federal, Millard county, Utah, in *Basin and Range Symposium and Great Basin Field Conference*, edited by C. G. Newman, 503-514, Rocky Mountain Association of Geology, Denver, Colo., 1979.
Pechmann, J. C., W. D. Richins, and R. B. Smith, Evidence for a "double Moho" beneath the Wasatch Front, Utah (abstract), *Eos Trans., AGU*, 65, 988, 1985.
Pedersen, L. B., Interpretation of potential field data - A generalized inverse approach, *Geophys. Prospect. 25*, 199-230, 1977.
Picha, F., and R. I. Gibson, Basement control of the Sevier Orogenic belt in Utah (abstract), *Geol. Soc. of Am.*, Abstr. With Programs, 15, 378, 1983.
Planke, S., Cenozoic structures and evolution of the Sevier Desert basin, west-central Utah, from seismic reflection data, M.S. thesis, 163 pp., Univ. of Utah, Salt Lake City, 1987.
Platt, J. P., Dynamics of orogenic wedges and the uplift of high-pressure metamorphic rocks, *Geol. Soc. of Am. Bull.*, *97*, 1037-1053, 1986.
Savage, J. C., and L. M. Hastie, Surface deformation associated with dip-slip faulting, *J. Geophys. Res.*, *71*, 4897-4904, 1966.
Serpa, L. F., Detailed gravity and aeromagnetic surveys in the Black Rock Desert area, Utah, M.S. thesis, 210 pp., Univ. of Utah, Salt lake City, 1980.
Sharp, J. W., West-central Utah; palinspastically restored sections constrained by COCORP seismic reflection data, M. S. thesis, 60 pp., Cornell Univ., Ithaca, N.Y., 1984.
Smith, R. B., Seismicity, crustal structure, and intraplate tectonics of the interior of the western Cordillera, in Cenozoic Tectonics and Regional Geophysics of the Western Cordillera, edited by R. B. Smith and G. P. Eaton, *Mem. Geol. Soc. Am. 152*, 111-141, 1978.
Smith R. B., and R. L. Bruhn, Intraplate extensional tectonics of the eastern Basin-Range; inference on structural style from seismic reflection data, regional tectonics, and thermal-mechanical modeling of brittle-ductile deformation, *J. Geophys. Res.*, 89, 5733-5762, 1984.
Smith, R. B., and W. D. Richins, Seismicity and earthquake hazard of Utah and the Wasatch front: Paradigm and paradox, in Proceedings of Conference XXVI; a Workshop on Evaluation of Regional and Urban Earthquake Hazards and Risks in Utah, edited by W. W. Hays, *U.S. Ge Surv. Open File Rep.*, 84-0763, 73-112, 1984.
Smith, R. B., and M. L. Sbar, Contemporary tectonics and seismicity of the western United States with emphasis on the Intermountain seismic belt, *Geol. Soc. Am. Bull.*, *85*, 1205-1281, 1974.
Smith, R. B., W. C. Nagy, K. A. Julander, J. J. Viveiros, C. A. Barker, and D. G. Gants, Geophysical and tectonic framework of the eastern Basin and Range-Colorado Plateau-Rocky Mountain transition, in Geophysical Framework of the Continental United States, *Geol. Soc. America Memoir. 172*, 205-233, 1989.
Villien, A., and R. Kligfield, Thrusting and synorogenic sedimentation in central Utah, in Sedimentation and Tectonics in the Rocky Mountain Region, edited by J. A. Peterson, *Am. Assoc. Petrol. Geol., 41*, 281-307, 1986.
Von Tish, D. B., R. W. Allmendinger, and J. W. Sharp, History of Cenozoic extension in central Sevier Desert west-central Utah, from COCORP seismic reflection data, *Am. Assoc. Petrol. Geol. Bull., 69*, 1077-1087, 1985.
Wernicke, B., Low-angle normal faults in the Basin and Range Province: Nappe tectonics in an extending orogen, *Nature*, *291*, 645-647, 1981.
Wernicke, B., J. D. Walker, and M. S. Beaufait, Structural discordance between neogene detachments and frontal Sevier thrusts, Central Mormon Mountains, Southern Nevada, *Tectonics*, *4*, 213-246, 1985.
White, N. J., J. A., Jackson, and D. P. McKenzie, The relationship between the geometry of normal faults and that of the sedimentary layers in their hanging walls, *J. Struct. Geol.*, *8*, 897-909, 1986.
Zoback, M. L., E. R. Anderson, and G. Thompson, Cainozoic evolution of the state of stress and style of tectonism of the Basin and Range province of the western United States, *Philos. Trans. R. Soc. London, Ser. A* 300, 407-434, 1981.

S. Planke, Institutt for Geologi, University of Oslo, P. O. Box 1047, Blindern, 0316 Oslo 3, Norway.
R. B. Smith, Department of Geology and Geophysics, University of Utah, Salt Lake City, UT 84112.

(Received September 18, 1989;
revised June 20, 1990;
accepted August 27, 1990.)

TECTONICS, VOL. 10, NO. 3, PAGES 577-586, JUNE 1991

SLIP LINE MODEL FOR SOUTHERN CALIFORNIA CRUSTAL KINEMATICS

Yongshun Chen[1] and J. Bernard Minster

Institute of Geophysics and Planetary Physics, Scripps Institution of Oceanography, La Jolla, California

Abstract. We propose a simple slip line model to explain the faulting and seismicity patterns of southern California. We assume the Sierra Nevada–Great Valley (SNGV) block to be rigid, in view of its low seismicity, and other regions to undergo plastic deformation. From this point of view, the complex deformation patterns observed in southern California, including the Borderland region, result from the "plowing" of the eastern margin of the Pacific plate by the nondeforming SNGV block. A simple analogy can then be made between regional tectonics in southern California and two-dimensional flow solutions obtained in metallurgy for the extrusion of rigid-plastic metals. We use a simplified geometry based on the geology and seismicity of southern California to calculate a two-dimensional slip line field which predicts the shape of the San Andreas fault near the "big bend" surprisingly well. The largely aseismic, high-topography western Mojave can then be interpreted as an analogue to the nondeforming "dead metal" zone which arises for certain metal extrusion geometries. The slip field agrees quite well with the strikes and slip orientation of major dextral faults in southern California, including the San Jacinto, Elsinore, and Newport-Inglewood faults. It also predicts correctly the strikes and slip orientation of sinistral "cross faults" found in some areas of the region. In the Transverse Ranges, where thrust faulting dominates, the slip lines are no longer potential fault planes, but a simple argument predicts that they should lie at 45° on the strikes of thrust faults, in fair agreement with the observations.

[1]Now at College of Oceanography, Oregon State University, Corvallis, Oregon.

Paper number 91TC00166.
0278-7407/91/91TC-00166$10.00

INTRODUCTION

Perhaps one of the most heavily studied fault systems in the world is the San Andreas fault system in California, which is part of the boundary between the Pacific and North American Plates in the western United States. In particular, the San Andreas fault system in southern California comprises a complex array of subparallel faults that form a plate boundary deformation zone up to 300 km wide, and raises several fundamental questions. For example, what causes the "big bend" of the San Andreas fault in southern California which offsets the fault about 150 km (Figure 1a)? Why does it have a curved shape instead of a simple left step? How are the major right-lateral faults in southern California, for instance, San Jacinto, Elsinore, Newport-Inglewood, related to the San Andreas? Why is the Mojave block, a triangle-shaped area bounded on the north by the Garlock fault and on the southwest by the San Andreas big bend, largely uncut by major active faults (Figure 1a), and why is it, in fact, almost aseismic by southern California standards (Figure 1b)?

In this paper we examine a simple mechanical model to explore these issues. Following previous authors [e.g., Hill, 1982; Minster and Jordan, 1984, 1987) we take the Sierra Nevada–Great Valley (SNGV) block to be rigid, in view of its low seismicity. We assume other regions in the plate boundary deformation zone to undergo plastic deformation. From this viewpoint, using a metallurgical analogy, the complex deformation pattern observed in southern California, including the Borderland region, results from the "plowing" of the eastern margin of the Pacific plate by the SNGV block, which acts as a rigid one-sided snowplow. We can then attempt to use simple two-dimensional flow solutions obtained in metallurgy for the machining of a rigid/plastic metal to describe the geometry and interpret the mechanics of tectonic faulting in southern California. In particular, we seek to predict correctly the geometry of faults of the San Andreas

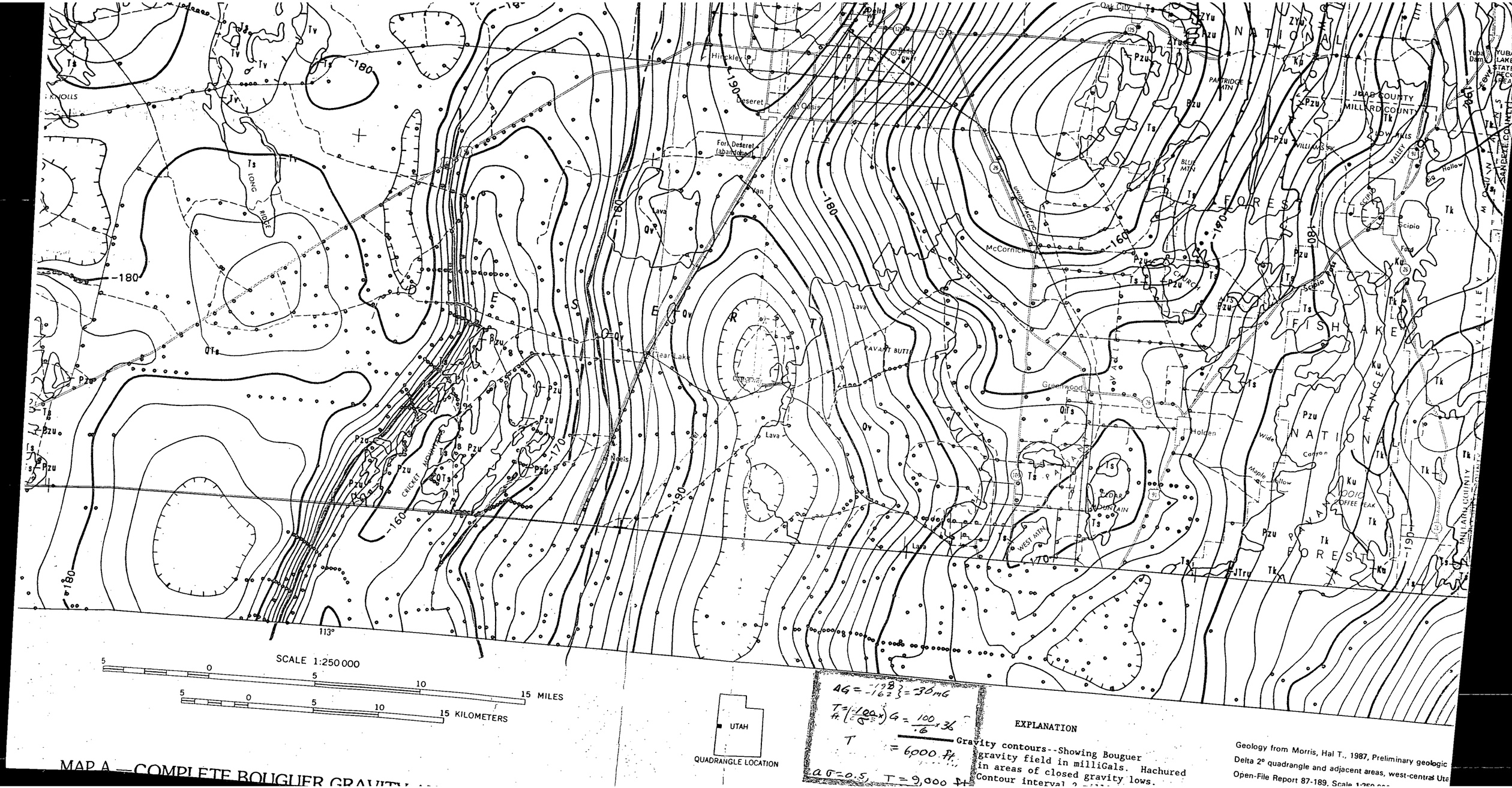

$\Delta G = -198 - (-162) = 36 mG$

$T = \left(\frac{100}{\sigma = 2}\right) G = \frac{100}{.6} \times 36$

$T = 6{,}000$ Ft.

$\sigma = 0.5$, $T = 9{,}000$ Ft

MAP A.—COMPLETE BOUGUER GRAVITY

6/03/93
H.P. Ross

Call to: Viki Bankey
USGS MS964
Box 25046 DFC
Denver, CO 80225
(303) 236-1348

Re: Delta Quad (AMS) Gravity Map
"Complete Bouguer gravity anomaly map of Utah"

① State of Utah Map, Cook, Bankey, DePangher and Makay, 1989
is also fully terrain corrected.

② 9-track tape of statewide data set is available from
Attn: Kent Hegge
EROS Data Center tel: (605) 594-6976
Souix Falls, SD 57198

cost: $80.00

Ken Cook has a copy of tape: she thought the UGS also ha
a copy, can't remember who;
Phil Wannamaker (UURI) should have a copy.

③ EROS Data Center also has tape of gravity data
for Nevada and Idaho

④ Note on Delta Quadrangle: Isotatic Map is 30 mGals too lo
so add +30 mGals. studying error source now.
A pure 30 mGal base level shift. (Viki Bankey, 6/03/93)

Thermal springs and wells in the United States (excluding Alaska and Hawaii)—Continued

No. on figure	Name or location	Temperature of water (°F)	Flow (gallons per minute)	Associated rocks	References on chemical quality	Remarks and additional references
			Utah (See fig. 7.) P17			
1	Warm Springs in sec. 20, T. 12 N., R. 15 W., 17 miles north-northwest of Terrace railroad station.	Warm	900	Alluvium		Water used for irrigation. Ref. 508.
2	Blue (Honeyville) Springs, in T. 13 N., R. 5 W., 18 miles southeast of Snowville.	86	B-13-5)	do	508	6 springs. Refs. 144, 521.
3	Udy's Hot Springs, near the Malad River 2 miles southwest of Plymouth.	90–122	3,500	Carboniferous strata near Wasatch fault.		8 main springs. Water is saline. Used for bathing. Resort. Refs. 144, 508.
4	Crystal Springs, in T. 11 N., R. 2 W., 12 miles north of Brigham City.	121–134	B-11-2	do	508	About 30 springs. Water used locally. Refs. 124, 133, 144, 505, 521.
4A	Near south end of Little Mountain, 7 miles west-northwest of Corinne.	Warm	Small	Paleozoic strata	508	
5	T. 6 N., R. 5 W., on east side of Promontory Point.	84	B-6-5	Faulted (?) schist and gneiss (Precambrian).		Ref. 144.
6	Utah (Bear River) Hot Springs, in T. 7 N., R 2 W., 8 miles northwest of Ogden.	131–144	B-7-2 110	Faulted quartzite (Cambrian).	20, 133, 137, 144, 409, 522.	12 springs. Water is saline and ferruginous. Ref. 138.
6A	Clay's Hot Springs, 10 miles north of Ogden.	140	50	Quartzite on Wasatch fault		2 springs. Water is saline and ferruginous. Used for bathing. Ref. 512.
7	Patio Spring, 12 miles northeast of Ogden	68	200	Lake beds (Quaternary)		Water used for bathing.
8	Ogden Hot Springs, in T. 6 N., R. 1 W., at mouth of Ogden Canyon.	121; 150	B-6-1 Small	Syenite on Wasatch fault	522	2 springs. Water used for bathing. Refs. 138, 144, 418, 505.
9	Big Springs, in T. 2 S., R. 8 W., on the west side of Stansbury Range.	74	C-2-8	Carboniferous strata near fault.		2 springs. Water is brackish. Ref. 144.
10	Grantsville Warm Springs, 5 miles northwest of Grantsville.	74–91	50	Wasatch Formation (Eocene).		6 springs. Water is brackish; used for bathing. Deposit of calcareous tufa. Refs. 138, 144, 508.
10A	Morgan's Warm Springs, 4 miles southwest of Stockton.	80	500	do		Water is ponded. Used for bathing and irrigation.
10B	Russell's Warm Springs, 4.5 miles southwest of Stockton.	90	200	do		Water is ponded. Used for irrigation.
11	Beck's Hot Springs, 4 miles north of Salt Lake City.	128		Paleozoic strata on Wasatch fault.	128, 133, 137, 418.	Several springs. Water smells of H_2S. Resort. Refs. 124, 144, 511, 512, 521, 685.
11A	Warm Springs, 2 miles north of Salt Lake City.	118	350	do	525	Water used for bathing. Refs. 137, 511–513, 523.
12	Wasatch Springs, in the northwestern part of Salt Lake City.	130	350	Limestone (Carboniferous) near Wasatch fault.	525	Water used for bathing. Sanitarium. Refs. 133, 137, 144, 513, 523.
13	Crystal Springs, in T. 4 S., R. 1 W., 4 miles southwest of Draper.	70	C-4-1	Alluvium		Several springs. Water used for bathing. Refs. 138, 144, 523.
14	Schneitter's Hot Pots, 4.5 miles northwest of Heber.	85–116	20	Wasatch Formation (Eocene) near Carboniferous limestone.	133, 137	20 main springs. Water used for bathing. Extensive deposit of tufa. Refs. 138, 144, 418, 514, 526.
14A	Luke's Hot Pots, 4 miles northwest of Heber.	78–110	30	do		Several springs. Water used for bathing. Ref. 514.
14B	Buhler's Springs, 3.5 miles northwest of Heber.	80–108	10	do		Several springs. Water used for bathing. Extensive deposit of tufa. Refs. 138, 510, 514.
15	Saratoga Springs, on northwest shore of Utah Lake.	111	211	Wasatch Formation (Eocene).		Several springs. Water used for bathing. Resort. Ref. 523.
16	T. 8 S., R. 1 E., on south shore of Utah Lake 8 miles northwest of Payson.	88	D-8-1 200	Alluvium		Water used locally. Ref. 523.
17	T. 10 S., R. 1 E., near the north end of Long Ridge 2 miles east of Goshen.	70	D-10-1 2,000	Faulted Carboniferous strata.		Several springs. Water used locally. Ref. 523.
18	Castilla Mineral Springs, in T. 9 S., R. 3 E., in Spanish Fork Canyon 15 miles south of Provo.	111; 145	D-9-3	Carboniferous strata near Wasatch fault.		3 springs. Resort. Refs. 138, 144, 523.
19	Sec. 14, T. 8 S., R. 5 E., on Diamond Creek 15 miles east of Springville.	Warm	D-8-5 700	Wasatch Formation (Eocene).		2 springs. Water smells of sulfur.
19A	12 miles northeast of Jensen, in canyon of Green River.	90	10	Paleozoic or Mesozoic strata.		2 springs issuing at river edge.
20	Hot Springs, in T. 11 S., R. 14 W., at north end of Fish Springs Mountains and 3 miles north-northeast of Fish Springs (town).	74–78	C-11-14	Alluvium near faulted Paleozoic strata.		Several springs. Water used locally. Refs. 138, 144, 506, 515, 520.
21	Big Spring, in T. 11 S., R. 14 W., 1 mile southeast of Hot Springs (No. 20).	85	C-11-14	do		3 springs. Refs. 144, 506, 520.
22	Fish Springs, in T. 11 S., R. 14 W., 4 miles southeast of Hot Springs (No. 20) and 3 miles east of Fish Springs (town).	80–140	C-11-14	do	406	7 springs. Water smells strongly of H_2S. Large deposit of tufa. Refs. 144, 406, 506, 515, 520.
23	Sec. 33, T. 14 S., R. 18 W., on Miller's Ranch 8 miles south of Trout Creek.	64	500	Alluvium		Several springs rising in pools. Water used for irrigation. Refs. 506, 520.
24	Abraham Springs in T. 14 S., R. 8 W., on Fumarole Butte, 19 miles north-northwest of Delta.	100–205	C-14-8 200	Fractured lava (Tertiary)	507	20 springs. Deposit of manganese. Refs. 109, 144, 509, 512, 516, 520.
25	Sec. 31, T. 15 S., R. 19 W., in Snake Valley 1 mile west of Gandy.	82	C-15-19)31 Large	Limestone (lower Paleozoic)		Several springs. Water used for irrigation. Deposit of tufa. Ref. 520.
26	Sec. 9, T. 16 S., R. 18 W., in Snake Valley 2 miles south of Foote's Ranch.	68	C-16-18)9 000	Alluvium		Several springs rising in pools. Water used for irrigation. Refs. 144, 520.
27	Knoll Springs, in sec. 11, T. 18 S., R. 18 W., in Snake Valley 12 miles southeast of Smithville.	68–71	C-18-18)11	Alluvium near Carboniferous strata.		Several springs. Water smells of H_2S. Used locally. Refs. 144, 520.
28	Sec. 24, T. 22 S., R. 6 W., 3 miles northwest of Hatton.	94	C-22-6)24 Large	Interbedded tuff and lava (Tertiary).		Water used for irrigation. Ref. 520.
29	Brewer's Springs, in secs. 13 and 24, T. 15 S., R. 2 E., 1 mile northwest of Wales.	57–62	400	Alluvium near faulted Wasatch Formation (Eocene).		3 springs. Water used for domestic purposes and irrigation. Ref. 524.
30	Lowry's Spring and Squires' Spring, in sec. 23, T. 18 S., R. 2 E., 3 miles south of Manti.	59; 62	40	Faulted Wasatch Formation (Eocene).		Water used for irrigation. Ref. 524.
31	Livingston Warm Springs, in sec. 13, T. 18 S., R. 2 E., 1 mile south of Manti.	62; 73	D-18-2)13 285	do		2 main springs. Water used for domestic purposes and irrigation. Ref. 524.
32	Manti Springs, in sec. 17, T. 18 S., R. 3 E., 2 miles southeast of Manti.	59; 65	30	do		Do.
33	Morrison Spring, in sec. 35, T. 18 S., R. 2 E., 2 miles northeast of Sterling.	61	2,500			Water used for irrigation. Ref. 524.
34	Gunnison Spring, in sec. 18, T. 19 S., R. 1 E.	61	8	Alluvium		Water supply for cattle. Ref. 524.

Thermal springs and wells in the United States (excluding Alaska and Hawaii)—Continued

No. on figure	Name or location	Temperature of water (°F)	Flow (gallons per minute)	Associated rocks	References on chemical quality	Remarks and additional references
			Utah—Continued			
35	Ninemile Warm Spring, in sec. 4, T. 19 S., R. 2 E.	72	D-19-2)4 900	Alluvium near faulted Wasatch Formation (Eocene).		Water used for domestic purposes and irrigation. Ref. 524.
36	Sec. 32, T. 20 S., R. 2 E., 8 miles northeast of Redmond.	58	15	Faulted Wasatch Formation.		Water used for irrigation. Ref. 524.
37	Redmond Springs, in secs. 11 and 12, T. 21 S., R. 1 W., near Redmond.	70	C-17-1)11, 12 6,000	do		Several springs. Water used for domestic purposes and irrigation. Ref. 524.
38	Salt Spring, in sec. 17, T. 21 S., R. 1 E., 2 miles northeast of Salina.	72	D21-1)17 2	Faulted Jurassic strata		Ref. 524.
39	Oak Spring and Christianson Spring, in sec. 1, T. 22 S., R. 2 W., 2 miles west of Aurora.	60	20	Faulted lava (Eocene)		Water supply for cattle. Ref. 524.
40	Herrin's Hole Spring, in sec. 23. T. 23 S., R. 2 W., 1 mile north of Glenwood.	63	450	do		Water used for irrigation. Ref. 524.
41	Cove Springs, in sec. 27, T. 23 S., R. 2 W., 1 miles west of Glenwood.	60	4,000	do		Several springs. Water used for irrigation. Ref. 524.
42	Richfield Hot Springs, in sec. 26, T. 23 S., R. 3 W.	74	C-23-3)36 1,500	Faulted limestone (Eocene)		Several springs. Water supply for town; also used for irrigation. Ref. 524.
43	Indian Spring and Parcel Creek Spring, in sec. 25, T. 23 S., R. 2 W., near Glenwood.	60	130	Faulted lava (Eocene)		Water used for domestic purposes and irrigation. Ref. 524.
44	Sec. 5, T. 24 S., R. 2 W., 2 miles southeast of Richfield.	52-61	4,500	Lava (Tertiary)		Several springs. Water used for irrigation. Ref. 524.
45	Sec. 25, T. 24 S. R. 3 W., 6 miles south of Richfield.	59	25	Alluvium overlying Wasatch Formation (Eocene).		Water used for domestic purposes and irrigation. Ref. 524.
46	Jericho Spring, in sec. 6, T. 25 S., R. 3 W., 2 miles northeast of Joseph.	65	700	Alluvium		Water used for irrigation. Ref. 524.
47	Johnson Spring, in sec. 27, T. 25 S., R. 3 W., 2 miles southeast of Monroe.	80	C-25-3)27 200	Faulted lava and tuff (Eocene).		Do.
48	Cooper Hot Springs, in sec. 15, T. 25 S., R. 3 W., 0.5 mile east of Monroe.	144-156	C-25-3)15 100	Faulted tuff (Tertiary)	524	Several springs. Water used for irrigation.
49	Joseph Hot Springs, in sec. 23, T. 25 S., R. 4 W., 1 mile southeast of Joseph.	135-146	C-25-4)23 30	Lava (Tertiary)		Several springs. Water used for irrigation. Deposit of tufa. Ref. 524.
50	Savier Spring, in sec. 32, T. 25 S., R. 4 W.	59	100	Alluvium		Water used for domestic purposes; also water supply for cattle. Ref. 524.
51	Roosevelt (McKean's) Hot Spring, in T. 27 S., R. 9 W., on west slope of Mineral Mountains 15 miles northeast of Milford.	192	C-27-9) 10	Granite	518	Water smells strongly of H_2S. Water supply for cattle. Deposits of tufa and sinter.
52	Warm Springs, secs. 21 and 28, T. 30 S., R. 12 W., 2 miles south-southwest of Thermo railroad siding.	90-175	C-30-12)21, 28 20	Alluvium near faulted(?) lava (Tertiary).	518	About 16 springs issuing from a low ridge. Deposits of dense calcareous tufa. Water supply for cattle.
53	Radium (Dotson's) Warm Springs, in sec. 7, T. 30 S., R. 9 W., 1 mile east of Minersville.	97	C-30-9)7 37	Quartzite	518	3 springs. Water used for bathing and irrigation.
54	La Verkin Hot Springs, on Rio Virgin 2 miles north of Hurricane.	108-132	1,000	Faulted Triassic strata		Several springs. Refs. 133, 144.
55	T. 37 S., R. 7 W., 25 miles southwest of Panguitch.	Warm		Lava (Tertiary) overlying Wasatch Formation (Eocene).		Ref. 138.
56	Undine Springs, in T. 25 S., R. 17 E., in Labyrinth Canyon of the Green River.	Warm		Sandstone (Triassic)		Many small springs. Deposit of tufa. Ref. 138.
57	Warm Spring Canyon near its junction with "Narrow Canyon" or "Dark Canyon" of the Colorado River.	91		do		Ref. 138.
			Virginia (See fig. 3.)			
1	Limestone Springs, near Compton	61-66		Folded or faulted Paleozoic strata.		3 springs. Water used locally. Refs. 133, 538, 541.
2	Warm Spring, 1 mile south of Bridgewater	64	500	do		Water used locally. Ref. 538.
3	Dice's Spring, 1 mile southeast of Burketown.	65	1,500-2,000	do		Do.
4	Fitzgerald Spring, near Middle River Bridge, 2.25 miles west of Fort Defiance.	61	60	do		Do.
5	Bragg Spring, 2.25 miles northeast of Bolar	75	50	do		Do.
6	Bolar Spring, 3 miles northeast of Bolar	72	4,500	do		Do.
7	Warm Sulphur Springs, at Warm Springs (town).	91-96	1,200	do	133, 144, 541, 543	4 springs. Resort. Refs. 529, 538.
8	Hot Springs, at Hot Springs (town)	72-106		do	20, 128, 133, 137, 144, 409, 541, 543.	7 springs. Resort. Refs. 529, 538, 542.
9	Healing (Rubino Healing, Sweet Alum) Springs, at Healing Springs (town).	82-88		do	133, 137, 139, 144, 409, 543.	4 springs. Water bottled and marketed. Resort. Refs. 538, 541.
10	Mill Mountain Springs, at Panther Gap 1.5 miles west of Goshen.	60; 65; 66	50; 800; 500	do		3 springs. Water used locally. Refs. 538, 541.
11	Rockbridge (Rockbridge Alum, Strickler's) Springs at Rockbridge Baths 10 miles north of Lexington.	72		do	137, 139	3 springs. Resort. Refs. 144, 529, 538, 541.
12	Layton (Keyser's) Springs, on the Jackson River 2 miles south of Falling Spring (No. 13).	63; 72	200	do		2 springs issuing on opposite banks of the river. Water used locally. Refs. 538, 541.
13	Falling Spring, 8 miles south of Healing Springs (No. 9).	74	7,000	do		Water used locally. Refs. 538, 541.
14	Sweet Chalybeate Springs, 3 miles north of Sweet Chalybeate.	63-68	280	do	133, 144, 541	3 springs. Resort. Ref. 538.
	Lee Carter Spring, 1.5 miles northeast of Sweet Chalybeate.	63	20	do		Water used locally.
15	C. B. Hunter Spring, 0.5 mile north of Sweet Chalybeate.	60	10	do		Do.
	R. O. Stone Spring, at Sweet Chalybeate.	73	100	do		Do.
	Sweet Chalybeate Spring, at Sweet Chalybeate.	76	1,000	do		Do.
16	Lithia (Wilson Thermal), on Mill Creek 3.25 miles east of Gala.	65	300	do	541	Water used locally. Ref. 538.
17	Blueridge (Buford's Gap) Springs, at Buford's Gap.	66-75		do		3 springs. Water used locally. Refs. 138, 541.

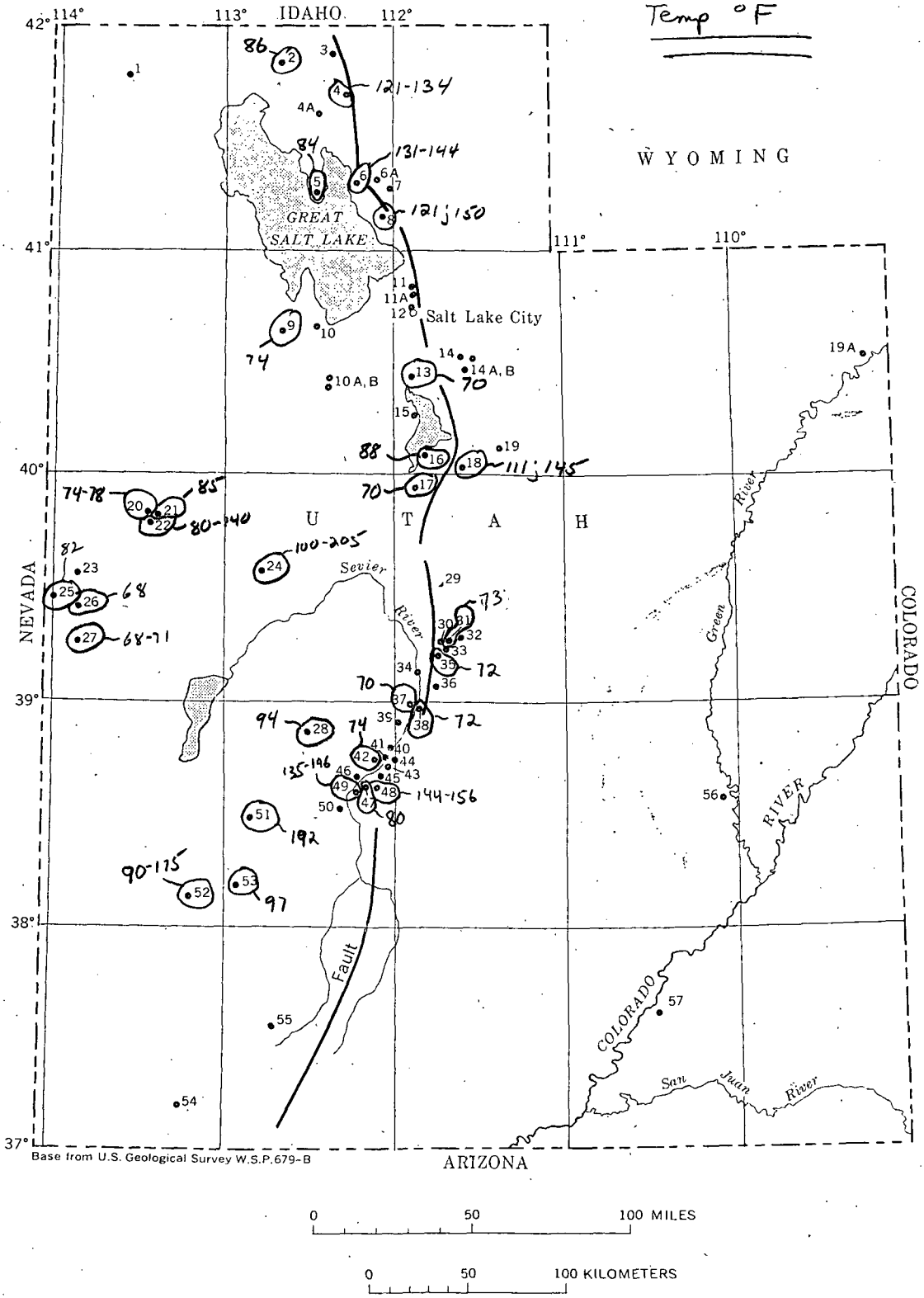

FIGURE 7.—Utah showing location of thermal springs. From ref. 148.

							HCO_3	CO_3	SO_4	Cl	F	B	Hardness	Dissolved solids	conductance	Ph
							Baker			USGS			Prof Paper 600D			
C-1 Temp 27	21		353	72	125	28	716	0	702	115	2.1	.7 NO_3 .1	1180	1840	2330	7.4
C-2 Temp 34	19		329 ~~34~~	70	111	25	686	0	643	103	2.2	.64 NO_3 .1	1110	1710	2180	7.7
C-3 Temp 32	21		329	88	163	33	584	0	805	150	2.7	.8 NO_3 0	1180	1980	2610	7.7
C-4 Temp 40	28		389	73	157	31	728	0	820	138	2.5	.74 NO_3 .1	1270	2040	2560	7.3
C-5 Temp 46	27		345	83	148	16	644	0	742	132	2.5	.64 NO_3 .4	1200	1910	2410	7.5
C-6 Temp 40	23		331	68	114	25	674	0	661	108	2.2	.67 NO_3 .1	1110	1730	2200	7.3
				C-1, 2, 3, 6			Hot pots									
				C 4, 5			Thermal Sp.									
				↙ 150 g/m		↘	1300	g/m								(4)

USGS Prof Paper 600D

Thermal springs near Midway

Temp °C

(5)

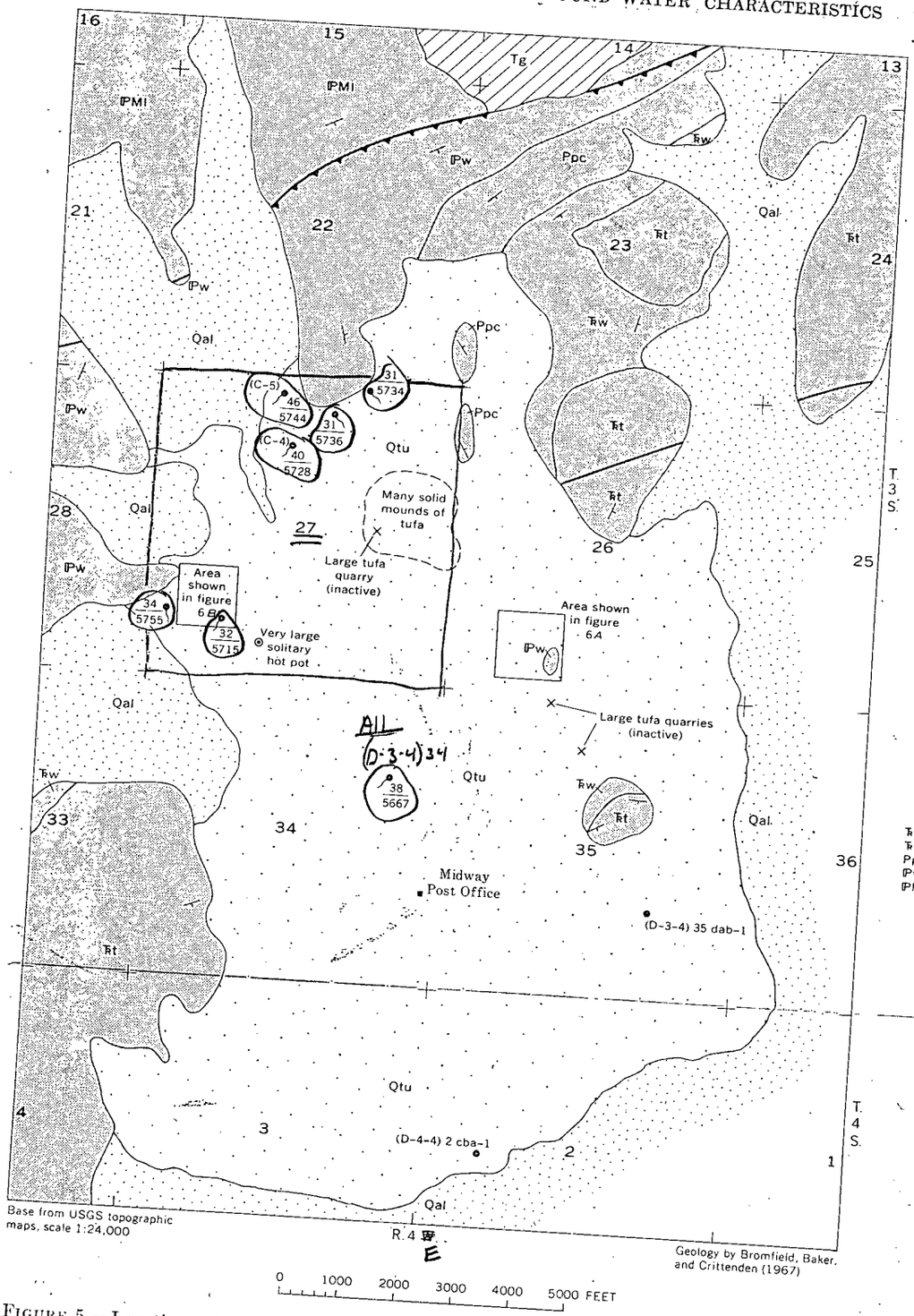

EXPLANATION

(C-4) 40 / 5728
Thermal spring
Upper number is water temperature in degrees C; lower number is altitude of water surface in feet above mean sea level. Number in parentheses identifies site sampled for chemical analysis (see table 1)

(D-3-4) 35 dab-1
Well and number referred to in text

Qtu
Tufa deposits (Quaternary)

Qal
Alluvial deposits (Quaternary)

Tg
Granodiorite (Tertiary)

Trt
Trw
Ppc
IPw
IPMi
Sedimentary rocks
Trt, *Thaynes Formation (Triassic)*
Trw, *Woodside Formation (Triassic)*
Ppc, *Park City Formation (Permian)*
IPw, *Weber Quartzite (Pennsylvanian)*
IPMi, *limestones (Pennsylvanian and Mississippian, undifferentiated)*

Contact

Strike and dip of beds

Fault

Thrust fault
Sawteeth on upper plate

FIGURE 5.—Locations of flowing thermal springs and principal areas of hot pots and solid mounds of tufa. Location of map area shown on figure 1.

All are (D-3-4)

titrated in the field to determine bicarbonate concentration, and another aliquot was acidified and sent to the laboratory for determination of calcium concentration. A clean 1-liter plastic bottle was filled with the filtered water, loosely capped, and stored. After 15 days the bottle was opened and the pH measured. A sample

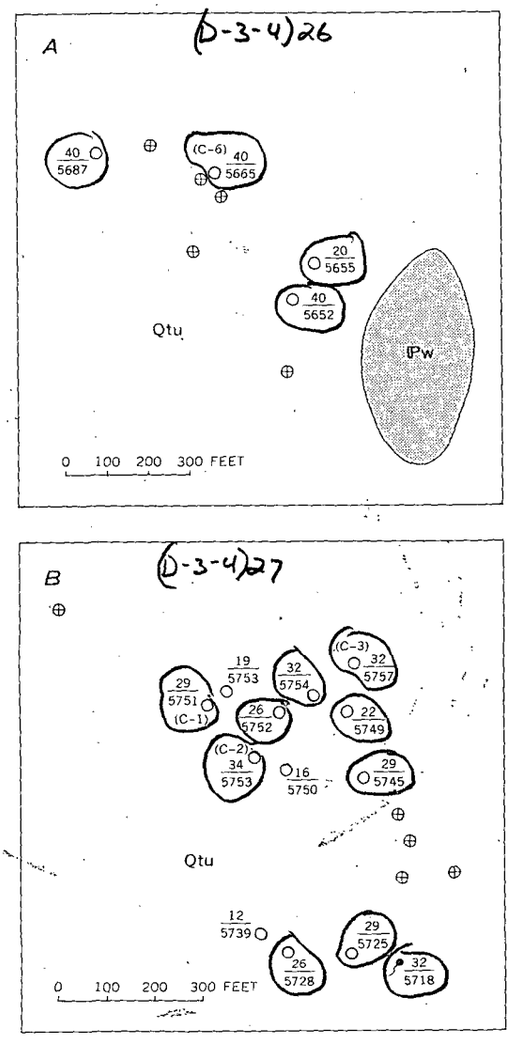

FIGURE 6.—Positions of hot pots and dry craters within the two principal clusters indicated in figure 5. *A*, eastern cluster; *B*, western cluster.

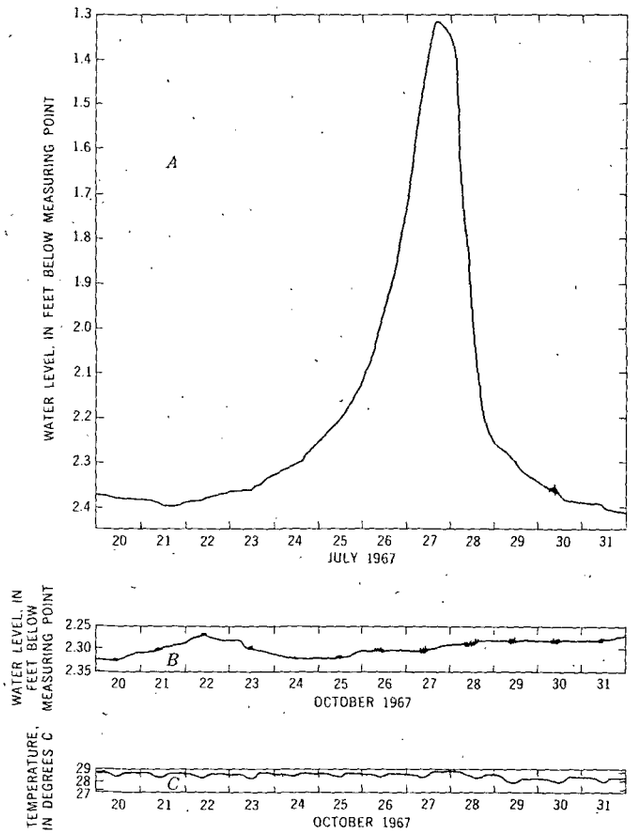

FIGURE 7.—Reproductions of charts from automatic recorders on hot pot at location C–1 (fig. 6*B*).
A, Hydrograph showing abrupt rise and fall of water level probably caused by slug of water (recharge) entering the aquifer.
B, Hydrograph showing small changes of water level caused by changes in barometric pressure and very small oscillations resulting from circulation of water within the pot due to cooling at the surface.
C, Thermograph record for the period covered by hydrograph *B*.

from the bottle was then filtered (a noticeable precipitate was present) and the concentrations of calcium and bicarbonate were determined in the laboratory. The procedure was repeated after 30 days and again after 45 days. The results are as follows:

	pH	Calcium (mg/l)	Bicarbonate (mg/l)
Field	6.8	[1] 394	780
15 days	7.3	335	644
30 days	7.5	208	276
45 days	7.7	164	122

[1] Acidified sample determined in the laboratory.

As a further comparison of the conditions existing in the laboratory and those prevailing in the aquifer, the pH required for the water samples to be in equi-

Location	well #	owner	Driller	date Drilled	size well	casing o screen	Driller's Log	Flow data	total Depth	water depth (Date)	temp/depth bhc!
					Fred Sayon Thesis						
A-4-3	31cab	Como Springs		1936	6"			200 g/m Test yield	46	26-46	84
	31cdc	Como Springs		1935	8			105 g/m test yield	146	126-146	82

chem

	Si	Fe	Ca	Mg	Na+K	HCO_3	SO_4	Cl	F	NO_3	SP cond	TDS	Hardness Ca, mg	Ph
	9	0	73	21	23	268	61	32	.43	5.8	635	370	270	7.9

Jour. Research U.S. Geol. Survey
Vol. 6, No. 1, Jan.–Feb. 1978, p. 133–147

PLEISTOCENE RHYOLITE OF THE MINERAL MOUNTAINS, UTAH—GEOTHERMAL AND ARCHEOLOGICAL SIGNIFICANCE

By P. W. LIPMAN; P. D. ROWLEY, H. H. MEHNERT;
S. H. EVANS, Jr., W. P. NASH, and F. H. BROWN;[1]
Hawaiian Volcano Observatory, Hawaii; Denver, Colo.; and Salt Lake City, Utah
With sections by G. A. IZETT and C. W. NAESER
and by IRVING FRIEDMAN, Denver, Colo.

Abstract.—Little-eroded rhyolitic tuffs, flows, and domes extend over about 25 km² along the western side of the Mineral Mountains, southwestern Utah, which is along the eastern edge of the Roosevelt KGRA (Known Geothermal Resource Area). Initial eruptions resulted in two low-viscosity lava flows of nonporphyritic rhyolite. These were followed by bedded pumice falls and nonwelded ash flows. The youngest activity produced at least nine viscous domes and small lava flows of rhyolite that contain 1–5 percent phenocrysts of quartz, plagioclase, sodic sanidine, and biotite; distinction between domes and eroded flow segments locally is difficult.

Potassium-argon ages indicate that all the rhyolite of the Mineral Mountains was erupted between 0.8 and 0.5 m.y. ago. The rhyolite rests on dissected granite of the Mineral Mountains pluton, the largest intrusion in Utah, which has yielded published K-Ar ages of 9 and 15 m.y. A small older dissected rhyolite dome, about 8 m.y. old, occurs just west of the range front. Whether the young ages of the pluton represent time of intrusion or of later reheating, they, in conjunction with the Pleistocene rhyolite in the Mineral Mountains, do indicate a major late Cenozoic thermal anomaly, the size and age of which is significant to evaluation of the Roosevelt KGRA. The rhyolite is also the only known source of implement-grade obsidian in the southwest between eastern California and northern New Mexico.

As part of the U.S. Geological Survey's geothermal energy program, age, composition, and distribution data are being obtained for upper Cenozoic volcanoes in the western United States that have erupted significant amounts of silicic rocks. Such silicic rocks, mostly rhyolites, are considered possible indicators of the subsurface presence of shallow magma chambers still sufficiently hot to have potential for geothermal resources. A rationale for this approach is outlined by Smith and Shaw (1975).

Large volumes of rhyolite associated with known geothermal resources have been described from Yellowstone National Park (Allen and Day, 1935; Christiansen and Blank, 1972), in the Jemez Mountains in New Mexico (Smith, Bailey, and Ross, 1970), and in the Long Valley area, California (Bailey, Dalrymple, and Lanphere, 1976). Around the margins of the Colorado Plateau, small volumes of similar silicic rocks that also seem worthy of reconnaissance evaluation in terms of geothermal significance occur in the San Francisco Mountains volcanic field, Arizona (Robinson, 1913; Moore, Wolfe, and Ulrich, 1974), in the Mount Taylor and Taos Plateau volcanic fields of New Mexico (Hunt, 1938; Lambert, 1966), and in the Mineral Mountains, Utah.

In the Mineral Mountains, southwestern Utah, young rhyolite masses extend discontinuously for about 15 km along the range crest and cover an area of less than 25 km²; these have been little studied and previously were interpreted as erosional remnants of a single large silicic volcano of late Tertiary age (Earll, 1957; Liese, 1957). This brief report presents new geologic data, including K-Ar ages which demonstrate that many separate lava domes, flows, and tuffs were erupted from vents along the range crest between 0.8 and 0.5 m.y. ago. Along one of the western range-front faults, about 2 km northwest of the nearest rhyolitic volcanic rocks, Roosevelt Hot Springs is located within a KGRA (Known Geothermal Resource Area) that is actively being developed for geothermal power production. The youthful silicic volcanism recorded by the rhyolite of the Mineral Mountains suggests the presence of a still-hot buried magma chamber that may be the heat source for the KGRA.

Acknowledgments.—Discussions with Glenn A. Izett and Irving Friedman, who examined the rhyolites, and Sr-Rb data on granite from the Mineral Mountains pluton by Carl E. Hedge aided the evolution of ideas on the rhyolite of the Mineral Mountains. We thank John S. Pallister and Alan Martz for assistance

[1] Department of Geology and Geophysics, University of Utah.

in the field and for making mineral separations for K-Ar dating and microprobe analyses, respectively. We also thank Gary L. Galyardt for information on the Roosevelt KGRA.

Research by authors from the University of Utah was supported by National Science Foundation Grant GI–43741 and U.S. Energy Research and Development Administration Contract no. EY–76–S–07–1601.

GENERAL GEOLOGIC SETTING

The Mineral Mountains, in west-central Utah (fig. 1), are a typical basin-range horst, which rises about 1 km above the adjacent alluviated basins, the Escalante Desert to the west and an unnamed valley to the east. The horst extends nearly 50 km in a northerly direction and is in general about 10 km wide.

On the western and northern sides of the range, metamorphic rocks of the Wildhorse Canyon Series of Condie (1960), of probable Precambrian age, are the dominant rocks, but on the southern, northern, and eastern sides of the range, Paleozoic and Mesozoic sedimentary rocks are exposed widely. These layered rocks are intruded by a distinctive body of granite, the Mineral Mountains pluton, which is the largest single exposed intrusive body in Utah, covering nearly 250 km². This granite and associated pegmatite and aplite may be as young as late Miocene, having yielded two K-Ar ages on feldspars of 15 and 9 m.y. from different sample sites (Park, 1968; Armstrong, 1970). These young apparent ages are supported in a general way by results of a Rb-Sr isotopic study. A Rb-Sr isochron, based on 11 analyses of whole-rock samples ranging in composition from diorite to aplite, shows exceptionally bad scatter but suggests that the age of the main batholith is about 35 m.y., with sizable chemical modification—especially Sr loss—having occurred 7–15 m.y. ago (C. E. Hedge, written commun., 1976).

Prior to the onset of late Cenozoic rhyolitic volcanism in the Mineral Mountains, the Mineral Mountains pluton and its country rocks were deeply dissected to form a rugged erosional topography with towering pinnacles rising above narrow usually dry valleys.

The Mineral Mountains are bounded on the west, and probably on the east side, by north-striking normal faults. The trend of the bounding faults on the west is marked locally in the Roosevelt KGRA by discontinuous elongate mounds of opaline sinter and other hot-spring deposits. Near the northern end of this trend is Roosevelt Hot Springs (Petersen, 1975). Water temperatures as high as 90°C have been recorded from Roosevelt Hot Springs, but sometime prior to 1966 the springs dried up (Mundorff, 1970). Phillips Petroleum Co., the successful bidder on the KGRA in 1974, is continuing exploration on the property. Numerous test wells so far drilled in the KGRA have documented the presence of a low-salinity liquid-dominated geothermal system (Berge, Crosby, and Lenzer, 1976; Greider, 1976). The thermal anomaly covers approximately 32 km², and reservoir temperatures exceed 250°C.

RHYOLITE OF THE MINERAL MOUNTAINS

Rhyolitic rocks in the Mineral Mountains include three stratigraphically distinct sequences. Lowermost are two nearly nonporphyritic obsidian-rich lava flows. These are overlain by a pyroclastic sequence, including both ash-fall and ash-flow tuffs. Stratigraphically highest are porphyritic rhyolite lava domes erupted from at least nine separate vents, most of which are along the range crest.

Flows of Bailey Ridge and Wildhorse Canyon

The oldest rhyolitic rocks in the Mineral Mountains are two lava flows of virtually nonporphyritic flow-layered rhyolite. One flow is exposed for about 3 km along Bailey Ridge and in Negro Mag Wash (fig. 2) northwest of Bearskin Mountain. The other is exposed for about 3.5 km along Wildhorse Canyon, west of Bearskin Mountain. Both flows were originally as much as 100 m thick and followed pre-existing valleys that drained the western side of the Mineral Mountains, with relief much like the present, and that were graded nearly to the present levels at valley fronts. Both flows are only slightly dissected, and much of their primary upper surfaces of frothy pumiceous perlitic rubble is preserved.

Where deeply dissected, both flows display similar cooling and crystallization zonations. The basal few meters of the flow, resting directly on medium- to coarse-grained Tertiary granite of the Mineral Mountains pluton, consists of dense black obsidian. The obsidian has well-developed flow lamination defined by alined microlites of feldspars and opaque oxides (fig. 3A). The basal obsidian zone grades upward within a meter or two into a well-layered zone, in which dark obsidian and light-gray or brown finely crystallized flow-layered lava alternate. The interior of the flow is as much as 10–30 m thick and consists of gray relatively structureless devitrified rhyolite, in places containing concentrations of ovoid gas cavities locally filled with vapor-phase crystallization products.

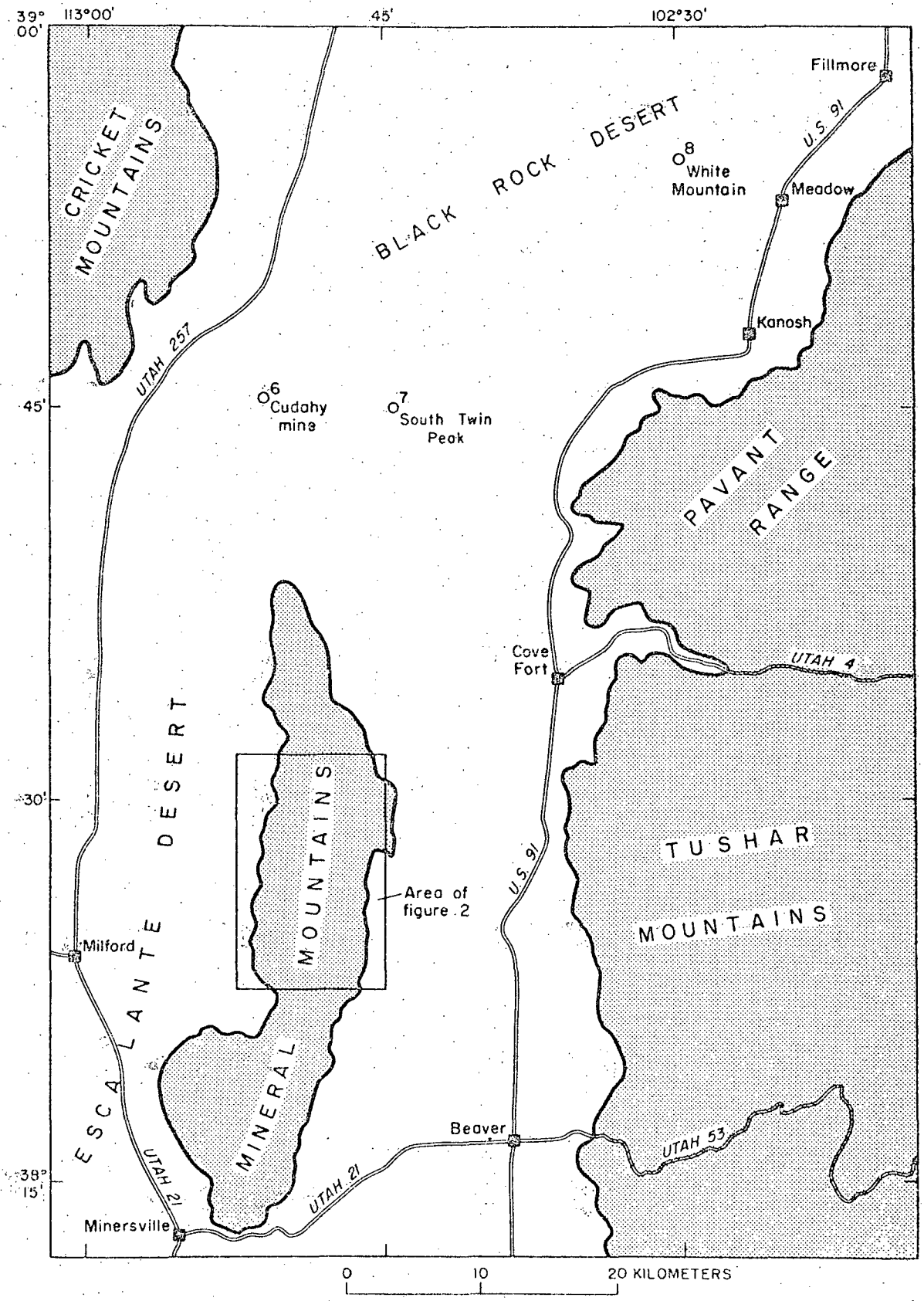

FIGURE 1.—Index map showing location of the Mineral Mountains and nearby areas, Utah. Numbers indicate locations of some dated samples (table 3); the others are shown on figure 2.

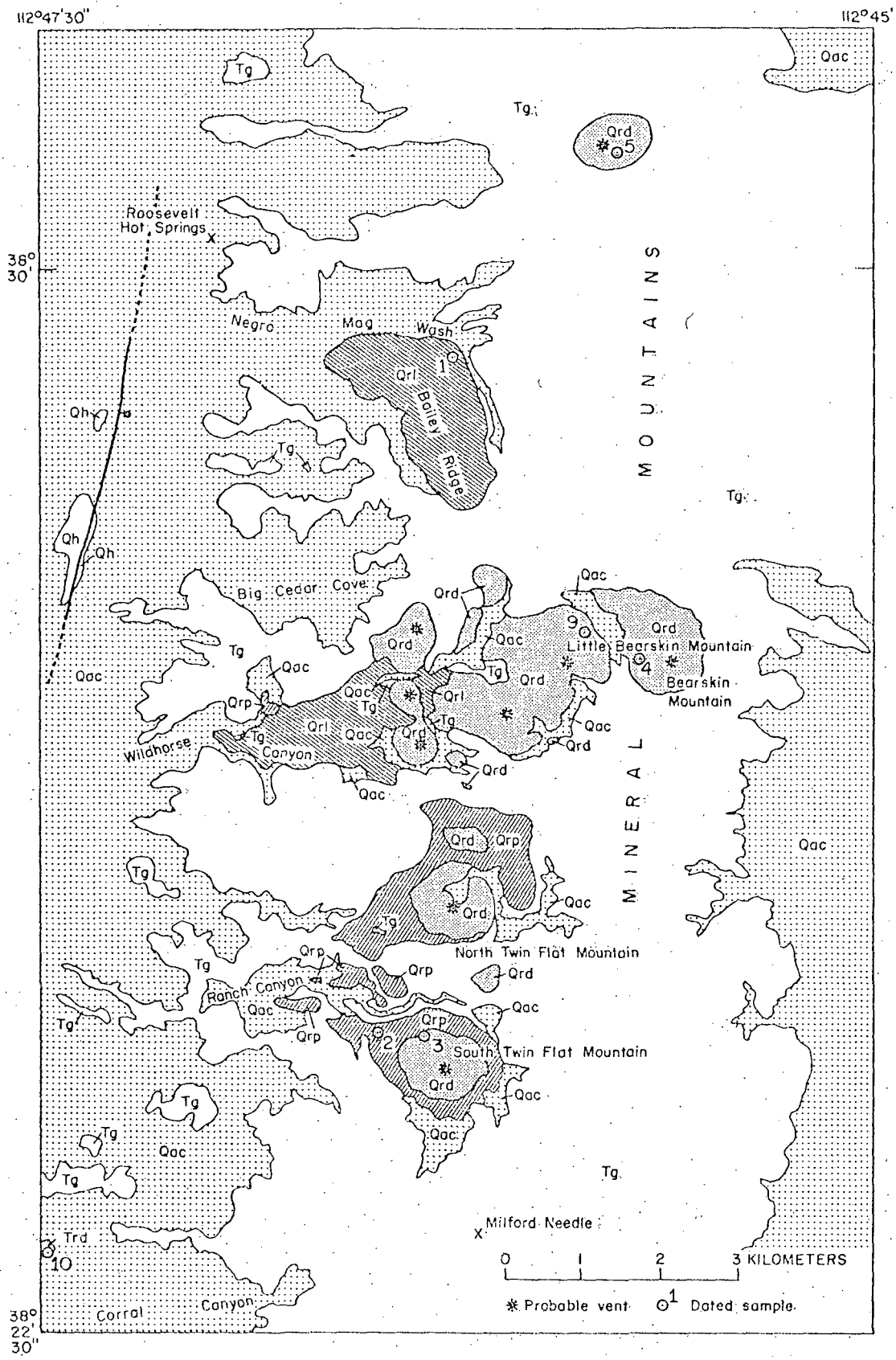

FIGURE 2.—Generalized geologic map of the central Mineral Mountains, Utah, showing distribution of Pleistocene rhyolitic rocks and locations of dated samples (table 3). Rock units, from oldest to youngest: Tg, Tertiary granite of Mineral Mountains; Trd, Tertiary rhyolite dome of Corral Canyon; Qrl, lava flows of Bailey Ridge and Wildhorse Canyon; Qrp, pyroclastic rocks; Qrd, lava domes; Qac, surficial deposits, primarily alluvium and colluvium; Qh, hot-spring deposits. Fault shown (bar and ball on downthrown side), named the Dome fault by Petersen (1975), is only one of many along the western range front.

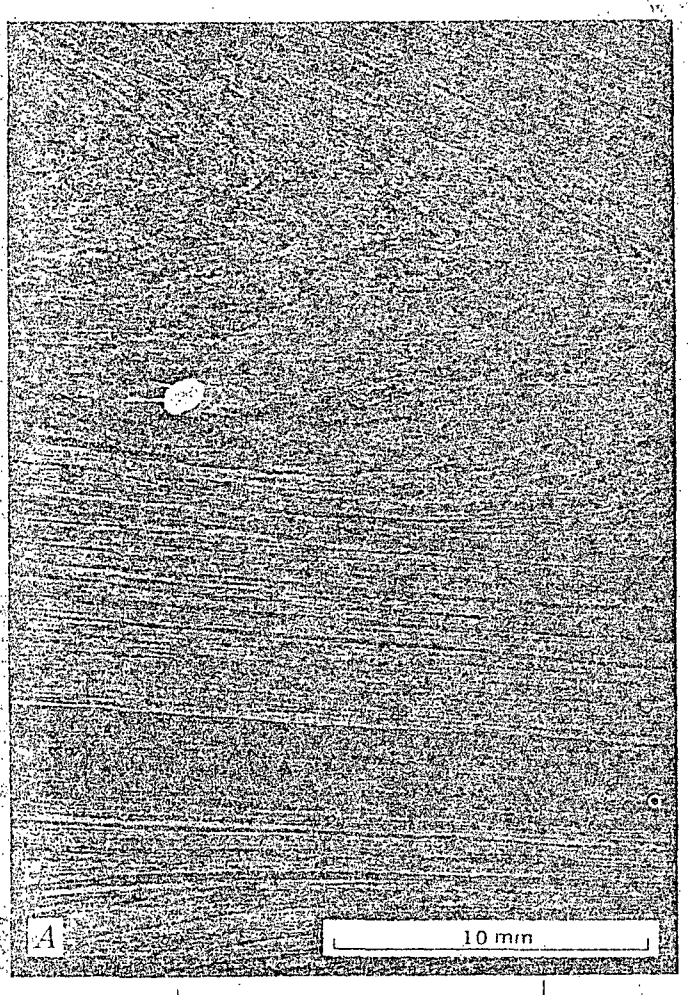

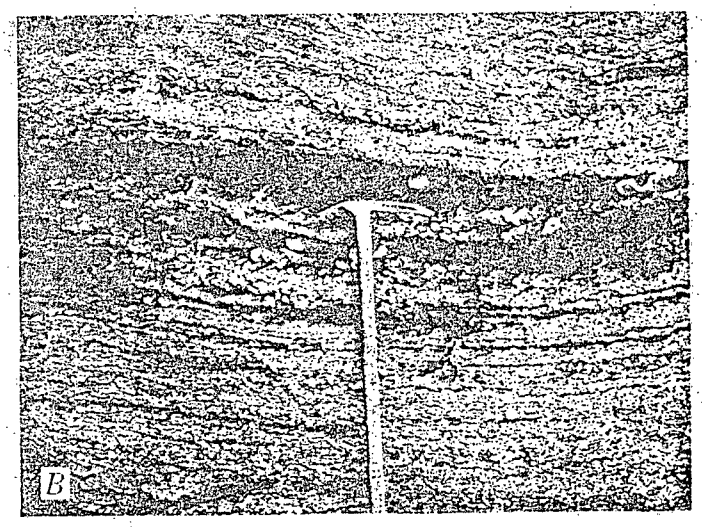

FIGURE 3.—Photographs of the Wildhorse Canyon flow. *A*, Photomicrograph showing recumbently folded flow lamination. Flow structures are defined by alined microlites. *B*, Alternating layers of obsidian and devitrified rhyolite in upper part of flow.

In upper parts of the flow a few meters of flow-layered obsidian are interlayered with devitrified rock (fig. 3*B*), passing upward into a more uniform dark glass zone or grading directly into a frothy rubbly breccia of tan perlitic pumice as much as 10 m thick at the top of the flow.

The flow layering and lamination in these rhyolitic lavas is remarkably planar and uncontorted as compared to the swirly internal structures typical of many rhyolitic lava flows. The "ramp structures" that occur commonly in upper parts of silicic flows (Christiansen and Lipman, 1966), are absent or poorly developed, and subhorizontal layering is typical throughout the Bailey Ridge and Wildhorse Canyon flows. The most common deviations from planar layering are small, typically rootless recumbent folds (fig. 3*A*), most limbs of which are less than 1 m long. These flowage features, as well as the relatively slight thickness of each lava flow as compared to its longitudinal extent, indicate that they were characterized by lower emplacement viscosities than many silicic lava flows.

Vents for these oldest flows of the Mineral Mountains have not been found. The Wildhorse Canyon flow appears to extend up drainage beneath younger lava domes in the upper part of the canyon, although exposures of the critical relations are poor because of cover by rubble. Probably the vent area for this flow is beneath the younger lavas to the east. If the Bailey Ridge flow vented from beneath its uppermost outcrop area, surface structures of this part of the flow give no indication of any concealed vent. This part of the flow is little dissected, however, and the vent area could be completely buried. Alternatively, the Bailey Ridge flow, and also the Wildhorse Canyon flow, might have come from higher on the slope, underneath the area now covered by the Bearskin and Little Bearskin Mountain lava domes. However, this would require that the upper portions of the flows be largely removed by erosion while the lower portions were left relatively undissected.

The Bailey Ridge and Wildhorse Canyon flows are petrographically similar. They contain less than 0.5 percent total phenocrysts, the majority of which are alkali feldspar (table 1). There are trace amounts of oligoclase, biotite, titanomagnetite, and ilmenite. The two flows are virtually identical in chemical composition (table 2). They are typical silicic rhyolites, containing about 76.5 percent SiO_2 and just over 9 percent total alkalis. The fresh obsidians contain more fluorine than water; secondarily hydrated pumice from the Bailey Ridge flow contains 2.4 percent total H_2O. The magmatic temperatures of these flows were about 750°C, as determined from compositions of iron-titanium oxides and coexisting plagioclase and alkali

TABLE 1.—*Modal compositions of radiometrically dated samples*

[Est., estimate; tr., trace; leaders (--), not present; *, microphenocrysts]

Field No.	Unit	Ground-mass	Plagio-clase	K-feldspar	Quartz	Biotite	Horn-blende	Clino-pyroxene	Opaques	Points counted
75L-17	Bailey Ridge flow, obsidian	99.9	--	tr.	tr.	--	--	--	--	Est.
75L-15	Tuff of Ranch Canyon obsidian block	98.2	0.6	0.8	0.4	tr.	--	--	tr.	3,615
75L-16	South Twin Flat Mountain dome, obsidian with patchy devitrification	92.6	1.2	3.9	2.3	tr.	--	--	tr.	3,034
75L-56	Bearskin Mountain, obsidian	97.2	.3	1.2	1.2	0.1	--	--	tr.	4,725
75R-53	Little Bearskin Mountain dome, obsidian	96.0	.9	1.9	1.0	--	--	--	0.1	2,000
75L-18A	Northern dome, frothy perlite	97.4	.4	1.3	.7	.1	--	--	.1	2,642
75L-19	Rhyolite of the Cudahy mine, obsidian	100	--	--	--	--	--	--	--	Est.
75L-21	Black Rock desert felsite plug	91.2	5.8	1.2	--	tr.	--	1.2	.6	3,188
75L-23	Rhyolite of White Mountain, obsidian	94	--	--	--	--	*6	--	--	Est.

TABLE 2.—*Chemical analyses and CIPW norms of rhyolites of the Mineral Mountains*

[Analyses by S. H. Evans, Jr., by standard wet chemical techniques. Key to analyses; 74-3A, Obsidian, Bailey Ridge flow; 74-8, Obsidian, Wildhorse Canyon flow; 75-14, Obsidian, Little Bearskin Mountain dome; 75-20, Basal Obsidian, North Twin Flat Mountain dome. Leaders (---) not present; tr., trace]

Chemical Analyses					CIPW Norms				
	74-3A	74-8	75-14	75-20		74-3A	74-8	75-14	75-20
SiO_2	76.52	76.51	76.42	76.45	Q	33.40	33.28	33.22	32.48
TiO_2	.12	.12	.08	.08	c	---	.26	.41	.45
Al_2O_3	12.29	12.29	12.79	12.79	or	30.96	31.20	27.89	27.95
Fe_2O_3	.31	.23	.20	.30	ab	32.15	31.90	37.40	37.15
FeO	.46	.51	.38	.29	an	1.00	1.02	---	---
MnO	.05	.05	.09	.10	di-wo	.37	.47	---	---
MgO	.08	.08	.11	.12	di-en	.11	.12	---	---
CaO	.64	.65	.44	.40	di-fs	.27	.38	---	---
Na_2O	3.80	3.77	4.42	4.39	hy-en	.09	.08	.27	.30
K_2O	5.24	5.28	4.72	4.73	hy-fs	.21	.26	.57	.34
P_2O_5	.02	.01	tr.	.06	mt	.45	.33	.29	.43
H_2O+	.12	.06	.13	.10	il	.23	.23	.15	.15
H_2O-	.06	.06	.01	---	ap	.05	.02	---	.14
F	.16	.15	.42	.44	fr	.33	.29	.61	.45
Sum	99.87	99.77	100.21	100.25	rest	.18	.12	.14	.10
Less F=O	.07	.06	.18	.19	Total	99.80	99.96	99.95	99.94
Total	99.80	99.71	100.03	100.06					

feldspar. The relatively low emplacement viscosities, indicated by the planar flow structures of these rhyolites, do not therefore seem related to exceptionally high emplacement temperatures.

A single K-Ar radiometric age determination of 0.79±0.08 m.y. (table 3, no. 1), from the toe of the Bailey Ridge flow, is the oldest age obtained from any rhyolite of the Mineral Mountains. The Bailey Ridge flow has a reversed paleomagnetic pole position (table 4) indicating, in conjunction with K-Ar data, that it was erupted toward the end of the Matuyama polarity epoch. The Wildhorse Canyon flow has not yet been dated radiometrically, but it also is characterized by a reversed polarity, which, in conjunction with morphological and chemical resemblance to the Bailey Ridge flow and its position beneath some of the pyroclastic rocks, suggests a similar age.

Pyroclastic rocks

South of Wildhorse Canyon, pyroclastic rocks of ash-fall and ash-flow origin are the lowest exposed rhyolitic rocks. The main area of pyroclastic rocks is in Ranch Canyon, where tuffs bury rugged paleotopography much like the present land surface.

The pyroclastic rocks are only weakly consolidated and are mostly poorly exposed, underlying alluviated slopes. All the pyroclastic deposits, both ash-fall and and ash-flow, are white to light tan. They occur over an altitude range from 1950 m in valley-bottom exposures in Ranch Canyon to as high as 2540 m on the surrounding slopes. They also occur in the Cove Fort area, where they are overlain by basalt lava flows (Nash and Smith, 1977). Much of the pyroclastic sequence has been removed by erosion in Ranch Canyon, and it is not clear to what extent this altitude range reflects an actual total thickness of the original deposit and to what extent the pyroclastic rocks were thinner but blanketed the preexisting topography. In Ranch Canyon these rocks are overlain by the large lava domes on North and South Twin Flat Mountains and by smaller masses of rhyolitic lava on adjacent ridges. Although contacts between these domes and the pyroclastic rocks are nowhere well exposed, this stratigraphic sequence is indicated by structural zones in the rhyolite domes of North and South Twin Flat Mountains. The lowest exposures are of a subhorizontal

TABLE 3.—*K-Ar age determinations on upper Cenozoic rhyolites of the Mineral Mountains, Utah, and adjacent areas*

[Constants: $K^{40}\lambda_c = 0.581 \times 10^{-10}$/yr, $\lambda_\beta = 4.963 \times 10^{-10}$/yr; atomic abundance: $K^{40}/K = 1.167 \times 10^{-4}$; *Radiogenic argon; Potassium determinations made with an Instrumentation Laboratories flame photometer with a Li internal standard. Figures 1 and 2 give sample locations. Ages of WM76-3 and MR76-26 determined by S. H. Evans, Jr., and F. H. Brown; other ages determined by H. H. Mehnert]

Sample	Field No.	Unit	Material dated	Location (Lat N Long W)	K_2O (percent)	$*Ar^{40}$ (10^{-10} moles/gram)	$*Ar^{40}$ (percent)	Age (m.y. ±2σ)
1	75L-17	Bailey Ridge flow-------	Obsidian--------	38°29′, 112°49′	5.10, 5.10	0.058	25.8	0.79±0.08
2	75L-15	Tuff of Ranch Canyon----	Obsidian block--	38°25′, 112°50′	4.63, 4.66	.047	47.1	0.70±0.04
3	75L-16	South Twin Flat Mountain dome----------	Sanidine--------	38°25′, 112°49′	8.14, 8.08	.059	18.1	0.50±0.07
4	75L-56	Bearskin Mountain dome--	Obsidian--------	38°27′, 112°47′	4.48, 4.49	.048	20.2	0.75±0.10
						.039	13.5	0.60±0.12
5	75L-18A	North Dome----------	Sanidine--------	38°31′, 112°47′	9.36, 9.35	.073	24.5	0.54±0.06
6	75L-19	Cudahy mine----------	Obsidian--------	38°45′, 112°51′	4.91, 4.93	.168	46.0	2.38±0.15
7	75L-21	South Twin Peak--------	Sanidine--------	38°45′, 112°47′	11.13, 11.12	.373	54.3	2.33±0.12
8	75L-23	White Mountain----------	Obsidian--------	38°55′, 112°30′	4.63, 4.70	.029	15.9	0.43±0.07
	WM76-3		Obsidian--------		5.23, 5.25	.030	21.5	0.39±0.02
9	75R-23	Little Bearskin Mountain dome--------	Sanidine--------	38°27′, 112°48′	9.31, 9.15 [1]9.26	.080	31.8	0.61±0.05
10	MR76-26	Corral Canyon dome------	Biotite---------	38°24′, 112°53′	8.72, 8.75	1.011	61.6	7.90±0.30

[1] Isotope dilution determination

TABLE 4.—*Preliminary data on magnetic polarities of rhyolites of the Mineral Mountains*

Unit	Number of samples	Declination	Inclination	Standard error (percent)
Normal samples:				
Northern dome----------	9	350	62	3
Big Cedar Cove dome------	4	23	67	4
Ranch Canyon dome--------	5	22	44	5
Corral Canyon dome-------	3	332	25	20
Ranch Canyon ash---------	2	356	46	29
Wildhorse Canyon ash-----	6	349	48	5
Reversed samples:				
Bailey Ridge flow--------	6	173	-63	6
Wildhorse Canyon flow----	4	168	-61	2

zone of basal flow breccia below the basal obsidian zone; this is the typical zonation expectable at the base of a lava flow or dome and would be an improbable relation if the pyroclastic rocks had been plastered against older lava domes. Thus, the lava dome of South Twin Flat Mountain overlies pyroclastic rocks that are at least 60 m and probably as much as 180 m thick, and these figures suggest minimum thicknesses of the pyroclastic unit.

The lower pyroclastic rocks are beds of air-fall pumice and ash at least 10 m thick and probably much thicker. Individual beds are a few centimeters to about a meter thick. Variable dips indicate that the ash was deposited on the underlying granite, on a surface as rugged as the present one. The pumice and ash contain several percent of small phenocrysts of quartz, oligoclase, alkali feldspar, biotite, magnetite, ilmenite, sphene, and allanite. This mineral assemblage is generally characteristic of the youngest rhyolite flows as well. Associated with the pumice and ash are a few percent of rhyolitic lithic debris, including devitrified rhyolite, perlite, and sparse obsidian fragments. Phenocrysts in the lithic debris are sparse, generally similar to those in the flows of Bailey Ridge and Wildhorse Canyon.

Ash-flow deposits widely overlie the ash-fall beds in Ranch Canyon. The ash-flow deposits locally are at least 50 m thick; probably the total thickness is much greater, but accurate estimates are difficult because of the poor exposures. The ash-flow deposits are everywhere nonwelded and only weakly consolidated; they tend to weather to small conical hills. On especially

steep slopes the ash-flow deposits rest directly against granite, with no intervening ash-fall material (fig. 4). In exceptionally good exposures, several flow units —each a few meters thick—can be recognized in the ash-flow deposits, with partings between the flow units marked by local concentrations of pumice, lithic debris, or better sorted ash.

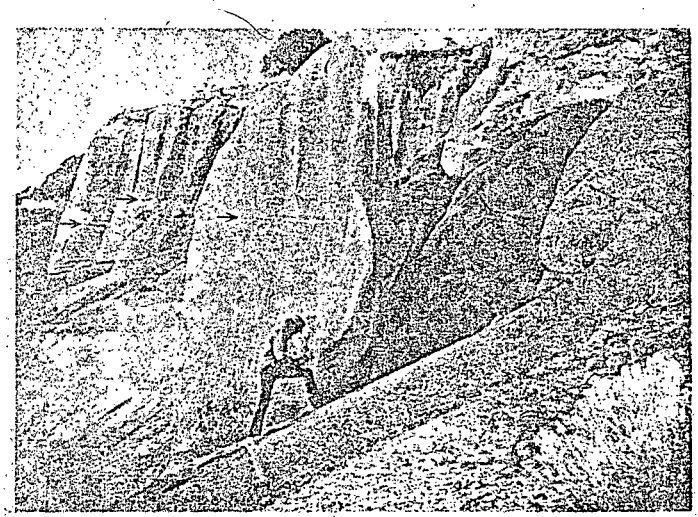

FIGURE 4.—Ash-flow tuff, resting on a rugged erosion surface cut on granite of the Mineral Mountains pluton. Arrows indicate faint parting between flow units of tuff. From northern side of Ranch Canyon at about 2105-m elevation.

On the northern side of lower Wildhorse Canyon, an isolated patch of pyroclastic material about 150 m across consists of finely laminated white fine-grained ash of lacustrine origin. These beds of water-reworked ash are younger than the Wildhorse Canyon flow and were deposited in a local basin dammed by the flow. The ash has a refractive index similar to that of the pyroclastic rocks in Ranch Canyon, one valley to the south, suggesting to us that it represents a reworked marginal facies of this deposit. In contrast, this patch of lacustrine tuff is interpreted by Glenn Izett (written commun., 1976) as airborne Bishop ash, from the Long Valley caldera in California, on the basis of small compositional differences with other rhyolites of the Mineral Mountains.

A single whole-rock K-Ar age on an obsidian clast from ash-flow tuff in Ranch Canyon yielded an age of 0.70 ± 0.04 m.y. (table 3, no. 2), providing an older limit for the age of the pyroclastic rocks. The pyroclastic deposits in Ranch Canyon, as well as the local lake beds in Wildhorse Canyon, have normal magnetic polarities in contrast to the reverse polarities of Bailey Ridge and Wildhorse Canyon flows. Thus, the pyroclastic rocks have been deposited during the Brunhes polarity epoch.

Porphyritic lava domes

The stratigraphically highest part of the upper Cenozoic volcanic assemblage in the Mineral Mountains is a group of at least nine separate perlite-mantled lava domes and small flows of porphyritic rhyolite. The domes tend to occur along the crest of the range, discontinuously over a zone about 15 km long. These domes form some of the highest topographic points in the Mineral Mountains, including Bearskin Mountain with an elevation of 2772 m (9095 ft). Individual domes are as much as 1 km across at their bases and stand as much as 250 m high, although dimensions are difficult to determine precisely because of the irregular pre-existing topography and subsequent erosion. Small stubby flows extend out from some of the domes, and some small isolated patches of rhyolite (fig. 2) may represent either eroded flow remnants or small separate domes.

The larger domes, such as Bearskin and Little Bearskin Mountains, are little eroded, and surface exposures consist largely of blocks of tan perlitic glass that are slightly modified remnants of the original brecciated frothy carapaces of the domes. Scattered fragments of dense black obsidian, derived from beneath the perlitic breccia, occur about a third of the way above the base of these domes. Float of well-layered devitrified rhyolite is exposed locally just above the zone of obsidian fragments. Pumiceous material, that in places ravels out from below the level of the obsidian zone, may represent an initial pyroclastic fall that is not well exposed.

Other domes, such as those of North and South Twin Flat Mountains (fig. 5), have been more deeply dissected, in this case by the reexcavation of Ranch Canyon, and their internal structural and crystallization features are better exposed. The internal features of all these late domes are in general similar. A basal black vitrophyric zone is everywhere well developed, in places resting on lighter colored glassy basal flow breccia. The vitrophyre zone, which is as much as 5–10 m thick, grades upward into devitrified rock through a transition zone a few meters thick in which flow-layered obsidian alternates with devitrified rock that is commonly highly spherulitic. The devitrified interiors of the flows tend to be light gray and contain conspicuous spherulites. In places, gas cavities several centimeters across contain lithophysal fillings. The interiors of the flows tend to be crudely flow layered, with the layering subhorizontal just above the basal glass zone, but becoming steeper in upper parts of the lava dome. Near-vertical riblike masses of flow-layered devitrified rock are commonly exposed high on the

FIGURE 5.—Rhyolite domes of North and South Twin Flat Mountains. Rugged terrain in distance, including Milford Needle (elev. 2920 m) on the left side of the picture, is underlain by granite of the Mineral Mountains pluton. Photographed from ridge between Ranch and Wildhorse Canyons.

domes, where erosion has stripped away the surface mantle of frothy perlite. The steeply dipping flow layering and ramp structures of these domes thus are in contrast to structures in the older lava flows of Wildhorse Canyon and Bailey Ridge.

The porphyritic domes typically lack well-developed central craters (for example, the South Twin Flat Mountain dome) although several have slight central depressions that have been breached and accentuated by erosion. Breached depressions are especially evident for the unnamed northern dome, which is on the range crest northeast of Negro Mag Wash (fig. 2), Bearskin Mountain dome, and North Twin Flat Mountain dome (fig. 5).

All the domes contain several percent phenocrysts of quartz, oligoclase, alkali feldspar, biotite, and iron-titanium oxides (table 1). Trace amounts of sphene and allanite occur in some domes. Hornblende, zircon, and allanite are present in the Corral Canyon dome, the southernmost exposure of rhyolitic volcanic rocks. The North and South Twin Flat Mountain domes have 5–8 percent total phenocrysts, distinctly more than any of the others. The obsidian zones of these two domes appear even more phenocryst-rich, because of the presence of small "snowflake" devitrification spots. The flows in upper Wildhorse Canyon and to the north contain only 2–3 percent total phenocrysts.

Two analyzed samples of the porphyritic domes (table 2) are chemically similar silicic alkalic rhyolite. In comparison with the older flows of Bailey Ridge and Wildhorse Canyon, the domes are slightly but significantly higher in Na_2O and F; they are lower in K_2O and CaO.

Lack of continuity, and thus absence of contact relations, between the domes makes relative ages of the domes difficult to determine. On the basis of amount of dissection, North and South Twin Flat Mountains may be among the oldest, and Bearskin Mountain among the youngest of the domes. The K-Ar ages (table 1), petrographic and chemical similarities, and the generally similar degree of erosional dissection indicate that the domes are about the same age. Stratigraphic relations on the northern side of the North Twin Flat Mountain dome suggest that this dome is older than the unnamed ridge-capping flow 0.5 km north of it (fig. 2). Bearskin Mountain and the three domes extending southwest from it appear compositionally homogeneous, consisting of phenocryst-poor rhyolite similar to the rhyolite that overlies the North Twin Flat Mountain dome. The Bearskin Mountain dome has yielded K-Ar ages on obsidian of 0.60 ± 0.12 and 0.75 ± 0.10 m.y. (table 3, no. 4), and the Little Bearskin Mountain dome has an indicated sanidine age of 0.61 ± 0.05 m.y. (table 3, no. 9). Sanidines from obsidian of South Twin Flat Mountain and the unnamed northern dome have yielded K-Ar ages of 0.50 ± 0.07 and 0.54 ± 0.06 m.y., respectively (table 3, nos. 3, 5). Magnetic-polarity determinations for several domes of this group are normal (table 4) indicating, in conjunction with the K-Ar ages, that they were erupted during the Brunhes polarity epoch.

One small dome of mostly devitrified alkalic rhyolite and minor vitrophyre in Corral Canyon, shown as Trd in the lower left corner of figure 2, has been dated at 7.90 ± 0.30 m.y. (table 3, no. 10). These volcanic rocks appear to be unrelated to the young rhyolites higher in the Mineral Mountains; the rhyolite in Corral Canyon is more eroded and contains a different

phenocryst assemblage than the other rhyolites. The thermal event about 8 m.y. ago, as represented by these lavas, may have been responsible for producing the anomalously young ages of 14 and 9 m.y. measured on the Mineral Mountains pluton.

DISCUSSION

The stratigraphic relations and K-Ar ages of rhyolites of the Mineral Mountains, newly reported here, indicate that these rocks were emplaced during a relatively brief period in the Pleistocene, between about 0.8 and 0.5 m.y. ago, but an older rhyolitic event occurred about 8 m.y. ago. The Mineral Mountains are flanked on the northern and eastern sides by upper Cenozoic basalt flows (Condie and Barsky, 1972; Hoover, 1974), roughly contemporaneous with and younger than the rhyolite of the Mineral Mountains, and this association of rhyolite and basalt constitutes a bimodal volcanic assemblage of a type that is being recognized widely in the western United States in upper Cenozoic volcanic sequences (Christiansen and Lipman, 1972).

A significant question is whether the thermal anomaly of the Roosevelt KGRA is due to proximity to the late Cenozoic volcanic centers in the Mineral Mountains. Roosevelt Hot Springs and other inactive hot springs are located along the mountain-front fault on the western side of the Mineral Mountains, about 2 km west of the nearest exposed rhyolite (fig. 2). The size and shape of the Pleistocene magmatic system underlying the Mineral Mountains cannot be determined with any precision from the surface distribution of rhyolite vents, yet the extent of the vents for 15 km along the crest of the range suggests the possibility of a sizable magmatic system at depth. The elongate trend of rhyolite vents might even mark a segment of a large evolving circular igneous structure, such as interpreted for the Coso rhyolite domes in California (Duffield, 1975). The rhyolites of the Mineral Mountains were extruded along the eroded core of the large Mineral Mountains pluton, itself a late Cenozoic intrusion of remarkably large size for so young an age. Proximity in space and time suggests that the rhyolite of the Mineral Mountains represents a late stage in the evolution of a complex magmatic system that earlier gave rise to the granite of the Mineral Mountains. Alternatively, the rhyolite volcanism might have evolved independently of the granite, but has been partly localized where the crust was still hot from an earlier plutonic event. It seems likely, though not provable, that this large complex magmatic system has also been the heat source for the Roosevelt KGRA, with the shallow thermal anomaly enhanced along the range front by deep fault-controlled convective circulation of hot water.

This interpretation of a complex shallow magmatic system is supported by limited available rare-earth element data (table 5), which indicate that the rhyolite of the Mineral Mountains had a magmatic residence time in a shallow environment for a sufficiently long time to undergo major low-pressure fractional

TABLE 5.—*Rare-earth element analyses of rhyolites of the Mineral Mountains*

[Analyses by J. S. Pallister and H. T. Millard by neutron activation, using a chemical concentration technique. (See Zielinski and Lipman, 1976.)]

	Bailey Ridge flow	Wildhorse Canyon flow	South Twin Flat Mountain dome	Bearskin Mountain dome
	(75L-17)	(75L-60A)	(75L-16)	(75L-56)
La------	43.5	44.3	24.9	25.0
Ce------	95.6	94.3	51.5	44.2
Nd------	27.0	25.5	9.6	7.5
Sm------	3.6	3.5	1.3	.90
Eu------	.42	.40	.037	.035
Gd------	2.8	2.5	1.3	.88
Tb------	.52	.49	.30	.20
Tm------	.38	.35	.47	.31
Yb------	2.9	2.9	4.2	3.0
Lu------	.52	.49	.79	.57

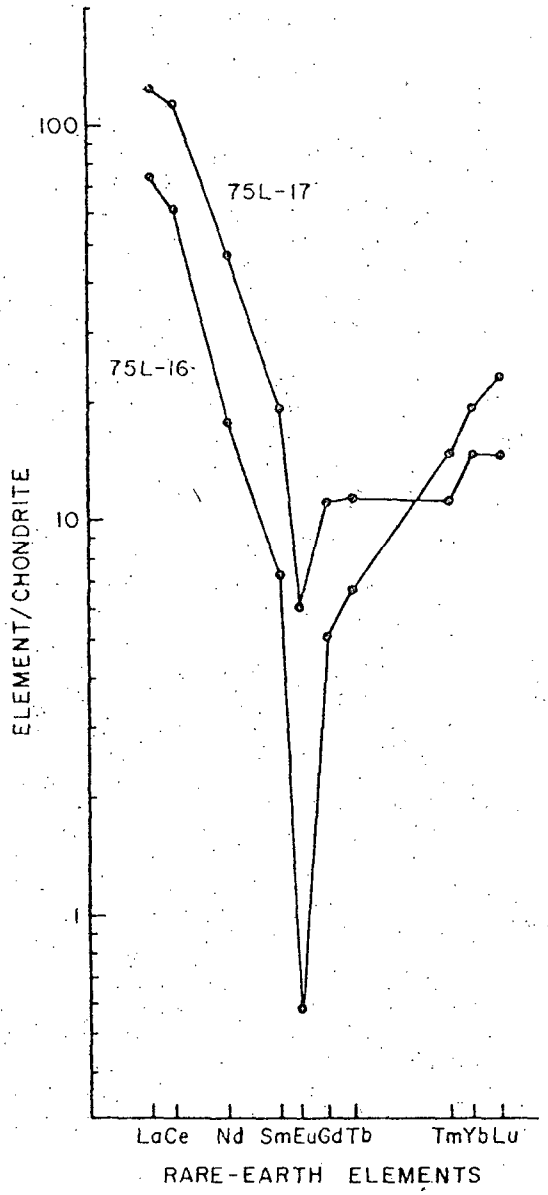

FIGURE 6.—Chrondite-normalized rare-earth-element plot for two rhyolites of the Mineral Mountains (75L–16 and 75L–17), showing negative Eu anomalies.

crystallization involving removal of feldspar. Chondrite-normalized analyses of two whole-rock samples show large negative Eu anomalies (fig. 6), indicative of major feldspar removal (Arth, 1976). This pattern contrasts with that of some other voluminous Cenozoic silicic rocks in the western United States (Zielinski and Lipman, 1976; P. W. Lipman, unpub. data, 1976) which show small or no Eu anomalies and appear to have developed their silicic compositions by processes not involving major feldspar fractionation, probably because the environment of differentiation was at pressures too high for feldspar to be stable.

Occurrences of upper Cenozoic alkalic rhyolite of possible geothermal significance in southwestern Utah are not restricted to the Mineral Mountains. We dated obsidian "Apache tears" from an eroded rhyolite flow at the Cudahy mine about 25 km north of the Mineral Mountains (fig. 1), as 2.38±0.15 m.y. (table 3, no. 6). A large rhyolite plug (South Twin Peak) in the Black Rock desert about 10 km east of the Cudahy mine yielded a similar K-Ar age of 2.33±0.12 m.y. (table 3, no. 7). Marginal obsidian from a small body of rhyolite at White Mountain, about 50 km northeast of the Mineral Mountains (fig. 1), yielded ages of 0.43±0.07 and 0.39±0.02 m.y. (table 3, no. 8), the youngest of any of our ages. The rhyolite at White Mountain contains inclusions of a distinctive dated basalt, indicating a maximum age for the dome of about 1 m.y. (Hoover, 1974). This rhyolite occurs less than 1 km from the nearest exposure of upper Pleistocene basalt of the Tabernacle volcanic field estimated to be 10 000–20 000 yr old (Hoover, 1974). Basalts of the Ice Springs volcanic field, 3 km north of White Mountain, are post-Lake Bonneville in age, that is, less than 12 000 yr old. These basaltic and rhyolitic rocks together offer another example of a bimodal basalt-rhyolite association in Utah. Thus, the potential for volcanic-related thermal anomalies in southwestern Utah is not confined to the Mineral Mountains. In fact, White Mountain is about 7 km north of Meadow and Hatton hot springs (Mundorff, 1970).

Another intriguing aspect of the rhyolites in the Mineral Mountains is their significance as a source of artifact obsidian. Implement-grade obsidian is relatively scarce in the southwestern United States, yet obsidian artifacts occur widely in archeological sites. Well-known sources of archeological obsidian include the Jemez Mountains in New Mexico, Coso Mountains and Long Valley areas in east-central California, Medicine Lake Highlands and associated rhyolitic centers in northeastern California, Newberry volcano and numerous small areas of rhyolite in eastern Oregon, and Yellowstone rhyolite plateau in Wyoming (fig. 7). The little known Mineral Mountains locality is in a region where high-quality obsidian is scarce, nearly equidistant from better known sources, yet it contains abundant obsidian suitable for implement manufacture. Individual blocks of nonporphyritic obsidian from the Bailey Ridge and Wildhorse Canyon flows are as much as 0.5 m across. Obsidian from the Mineral Mountains has recently been recognized in several archeological sites in southwestern Utah and adjacent parts of Nevada (Umshler, 1975), but how widely it has been distributed has yet to be established.

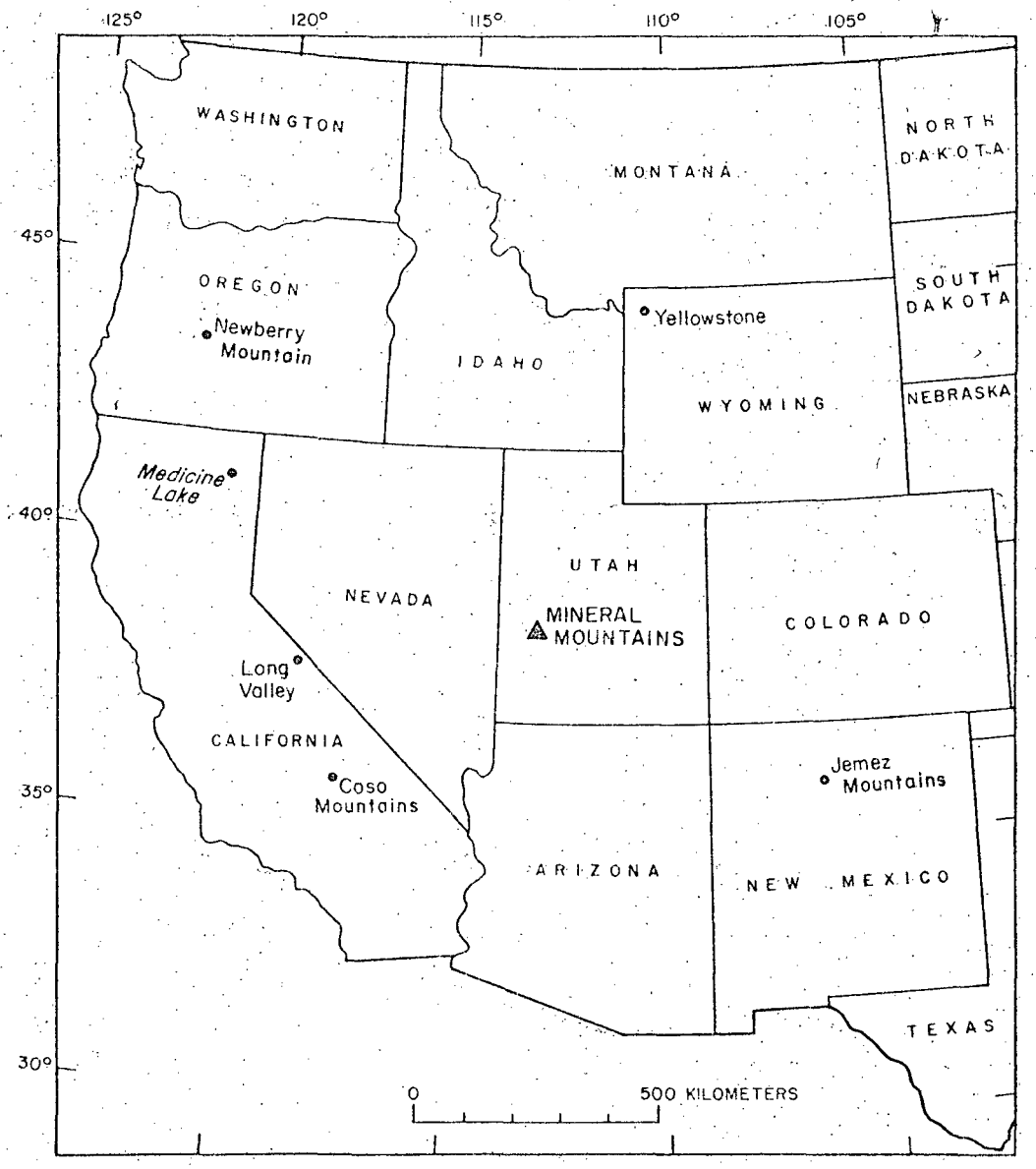

FIGURE 7.—Well-known sources for archeological obsidian in the western United States.

Available compositional data indicate that obsidian artifacts derived from the Mineral Mountains should be distinguishable, especially by minor-element compositions, from those of most of the better known obsidian sites.

Fission-track age dating, by G. A. Izett and C. W. Naeser, and obsidian-hydration age dating, by Irving Friedman, were conducted—independently of our study—on selected samples of rhyolite from the Mineral Mountains. The ages determined by these two other techniques provide a cross-check on the ages presented above that were determined by the K-Ar isotope method. Comparisons of the results of the three techniques are presented separately, in the sections that follow.

FISSION-TRACK DATING

By G. A. Izett and C. W. Naeser

Fission-track age determinations were made on samples of obsidian from the Bailey Ridge flow and the Bearskin Mountain dome. The fission-track age of the Bailey Ridge obsidian is in fair agreement with the K-Ar age of the obsidian, but the fission-track age of the Bearskin Mountain obsidian is anomalously younger than the K-Ar age. Th sample we dated of the Bearskin Mountain obsidian contains no fossil fission tracks; however, the age can be estimated by assuming the presence of one fossil track as shown in the table below. The anomalously young fission-track age of the Bearskin Mountain obsidian probably is due to the annealing of fossil tracks from a recent thermal event. The fission-track analytical data follow:

Fission-track analytical data

[Fission tracks etched for about 10 seconds in 48 percent hydrofluoric acid; ± 1 sigma about the mean. $\lambda f = 6.85 \times 10^{-17} yr^{-1}$]

Locality	ϕ (neutrons cm^{-2})	ρ_s (tracks cm^{-2})	ρ_i (tracks cm^{-2})	Fission track glass age x 10^6 years	K-Ar glass age x 10^6 years[1]
Bearskin Mountain dome	8.72×10^{14}	$<3.37 \times 10^1$(1)	1.25×10^5(309)	<0.02	0.75 ± 0.1 0.60 ± 0.12
Bailey Ridge flow	0.5×10^{15}	7.89×10^2(3)	4.40×10^4(213)	0.55 ± 0.30	0.79 ± 0.08

[1]See table 3.

OBSIDIAN-HYDRATION DATING

By Irving Friedman

Four rhyolite lava flows or domes from the Mineral Mountains, Utah, were dated by the obsidian-hydration technique. Most of the results agree with K-Ar and fission-track dates of the same flows.

Obsidian-hydration dating depends upon the fact that a newly formed surface on obsidian, such as a cooling crack, adsorbs water from the atmosphere. This adsorbed water slowly diffuses into the obsidian, and the depth of penetration of the water can be measured under the microscope in a thin section cut normal to the surface (Friedman and Smith, 1960). The rate at which the water diffuses into the obsidian is dependent upon temperature and glass composition (Friedman and Long, 1976).

The thickness of the hydrated layer (in micrometers) for the rhyolite units is tabulated below. Also listed is the expected rate of hydration (in $\mu m^2/10^3$ yr) for each flow, calculated for an estimated effective hydration temperature of 8°C and from the chemical composition of the obsidian. (See Friedman and Long, 1976.) The calculated obsidian-hydration age is also given, as is the K-Ar age.

Although the effective hydration temperature is assumed to be the same for all the flows sampled, the differing whole-rock chemistry of the obsidian gives different calculated hydration rates. Compositions of two of the obsidians are from table 2 in this paper; the analysis of the Bearskin Mountain dome is from S. H. Evans (written commun., 1976). No analysis is available for the South Twin Flat Mountain dome. An analysis for the North Twin Flat Mountains (table 2) was used instead; the hydration rate and calculated age are accordingly uncertain.

The calculated hydration rates vary by a factor of 2.5, owing mainly to differences in the amount of CaO+MgO. The chemical analyses were on whole-rock samples, but the hydration-rate calculation should be based on glass compositions. The Wildhorse Canyon and the Bailey Ridge glasses are almost free of phenocrysts, but the Bearskin Mountain and particularly the

Rhyolite	Thickness of hydration μm (± 1 μm)	Chemical index	Calculated hydration rate $\mu m^2/10^3$ yrs	Calculated age 10^6 yrs	Corrected age	K/Ar age
Wildhorse Canyon flow	41	42.5	2	0.85	0.85	([1])
Bailey Ridge flow	40	41.7	2	.80	.80	0.79
Bearskin Mountain dome	31	47.4	4	.24	.48	.75 .60
South Twin Flat Mountain dome	22	51.1(?)	5(?)	.10(?)	.25	.50

[1]No determination

South Twin Flat Mountain glasses are porphyritic. Obsidian from Wildhorse Canyon, Bailey Ridge, and South Twin Flat Mountain all have refractive indices of 1.4847 ± 0.0005, whereas Bearskin Mountain dome has a slightly higher index, 1.4856 ± 0.0005. The similarity in index of all four glasses makes any assumption of greatly differing hydration rates for these samples unrealistic. If we assume that the chemical compositions of the glass phase of all four samples are similar, then the hydration rates also will be similar and the dates shown in the column "Corrected age" should apply.

The corrected ages agree with the K-Ar dates, except for the date for the South Twin Flat Mountain dome, where the hydration date is about half that derived by K-Ar dating. The reasons for this discrepancy are not known, but we may not have sampled sufficiently to find an original surface on the samples from this site. Alternatively, the discrepancy may be due to some inherited argon in the sanidine used for K-Ar dating.

REFERENCES CITED

Allen, E. T., and Day, A. L., 1935, Hot spring of the Yellowstone National Park: Carnegie Inst. Washington Pub. 466, 525 p.

Armstrong, R. L., 1970, Geochronology of Tertiary igneous rocks, eastern Basin and Range province, western Utah, eastern Nevada, and vicinity, U.S.A.: Geochim. et Cosmochim. Acta, v. 34, p. 203–232.

Arth, J. G., 1976, Behavior of trace elements during magmatic processes—A summary of theoretical models and their application: U.S. Geol. Survey Jour. Research, v. 4, no. 1, p. 41–48.

Bailey, R. A., Dalrymple, G. B., and Lanphere, M. A., 1976, Volcanism, structure, and geochronology of Long Valley caldera, Mono County, California: Jour. Geophys. Research, v. 81, p. 725–744.

Berge, C. W., Crosby, G. W., and Lenzer, R. C., 1976, Geothermal exploration of Roosevelt KGRA, Utah [abs.]: Rocky Mtn. Section, AAPG and SEPM 25th Annual Mtg., Billings, Mont., Program, p. 52–53.

Christiansen, R. L., and Blank, H. R., 1972, Volcanic stratigraphy of the Quaternary rhyolite plateau in Yellowstone National Park: U.S. Geol. Survey Prof. Paper 729–B, 18 p.

Christiansen, R. L., and Lipman, P. W., 1966, Emplacement and thermal history of rhyolite lava flow near Fortymile Canyon, southern Nevada: Geol. Soc. American Bull., v. 77, no. 7, p. 671–684.

———1972, Late Cenozoic, Pt. 2 *of* Cenozoic volcanism and plate-tectonic evolution of the western United States: Royal Soc. London Philos. Trans., ser. A., v. 217, p. 249–284.

Condie, K. C., 1960, Petrogenesis of the Mineral Range pluton, southwestern Utah: Utah Univ., M.S. thesis, 94 p.

Condie, K. C., and Barsky, C. K., 1972, Origin of quaternary basalts from the Black Rock Desert Region, Utah: Geol. Soc. America Bull., v. 84, no. 2, p. 333–352.

Duffield, W. A., 1975, Late Cenozoic ring faulting and volcanism in the Coso Range area of California: Geology, v. 3, p. 335–338.

Earll, F. N., 1957, Geology of the central Mineral Range, Beaver County, Utah: Utah Univ., Ph. D. thesis, 112 p.

Friedman, Irving, and Long, W. D., 1976, Hydration rate of obsidian: Science, v. 191, no. 4225, p. 347–352.

Friedman, Irving, and Smith, R. L., 1960, A new dating method using obsidian: Part 1, the development of the method: Am. Antiquity, v. 25, no. 4, p. 476–522.

Greider, B., 1976, Geothermal energy, Cordilleran hingeline—West, *in* Hill, J. G., ed., Geology of the Cordilleran hingeline: Denver, Rocky Mountain Assoc. Geologists, p. 351–362.

Hoover, J. D., 1974, Periodic Quaternary volcanism in the Black Rock Desert, Utah: Brigham Young Univ., Geology studies, v. 21, p. 3–72.

Hunt, B. B., 1938, Igneous geology and structure of the Mount Taylor volcanic field, New Mexico: U.S. Geol. Survey Prof. Paper 189–B, p. 51–80.

Lambert, Wayne, 1966, Notes on the late Cenozoic geology of the Taos–Questa area, New Mexico, *in* Guidebook of Taos Raton Spanish Peaks country, New Mexico and Colorado, New Mexico Geol. Soc. 17th Field Conf., 1966: Socorro, N. Mex., New Mexico Bur. Mines and Mineral Resources, p. 43–50.

Liese, H. C., 1957, Geology of the northern Mineral Range, Millard and Beaver Counties, Utah: Utah Univ., M.S. thesis, 88 p.

Moore, R. B., Wolfe, E. W., and Ulrich, G. E., 1974, Geology of the eastern and northern parts of the San Francisco volcanic field, Arizona, *in* Geology of Northern Arizona: Geol. Soc. America, Rocky Mtn. Section Mtg., p. 465–494.

Mundorff, J. C., 1970, Major thermal springs, Utah: Utah Geol. and Mineralog. Survey Water-Resources Bull. 13, 60 p.

Nash, W. P., and Smith, R. P., 1977, Pleistocene volcanic ash deposits in Utah: Utah Geology, v. 4, no. 1, p. 35–42.

Park, G. M., 1968, Some geochemical and geochronologic studies of the beryllium deposits in western Utah: Utah Univ., M.S. thesis, 195 p.

Petersen, C. A., 1975, Geology of the Roosevelt hot springs area, Beaver County, Utah: Utah Geology, v. 2, no. 2, p. 109–116.

Robinson, H. H., 1913, The San Francisco volcanic field, Arizona: U.S. Geol. Survey Prof. Paper 76, 213 p.

Smith, R. L., Bailey, R. A., and Ross, C. S., 1970, Geologic map of the Jemez Mountains, New Mexico: U.S. Geol. Survey Misc. Geol. Inv. Map I–571.

Smith, R. L., and Shaw, H. R., 1975, Igneous-related geothermal systems: U.S. Geol. Survey Circ. 726, p. 58–83.

Umshler, D. B., 1975, Source of the Evan's Mound obsidian: Socorro, New Mexico Inst. Mining and Technology, M.S. thesis, 38 p.

Zielinski, R. A., and Lipman, P. W., 1976, Trace-element variations at Summer Coon volcano, San Juan Mountains, Colorado, and the origin of continental-interior andesite: Geol. Soc. America Bull., v. 87, p. 1477–1485.

☆U.S. GOVERNMENT PRINTING OFFICE: 1977—261-198/1

AREA
UT
KGRAs

DISTRIBUTION OF KGRAs

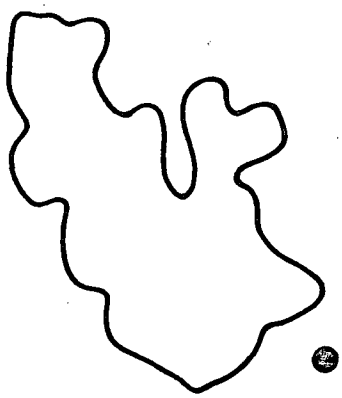

Salt Lake City

CRATER SPRINGS

WAH WAH-TUSHAR MINERAL BELT

COVE FORT-SULPHURDALE

Richfield

MONROE-JOSEPH

Milford

ROOSEVELT HOT SPRINGS

THERMO HOT SPRINGS

LUND

NEW CASTLE

NAVAJO LAKE

St. George